Negative dispersion without absorption in atomic ensembles

Dem Fachbereich Physik
der Universität Hannover
zur Erlangung des Grades

DOKTOR DER NATURWISSENSCHAFTEN
– Dr. rer. nat. –

genehmigte Dissertation von

Dott. Alessandra Rocco

geboren am 27. Februar 1968 in Milano

November 2001

Referent: Prof. Dr. K. Danzmann
Korreferent: Prof. Dr. M. Kock

Tag der Prufüng: 18. Dezember 2001

Kurzzusammenfassung

Dott. Alessandra Rocco

Negative Dispersion ohne Absorption in atomaren Ensembles

In dieser Arbeit werden die optische Eigenschaften von freien Atomen in einem Atomstrahl untersucht, um die Realisierungsmöglichkeit zu erforschen, ein optisches Medium zu schaffen, das anomale Dispersion ohne Absorption zeigt. Erzeugt wird dies Medium durch eine kohärente Überlagerung der atomaren Eigenzustände eines Zwei-Nieveau-System, das nach der Theorie ein endsprechendes Verhalten zeigt. Mit einem optischen Medium mit diesen Eigenschaften kann ein breitbandiger Resonator mit hoher Güte realisiert werden.

Für diese Untersuchungen wirde ein Messverfahren gewählt, das die Vorteile der optischen Interferometrie mit der Fm-Spektroskopie verbindet. Es ist ein Mach-Zehnder- Interferometer mit phasenmodulierten Arm, das seismisch isoliert ist und komplett in Hochvakuum arbeitet. Es erlaubt eine sehr empfindlich simultane Messung von Absorption und Phasenverschiebung. Der Interferometeraufbau wurde weiterentwickelt, um die Leistung des treibenden Feldes und die Teilchendichte in der Wechselwirkungszone zu erhöhen.

Als optisches Medium wird Ca gewählt. Die Frequenz des treibenden Feldes ist auf dem Resonanzübergang $4s^2\,^1S_0 \rightarrow 4s4p\,^1P_1$ bei $423nm$ stabilisiert. Die Absorption und Phasenverschiebung eines Zwei-Nieveau-System werden zum ersten Mal systematisch als Funktion der Feldstärke des treibenden Feldes gemessen. An die gemessenen Signalstrukturen wirdn die theoretischen Profile für ein getriebenes Zwei-Nieveau-System angefittet und so die Absorption und der Brechungsindex auf der Resonanzfrequenz bestimmt. Es zeigt sich, dass die Absorption stärker als die Dispersion mit steigender Feldstärke des treibenden Feldes abnimmt. Verglichen mit dem nichtgetriebenen System nimmt die Dispersion um den Faktor 53 und die Absorption um den Faktor 330 ab bei der maximalen Treiberfeldstärke von $\Omega_D = 2\pi 54.4 MHz$. Diese Abhängigkeit der Messwerte bestätigt sehr gut die Theorie.

Die Möglichkeit, ein solches Medium innerhalb eines optischen Resonator zu benutzen, wird auch untersucht. Die Daten-Analyse zeigt, dass λ Kompensation erreicht ist und dass aber bei dem Wert der erreichten experimentellen anomalen Dispersion die Restabsorption noch zu groß ist, um einen Weisslichtresonator zu realisieren. Es werden Lösungswege für dies benutzte atomare System aufgezeigt. Andere atomare Systeme, die auf den ersten Blick sehr erfolgversprechend erscheinen, werden auf ihre Realisierungsmöglichkeit hin überprüft.

Schlüsselworte

Anomal Dispersion, electromagnetisch induzierte Trasparenz, Frequenzverdopplung

Abstract

Dott. Alessandra Rocco

Negative dispersion without absorption in atomic ensembles

In this work the optical properties of a calcium atomic beam, strongly driven on the transition, are investigated, in order to obtain a coherently prepared medium with the right amount of negative dispersion at a point of zero absorption. From the theory it is well known that a strongly driven Two-Level system exhibits such properties. Such a medium could in particular be used to fill an optical resonator in order to obtain a broadband high finesse cavity (White Light Cavity).

For the investigations a spectroscopic method had been used, consisting of a Mach-Zehnder interferometer with a phase modulated arm. In this way it is possible to perform a high sensitive simultaneous measurement of both phase shift and absorption profiles in a calcium atomic beam, for an increasing driving field, which frequency is stabilized on the transition $4s^2\,^1S_0 \rightarrow 4s4p\,^1P_1$ at $423nm$. For the first time both absorption and phase shift were systematic investigated as function of the driving field intensity, while it was developed a new geometrical configuration for the atomic oven which permitted to reach a higher particle density in the interaction zone.

It was then possible to calculate the values of derivative of phase shift and absorption at the transition frequency, where the dispersion results anomalous, having fitted the measured curves to the phase shift and absorption profiles for a strongly driven Two-Level Atom.

An analysis of the evolution of the both the quantities as driving field function could be then performed. The theoretical analysis of the strongly driven two level system could then be experimentally verified, especially that the absorption decreases stronger than dispersion with an increasing driving field. It was in fact measured a decreasing of a factor 53 in the dispersion, between the not driven and driven atomic system while the corresponding absorption decreased of a factor 330, for a value of the driving field of $\Omega_D = 2\pi 54.4 MHz$.

The possibility of inserting the medium inside an optical resonator to obtain a broadband high finesse cavity has also been discussed. The data analysis showed that even if the λ compensation was reachable in the achieved condition, the residual absorption was still too high to realize a White Light Cavity. The configuration for further development of the system which should allow this realization was also analyzed, together with a comparison with the performances of different atomic systems.

Keywords

Contents

Contents

vi

Used symbols

Symbol	Unit	Meaning
$\lvert a \rangle, \lvert b \rangle$		Ground and excited atomic eigenstates
$< A >$	A	Expectation value of operator A
b_1		Fundamental wave confocal parameter
Δ	rad	Round-trip phase shift
$\Delta\omega_{FWHM}$	rad/s	FWHM-resonator bandwidth
$\Delta\omega_{FWHM}^{WLC}$	rad/s	FWHM- white light resonator bandwidth
$\Delta\omega_{FSR}$	rad/s	Resonator free spectral range
$\mathcal{D}$	Cm	Element of dipol matrix
$\mathcal{E}$	V/m	Electric field
$\alpha(\omega)$	m^{-1}	Absorption coefficient
α_0	m^{-1}	Absorption coefficient on the transition
E_i	J	Eigenenergy in the basis state $\lvert i \rangle$
$E_p(t)$	Vm^{-1}	Probe field
$E_D(t)$	Vm^{-1}	Driving field
$\vec{E}$	Vm^{-1}	Electric field
$\vec{e}_i$		Polarization unity vector
$\mathcal{F}$		Finesse
FOM	m	Figure of merit
g	s^{-1}	Transition linewidth
G		Gain
Γ_{BK}	1/(Wm)	Material constant for frequency doubling
γ_1	s^{-1}	Longitudinal relaxation rate
γ_2	s^{-1}	Transversal relaxation rate
θ	rad	Tilting angle of an optical element
ξ_{BK}		Boyd-Kleinmann factor
H	J	Hamilton-Operator
I	W/m^2	Intensity
I_{Sat}	W/m^2	Saturation intensity
I_{PD}	A	Photocurrent
J_n		Bessel function of order n
$\vec{k}$	m^{-1}	Wave vector
λ	m	Optical wavelenght

Used symbols

L_k	m	Crystal lenght
$\mathcal{L}$		Linear loss of fundamental wave in resonator
l_{int}	m	Interaction lenght
m	kg	Mass
M		Modulation index
M_{FMS}		FMS Modulation index
$n(\omega)$		Refraction index
$n'(\omega)$	Hz^{-1}	Dispersion
n'_0	Hz^{-1}	Dispersion at the transition
N_{at}	m^{-3}	Particle density
N	m^{-3}	Particle density
ν	s^{-1}	Optical frequency
Ω	s^{-1}	Frequency of modulation amplitude
P_1	W	Fundamental wave power
P_2	W	Second harmonic power
$\vec{P}$	Cm^{-2}	Polarisation
φ	rad	Optical phase
q	m	Complex beam parameter
r_1, r_2		Amplitude transmission coefficient for the mirrors
r_m		Amplitude transmission coefficient for the medium
ρ	m^{-3}	Density matrix, statistical Operator
t	s	Time
t_1, t_2		Amplitude transmission coefficient for the mirrors
t_{EOM}		Amplitude transmission coefficient for the EOM
T	K	Temperature
U_m	V	Mixer output voltage
v_g	ms^{-1}	Group velocity of an optical pulse
w_0	m	Beam waist for a Gaussian beam
$w(z)$	m	Beam radius for Gaussian beam
χ		Dielectric susceptibility
z	m	Coordinates in the propagation direction
z_R	m	Rayleigh-Length
Ω_p	s^{-1}	Probing field Rabi frequency
Ω_D	s^{-1}	Driving field Rabi frequency
ω_c	s^{-1}	Carrier frequency
ω_m	s^{-1}	Modulation frequency
Ω_{LO}	s^{-1}	Local oscillator circular frequency
Ω	s^{-1}	Modulation frequency
ω_p	s^{-1}	Probe laser circular frequency
ω_D	s^{-1}	Driving laser circular frequency

Physical Constants

Symbol	Value	[Units]	Name
c_0	299792458	[m/s]	Light velocity in vacuum
ϵ_0	$8.854187817 \, 10^{-12}$	[F/m]	Permittivity of free space
μ_0	$1.256637061 4 \, 10^{-6}$	[N/A^2]	Permeability of free space
e	$1.60217733(49) \, 10^{-19}$	[C]	Electron elementary charge
amu	$1.6605402(10) \, 10^{-27}$	[kg]	Atomic mass unit (=Masse ^{12}C-Atom/12)
$\hbar$	$1.05457266(63) \, 10^{-34}$	[J s]	Planck's constant/2π
k_B	$1.380658(12) \, 10^{-23}$	[J/K]	Boltzmann constant

List of Figures

List of Figures

1 Introduction

It is well known that the preparation of atoms by coherent driving fields cause changes in both the absorptive and dispersive properties of atomic samples. In this way it is possible to realize new kind of optical media, which provide many interesting applications.

Many studies have been performed over the last decades about the effect of the introduction of atomic coherence or the utilization of quantum interference to gaseous and solid media, and many of these effects were also verified experimentally. The investigation of lasing without inversion (LWI), which provide the possibility to realize coherent light source at the UV and the X-ray wavelength was initiated by Harris [19] and Scully [42], and theoretical [43], [44], and experimental [36] studies followed.

Furthermore the strong suppression of absorption in correspondence of an enhanced index of refraction [12] have also been theoretically and experimentally investigated [43]. Such media could result useful in application where strong refractive index are required as to realize ultra-sensitive magnetometers [13], [60].

Strongly positive dispersive transparent media can be used to decrease the group velocity [21], [28]. On the other hand strongly negative dispersive media have been recently studied in order to realize light pulse with 'superluminal' group velocity [52], [7], [10], [48].

An anomalous dispersive medium, exhibiting just the right amount of dispersion and with absorption sufficiently suppressed, could be furthermore used to realize high finesse broadband optical cavity [54]. If in fact a well defined negative dispersion at a point of vanishing absorption were achieved (λ compensation), a high internal build-up but nevertheless broad band response cavity ("white light cavity") could be realized. Such kind of cavity might be useful to enhance the performances of laser interferometry gravitational wave detectors [57]. In the contest of white light cavities a double lambda scheme was analyzed by Wicht et al. [57] but the central resonance structure of a two level system (TLA) presents some advantages with respect to the former, needing only one field to establish coherence.

Aim of this work was to study the optical properties of a negative dispersive, with decreased absorption medium. It can be obtained strongly driving a two level system, in order to achieve a so called white light cavity.

The early theoretical study performed by Mollow [33] at the end of the sixties predicted a

three peaked fluorescence spectrum for strongly driven atoms. With the use of the so called dressed states model developed Haroche and Cohen-Tannoudji [8], [18], the description of the three peaked spectrum, resulted intuitively understandable.

Theory predicts in fact that a medium has negative dispersive properties on the transition. But for this frequency the medium results also strongly absorptive and even at very low densities a probing field would be completely absorbed.

On the other hand electromagnetically induced transparency (EIT) [19] could be realized with help of a coherent electromagnetic wave. The medium results transparent: i.e. two laser fields pass a gas without losses, while each of them would be, if alone, completely absorbed. It results then interesting what happens to a medium index of refraction when transparency have been electro magnetically induced.

For the latter it was in fact theoretically demonstrated by Wicht [54] that dispersion on the resonance remains negative and even if decreasing with an increasing driving field, its decreasing resulted weaker than the absorption one . We verified experimentally such behavior.

Subsequently it is possible to imagine that using a suited driving laser field, it can be created a so called λ compensated medium. For such a medium is valid that the dispersion on the transition assumes the inverse value of the transition frequency itself, i.e.

$$n'(\omega_0) = \frac{\partial n}{\partial \omega} \bigg|_{\omega = \omega_0} = -\frac{1}{\omega_0} \ . \tag{1.1}$$

Performing consequently an expansion of the $n(\omega)$ around the transition frequency, and not considering higher order terms, the refraction index in the medium results independent from the frequency of the radiation: all the radiation frequencies which are are near enough to the atomic transition frequency ω_0 would experience, when passing through the medium, the same phase shift.

In order to appreciate the properties of a medium prepared in such a way, we need to remember that the phase shift experienced from an electromagnetic wave plays an important role in the analysis of the resonance condition of an optical resonator. An empty optical resonator of length L results in fact resonant, i.e. the transmitted intensity becomes maximal, when the round trip phase shift results $\phi = \omega \frac{L}{c} = 2\pi N$ with N an integer.

When a medium is present in the resonator both the round trip phase shift and absorption play a role in the expression of the transmitted intensity. For a λ compensated medium, for which the absorption had been electromagnetically suppressed, the optical cavity would at least in principle, result to have a broad band and high finesse.

Aim of the present work was consequently to perform an high sensitive simultaneous measurements of phase shift and absorption profiles for a two level system, driven on the transition, in correspondence of different driving field intensities. A systematic analysis of the results obtained was also performed, and the correspondence between the predicted

theory and the experimental results was verified. The characteristics needed to realize a "white light resonator" were also analyzed even if the actual limits of the system were reached.

In the first chapter of this work it is presented the semi-classical model, analyzed by Wicht [55], which is used to predict the behavior of the optical properties of our two level atom (TLA): the atomic system is considered a quantized two level system, while the electromagnetic fields are considered classical ones. The introduction of such a medium inside an optical resonator is also investigated.

The measuring system which have been developed by Wicht et al. [56], a Mach Zehnder interferometer with a phase modulated arm is described in the second chapter of this work. It allowed a high sensitive (shot noise theoretically limited for the phase shift measurement) simultaneous measurement of absorption and phase shift profiles. The advantages of using such a measuring system are illustrated in [56].

The implemented laser systems are also described. Laser diodes constitute a compact, convenient source of coherent light. Furthermore they are particularly suitable in application where an easy tunability is required: they result consequently particularly useful in the investigation of atomic spectral profiles. Two similar systems consisting in IR diode laser, in a master slave configuration were used. To study the Ca atomic transition $4s^2\,^1S_0 \rightarrow 4s4p\,^1P_1$ @ $423nm$ it was set up, as second harmonic generator, a ring resonator (containing a $KNbO_3$ crystal) in a bow tie configuration .

To increase the driving blue power available the infrared (IR) laser diode was substituted with a more powerful one ($200mW$ instead of $150mW$) and the performances of the new system are analyzed.

The different measurements realized are presented in the third chapter of this work: in order to characterize the performances of the system the profiles in absence of the driving field and for different atomic densities were measured. Measurements of the absorption and phase shift profiles for different driving field powers were also performed.

Different fitting methods were compared and a new routine was developed: it allowed to obtain the parameter characterizing the system (atomic density, transition line width, transition frequency, driving field intensity, etc.) and then to calculate the dispersion and absorption at the transition frequency. An analysis of the latter parameters as a driving field function is also presented. It is followed by a discussion about the results achieved.

1   Introduction

4

2 Theory of operation

2.1   Introduction

Aim of this work was the creation of a particular medium, which could be suited for application inside an optical resonator: it could in fact allow the realization of a cavity featuring simultaneously high internal build up and large bandwidth.

Such a medium, which should present a right amount of negative (anomalous) dispersion and simultaneously be transparent, could be realized using a strong driving field which is resonant with a two levels system.

It is in fact well known that it is possible to manipulate the optical properties of media, using coherent electromagnetic field. In this chapter it will be briefly described the theory of a strongly driven two level system, probed by a weak field using the dressed state approximation which had been developed by Haroche and Cohen Tanoudji [18], [8].

A semiclassical model is used: the atomic system is a quantized two level system (depicted in 2.1), while the electromagnetic fields are considered classical ones. The spectra resulted then intuitively understandable.

For our aim was also important to observe the evolution of both phase shift and absorption, calculated on the resonance, with increasing intensity of the driving field, in order to obtain the desired quantity of negative dispersion (in particular we wanted to achieve the λ compensation condition i.e. $\frac{\partial n}{\partial \omega}\Big|_{\omega_0} = -\frac{1}{\omega_0}$) for an electromagnetically induced transparent medium.

The Ca transition $4s^2\,{}^1S_0 \rightarrow 4s4p\,{}^1P_1$ @ 423nm is studied, and the spectra corresponding to different driving powers were analyzed.

The theory of an optical cavity is also briefly described. In particular it is analyzed, which would be the cavity properties (bandwidth and internal build-up) evolution, when filled with an anomalous dispersive transparent medium. When the λ compensation condition is in fact fulfilled, all the radiation frequencies which result near enough to the cavity resonance frequency ω_0, experience, when passing through the medium, the same phase-shift. If the absorption of the medium is furthermore suppressed, it is, at least in principle, possible to obtain a broad band high finesse optical cavity ("white light cavity" [57]). The

fulfillment of the requirements to create such a cavity using our particular medium have been also analyzed in this chapter.

2.2 Strongly driven two level system

The optical properties of a medium are related to the complex parameter $\chi = \chi' + i\chi''$ representing its susceptibility [55]. It describes a complex index of refraction $n_c = n + in_i$ through the relation:

$$(n + in_i)^2 = 1 + \chi = 1 + \chi' + i\chi''. \tag{2.1}$$

Let us consider an electromagnetic wave passing through a medium of length l, from the geometrical optic we have that

$$e^{-ik_0(n+in_i)l} = e^{-ik_0nl}e^{k_0n_il} = e^{ik_0nl}e^{-\alpha l}, \tag{2.2}$$

i.e. n represents the index of refraction and α the absorption coefficient of the medium. For α it is then valid:

$$\alpha = -k_0n_i = -\frac{\omega_0}{c_0}n_i. \tag{2.3}$$

The relation between the index of refraction, the absorption coefficient and the complex susceptibility results then:

$$n = 1 + \frac{1}{2}\chi' \qquad\qquad n_i = \frac{1}{2}\chi'', \tag{2.4}$$

under the hypothesis that we are in the presence of a low density medium, i.e. $|n_c - 1| \ll 1$. On the other hand the susceptibility gives the response of a medium to an electrical field applied to the system, and is related to the density matrix [63] through [50]:

$$\chi = \frac{2Np^2}{\epsilon_0\hbar\Omega_P}\rho_{ab|\Delta}. \tag{2.5}$$

The preceding relation is calculated for a two level system (TLA) with lower level $|a\rangle$ and upper level $|b\rangle$ (represented in Fig 2.1). The polarization of the medium is represented by two classical fields with angular frequency respectively ω_P (probe) and ω_D (drive) and amplitude described by:

$$\Omega_i = p\mathcal{E}_i/\hbar, \tag{2.6}$$

where p denotes the expectation value of the dipole operator and $i = P, D$. Furthermore in the relation (2.5), N represents the number of the two level systems considered (in our case then the particle density) with transition frequency ω_0, $\Delta = \omega_P - \omega_D$ the frequency difference of the two electrical fields and ρ_{ab} are the off diagonal terms of the density
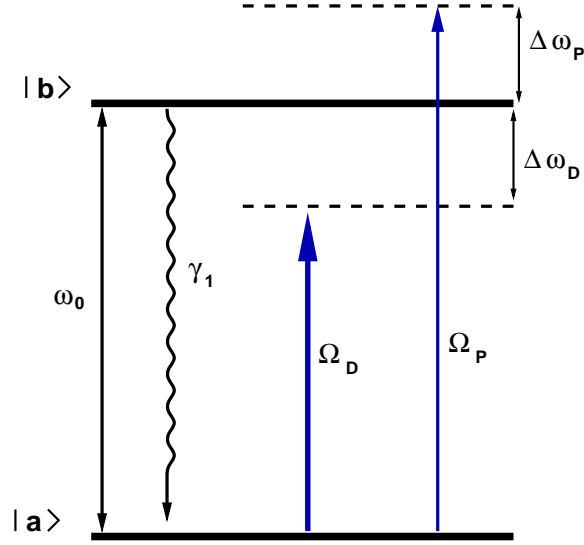
Figure 2.1: Term scheme for a two-level system (**TLA**) experiencing two electromagnetic fields: probe (P) and drive (D). They couple the levels $|a\rangle$ (lower) and $|b\rangle$ (higher). The fields intensities are defined through their Rabi frequencies Ω_P and Ω_D and their frequencies through $\Delta\omega_P = \omega_P - \omega_0$ and $\Delta\omega_D = \omega_D - \omega_0$, where ω_0 represents the transition frequency. The relaxation due to spontaneous emission from $|b\rangle$ to $|a\rangle$ is γ_1

matrix ρ in the bare atoms basis. Our aim is subsequently to calculate such density matrix. In the case of a strongly resonant driving field i.e. $\omega_D = \omega_0$ and consequently $\Delta_D = \omega_0 - \omega_D = 0$ the Hamiltonian of the system can be written in the form [55]:

$$
\begin{aligned}
\mathcal{H} =&-\frac{\hbar\omega_0}{2}(|b\rangle\langle b| - |a\rangle\langle a|) \\
&-\frac{1}{2}p\mathcal{E}_P[|b\rangle\langle a|e^{\omega_P t} + |a\rangle\langle b|e^{-\omega_P t}] \\
&-\frac{1}{2}p\mathcal{E}_D[|b\rangle\langle a|e^{\omega_D t} + |a\rangle\langle b|e^{-\omega_D t}].
\end{aligned}
\tag{2.7}
$$

Furthermore, it is possible to consider the so-called dressed states [8] $|+\rangle$, $|-\rangle$ as a useful basis for this problem, where the dressed states are the eigenstates of the two level system plus the driving field (excluding the contribution of the probing field). The relation between the $|+\rangle$, $|-\rangle$ and $|a\rangle$, $|b\rangle$ are:

$$
|-\rangle = \frac{1}{\sqrt{2}}(|a\rangle - |b\rangle),
\tag{2.8}
$$

$$
|+\rangle = \frac{1}{\sqrt{2}}(|a\rangle + |b\rangle).
\tag{2.9}
$$

And the complete Hamiltonian can be represented in this base [49], where we have furthermore to take account of the decaying rate γ_1 of the upper state population and the

Figure 2.2: Phase shift and absorption profiles calculated for a two level system in presence of two electromagnetic fields, one of which is very weak ($\Omega_P = 10^{-6} \times \gamma_1$ where γ_1 represents the natural line width of the transition). The transition considered is the $4s^2\,^1S_0 \rightarrow 4s4p\,^1P_1$ of Ca at $423nm$ with $\gamma_1 = 2\pi \times 34MHz$. The particle density is supposed to be $N_{at} = 5 \times 10^{16}m^{-3}$, and the interaction length $l_{int} = 1mm$. Two situations are represented: in the first one $\Omega_D = 0$ (no driving field) is present, and in the second one $\Omega_D = 0.11 \times \gamma_1$. It is possible to observe the decreasing of both phase shift and absorption. No Rabi side band structure is to be recognized

coherence is assumed to decay purely radiatively, i.e. $\gamma_{coh} = \gamma_2 = \gamma_1/2$ [49].
The time evolution equation, describing the time evolution of the density matrix is given by [63]:

$$i\hbar\frac{\partial\rho}{\partial t} = [\mathcal{H}, \rho].\tag{2.10}$$

The transformations which relate the density matrix ρ_{ab} in the $|a\rangle$, $|b\rangle$ basis and in the $|+\rangle$, $|-\rangle$ is

$$\rho_{ab} = \frac{1}{2}(\rho_{++} - \rho_{--}) - i\Im(\rho_{+-}).\tag{2.11}$$

It is then possible to solve the motion equation (2.10) of the term using a Floquet expansion [49]:

$$\begin{aligned}
\rho_{++} - \rho_{--} &= \sum_n p_n e^{in\Delta}, \\
\Re(\rho_{+-}) &= \sum_n q_n e^{in\Delta}, \\
\Im(\rho_{+-}) &= \sum_n r_n e^{in\Delta},
\end{aligned}\tag{2.12}$$

supposing that $\Phi = \Phi_D - \Phi_P$ where the latter represent an arbitrary phase. Considering the steady state solutions ($\dot{p}_n = \dot{q}_n = \dot{r}_n = 0$) this leads to a linear system of infinite

coupled equations. Solving the system with iteration method, and considering recurrence relations [49] this leads, for the density matrix:

$$\rho_{ba}^{\omega_p} = \frac{\Omega_P + \Omega_D Z_1^\star}{\Delta\omega_P - i\gamma_2} \frac{i\gamma_1}{P_0 + 2i\Im(R_0\Omega_D\Omega_P Z_1)}, \tag{2.13}$$

and Z_1 is recursive solved through the relation:

$$Z_n = \frac{Q_n\omega_D\Omega_p}{P_n - R_n(\Omega_P\Omega_D)Z_{n+1}}, \tag{2.14}$$

and

$$
\begin{aligned}
P_n =\ & -n(\omega_P - \omega_D) + i\gamma_1 \\
& -4[n(\omega_P - \omega_D) - i\gamma_2]\left\{ \frac{\Omega_D^2}{\Delta\omega_D^2 - [n(\omega_P - \omega_D) - i\gamma_2]^2} + \right. \\
& \left. + \frac{\Omega_P^2}{\Delta\omega_P^2 - [n(\omega_P - \omega_D) - i\gamma_2]^2} \right\},
\end{aligned}
\tag{2.15}
$$

$$Q_n = \frac{(2n-1)(\omega_P - \omega_D) - i2\gamma_2}{[\Delta\omega_D - n(\omega_P - \omega_D) + i\gamma_2][\Delta\omega_P - n(\omega_P - \omega_D) - i\gamma_2]}, \tag{2.16}$$

$$R_n = \frac{(2n+1)(\omega_P - \omega_D) - i2\gamma_2}{[\Delta\omega_D - n(\omega_P - \omega_D) - i\gamma_2][\Delta\omega_P - n(\omega_P - \omega_D) + i\gamma_2]}. \tag{2.17}$$

In the limit of a weak probe field ($\Omega_P \ll \gamma_1$) it is necessary, in the calculation of the density matrix, to take only account of first order terms in Ω_P and consequently the density matrix results in the form [55]:

$$\rho_{ab}^{\omega_P} = \Omega_P \frac{1 + \Omega_D^2 Q_1^\star/P_1^\star}{\Delta\omega_P - i\gamma_2} \frac{i\gamma_1}{P_0}, \tag{2.18}$$

where:

$$P_0 = i\gamma_1 + 4(i\gamma_2)\left\{ \frac{\Omega_D^2}{\Delta\omega_D^2 - (-i\gamma_2)^2} + \frac{\Omega_P^2}{\Delta\omega_P^2 - (-i\gamma_2)^2} \right\}, \tag{2.19}$$

$$
\begin{aligned}
P_1 =\ & -(\omega_P - \omega_D) + i\gamma_1 - 4(\omega_P - \omega_D) \times \\
& \times \left\{ \frac{\Omega_D^2}{\Delta\omega_D^2 - (\omega_P - \omega_D - i\gamma_2)^2} + \frac{\Omega_P^2}{\Delta\omega_P^2 - ((\omega_P - \omega_D) - i\gamma_2)^2} \right\},
\end{aligned}
\tag{2.20}
$$

$$Q_1 = \frac{\omega_P - \omega_D - i2\gamma_2}{(\Delta\omega_D - (\omega_P - \omega_D) + i\gamma_2)(\Delta\omega_P - (\omega_P - \omega_D) - i\gamma_2)}. \tag{2.21}$$

Using the equation (2.18) it is possible, with the help of relation (2.5) to calculate the susceptibility of the system and consequently, considering the relation (2.4) to calculate the absorption coefficient and the index of refraction. The latter represent the functions to
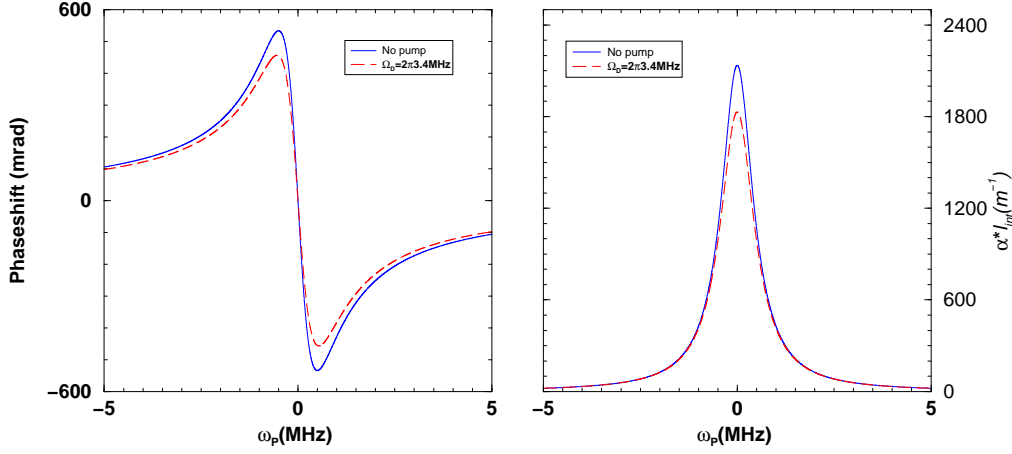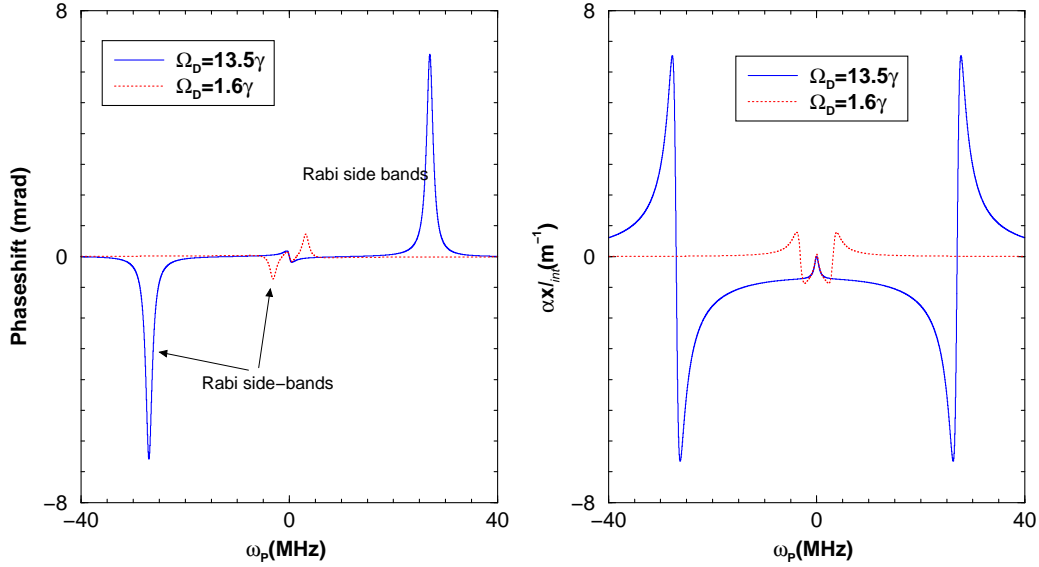
Figure 2.3: Phase shift and absorption profiles calculated for a two level system in presence of two electromagnetic fields, one of which is very weak ($\Omega_P = 10^{-6} \times \gamma_1$, where γ_1 represents the natural line width of the transition). The transition considered is the $4s^2\,^1S_0 \rightarrow 4s4p\,^1P_1$ of Ca at $423nm$ with and $\gamma_1 = 2\pi \times 34MHz$. The interaction length $l_{int} = 1mm$. Two situations are represented: in the first one $\Omega_D = 13.5 \times \gamma_1$ and the particle density is $N_{at} = 5 \times 10^{16}m^{-3}$, in the second one $\Omega_D = 1.6 \times \gamma_1$ and $N_{at} = 0.077 \times 10^{16}m^{-3}$. In both cases it is possible to recognize the Rabi side bands structure, and their evolution when increasing driving field power.

which we will fit the measured profiles.

Let us now discuss the form of the profiles which are depicted in the Fig 2.2 and Fig 2.3. In the first one it is possible to observe the evolution of the profiles when passing from no driving field to a weak driving field. In the second one (Fig 2.3) two different situations are represented, corresponding to two different intensities of the driving field. In both cases the particle density is so chosen, to obtain the same value for the dispersion on the transition (so that the λ compensation requirement is fulfilled). It is possible to observe that near the resonance the dispersion results negative. For the stronger driving field the absorption results strongly suppressed: a residual absorption is present in the medium ($\approx 1 \times 10^{-3}m^{-1}$) but it is not well resolved in the figure. Furthermore the structure of the spectrum results such that at first order and around ω_0, the absorption results independent from ω_P.

Once obtained the forms for the phase shift and the absorption for a strongly driven two level system, it is possible to proceed further. We study the evolution of the dispersion (derivative of the index of refraction with respect to the frequency) and the absorption on the transition (ω_0) when the medium is strongly driven by a field of frequency ω_0. If we
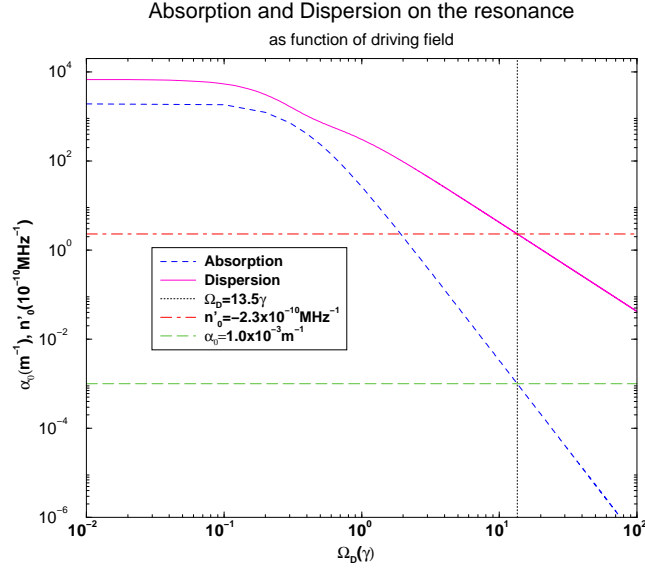
Figure 2.4: Dispersion and absorption on the resonance as function of the driving field. Calculated for a particle density $N_{at} = 5 \times 10^{16}m^{-3}$. Driving field is expressed in $\gamma_1 = 2\pi 34 MHz$ natural line width units. For $\Omega_D = 13.5\gamma_1$ the λ-compensation condition is achieved: $n_0' = -1/\omega_0 = 2.3 \times 10^{-10}MHz^{-1}$ the residual absorption results $\alpha_0 = 1.0 \times 10^{-3}m^{-1}$

calculate both the the dispersion on the resonance and the absorption we obtain [55]:

$$\alpha_{P,0} = 2\frac{\omega_0}{c_0}N_{at}\frac{3\pi c_0^3}{2\omega_0^3}\frac{1}{[1+8(\Omega_D/\gamma_1)^2]^2}, \tag{2.22}$$

$$n_{P,0}' = -\frac{2}{\gamma_1}N_{at}\frac{3\pi c_0^3}{2\omega_0^3}\frac{1+32(\Omega_D/\gamma_1)^4}{[1+8(\Omega_D/\gamma_1)^2]^3}, \tag{2.23}$$

Looking at the representation of the latter two functions in Fig 2.4 we observe that both absorption and dispersion decrease with increasing driving field, but there is a regime where the absorption decreasing is stronger than the dispersion one.

2.3 The medium in a cavity

Let us consider now, what would happen if we filled an optical resonator with a medium. We have in fact to observe that the presence of a medium in an optical resonator changes its properties.

First we need to define the transfer function of the resonator, as the ratio of the transmitted I^t to injected I^{in} intensity. This relation is described by the well-known Airy function [55]:

$$\frac{I^t}{I^{in}} = \frac{\mathcal{T}^2}{(1-\mathcal{R})^2}\frac{1}{1+4\frac{\mathcal{R}}{(1-\mathcal{R})^2}\sin^2\frac{\Delta}{2}}, \tag{2.24}$$

where $\mathcal{R}^2 = R_1 R_2(t_m^2)$, $\mathcal{T}^2 = T_1 T_2 t_m^2$ and R_1, R_2, T_1, T_2 represent the reflection and transmission coefficients of the input 1 and output 2 mirrors. t_m is the amplitude transmission coefficient due to the presence of the medium of index of refraction $n(\omega)$ inside the cavity of length L_r. $\frac{\Delta}{2} = \Phi_m = \frac{\omega}{c_0} n(\omega) L_r$ is the phase shift experienced by the field in a round trip under the hypothesis that the mirrors do not cause a further phase shift.

Let us now consider the expression (2.24). The maximum of the transmitted intensity is obtained maximizing the function (2.24) and in the particular case of an empty resonator (for which $t_m = 1$ and $n(\omega) = 1$), this would correspond to $\Delta = 2\pi N$ with N an integer. We also have to underline that the first term in the product, which depends also on the absorption coefficient of the medium present in the resonator, gives the amplitude of the transmitted field in the resonance condition. The form of the transmission profile is contained in the second term of the product.

From the transmission profile form it is possible to define a further characteristic describing the properties of an optical resonator: its bandwidth (or better the full width at half maximum $\Delta\omega_{FWHM}$). It is defined as twice the frequency interval between the frequency corresponding to the maximum, and the frequency where the intensity is decreased by a factor $1/2$.

A third quantity describing the properties of a resonator is its finesse $\mathcal{F}$ [9] defined as the ratio between the free spectral range (frequency distance between two consecutive transmission peaks) and the half bandwidth. For an impedance matched resonator (where the relation $R_1 = R_2 t_0^2$ is verified, with $t_0 = t_m(\omega_0)$) the finesse takes the form:

$$\mathcal{F} := \frac{\pi}{2} \sqrt{\frac{4 R_2 t_0^2}{(1 - R_2 t_0^4)^2}}. \tag{2.25}$$

Let us consider a resonator filled with a medium which has a transition at the frequency $\omega = \omega_0$. We can subsequently think of expanding both the optical properties (index of refraction and absorption) of the medium with respect to the frequency, around ω_0. We have, if $n(\omega_0) = 1$:

$$n(\omega) \approx 1 + n'(\omega_0)(\omega - \omega_0) + n''(\omega_0)(\omega - \omega_0)^2 + n'''(\omega_0)(\omega - \omega_0)^3 + ..., \tag{2.26}$$

$$\alpha(\omega) \approx \alpha(\omega_0) + \alpha'(\omega_0)(\omega - \omega_0) + \alpha''(\omega_0)(\omega - \omega_0)^2 + + \alpha'''(\omega_0)(\omega - \omega_0)^3 + ... \tag{2.27}$$

If the resonator resonance frequency is ω_0 (i.e. it is valid that $\frac{\omega_0 L_r}{c_0} = N\pi$) the phase shift in a round trip becomes, using the index of refraction expansion (2.26):

$$\Phi_m(\omega) = \Phi_m(\omega_0 + \Delta\omega) = \frac{\omega}{c_0} n(\omega) L_r = \frac{L_r}{c_0}\omega_0 + \frac{\Delta\omega L_r}{c_0}[1 + \omega_0 n_0'] + \mathcal{O}(\Delta\omega^2), \tag{2.28}$$

where $\mathcal{O}(\Delta\omega)$ are higher order terms in $\Delta\omega = \omega - \omega_0$.

With the latter expression and considering the finesse definition, the bandwidth of the resonator becomes:

$$\Delta\omega_{FWHM} = \Delta\omega_{FSR}\frac{1}{\mathcal{F}}[(1 + \omega_0 n_0') + n_0'\Delta\omega_{FWHM} + \mathcal{O}(\Delta\omega_{FWHM}^2)]^{-1}, \tag{2.29}$$

where $\Delta\omega_{FSR} = \frac{\pi c_0}{L_r}$ is the free spectral range of the resonator [9].

If it was possible to prepare the medium in a way such that:

$$n_0' = -\frac{1}{\omega_0}. \tag{2.30}$$

It is then valid that. at first order, for frequencies of the injected field such that the higher order terms $\Delta\omega = \omega - \omega_0$ in eq.(2.28) are negligible:

- $\Phi_m(\omega) = N\pi,$

i.e. the phase shift experienced by the field in one round trip is no longer be dependent on the frequency of the field. Furthermore, considering the round trip phase shift it is valid:

$$\Delta \propto \omega n(\omega)\frac{L_r}{c_0} = \frac{2\pi c}{\lambda_0}n(\omega)\frac{L_r}{c_0} = 2\pi\left(\frac{n(\omega)}{\lambda_0}\right)L_r = \frac{2\pi}{\lambda_m}L_r, \tag{2.31}$$

where $\lambda_m = \frac{\lambda_0}{n(\omega)}$ is the wavelength of the field in the medium (while λ_0 is the vacuum wavelength).

If the condition (2.30) is verified then the wavelength of the field in the medium results independent from its frequency: we can talk of λ **compensation** i.e. the dispersion of the medium compensates the frequency dependence of the vacuum wavelength.

It is important once more to underline that the expression is valid only for frequencies of the field near enough to the resonance frequency (which corresponds also to the medium transition frequency), such that, in the expansion of index of refraction, higher order terms can be neglected.

Let us now consider the modifications of the resonator characteristics expressed by (2.24), (2.25), (2.29) in presence of a λ compensated medium. We can recall that a medium exhibits an anomalous dispersion (i.e. a negative derivative of the index of refraction with respect to frequency) around a transition. At the same frequency the medium results, on the other hand, strongly absorptive but the absorption can be diminished (and almost suppressed) with aid of a strongly, resonant driving field.

To obtain λ compensation for Ca at the transition @ 423nm the dispersion should reach the value $n_0' = -2.2 \times 10^{-10} MHz^{-1}$.

It would be then verified (see 2.29), that compared to the FWHM of an empty resonator:

$$\Delta\omega_{FWMH}^{neg} = \sqrt{\frac{\omega_0\mathcal{F}}{\Delta\omega_{FSR}}}\Delta\omega_{FWHM}^{empty} = \sqrt{\frac{\mathcal{F}L_r}{\lambda_0}}\Delta\omega_{FWHM}^{empty}, \tag{2.32}$$

the bandwidth would result increased.

Let us consider for example a cavity with a finesse of $\approx 10^4$, and a length of $1cm$, for which λ compensation had been achieved. Its $\Delta\omega_{FWMH}$ would be increased of a factor $\approx 5 \times 10^4$ with respect to to an empty one, if the residual absorption had been completely suppressed.

The latter affirmation can not be considered completely true: the real bandwidth of the resonator is in fact limited from the frequency interval for which the higher order terms in the expansion of refraction index (2.26) are negligible.

In order to realize a λ compensated transparent medium, we have once more to observe
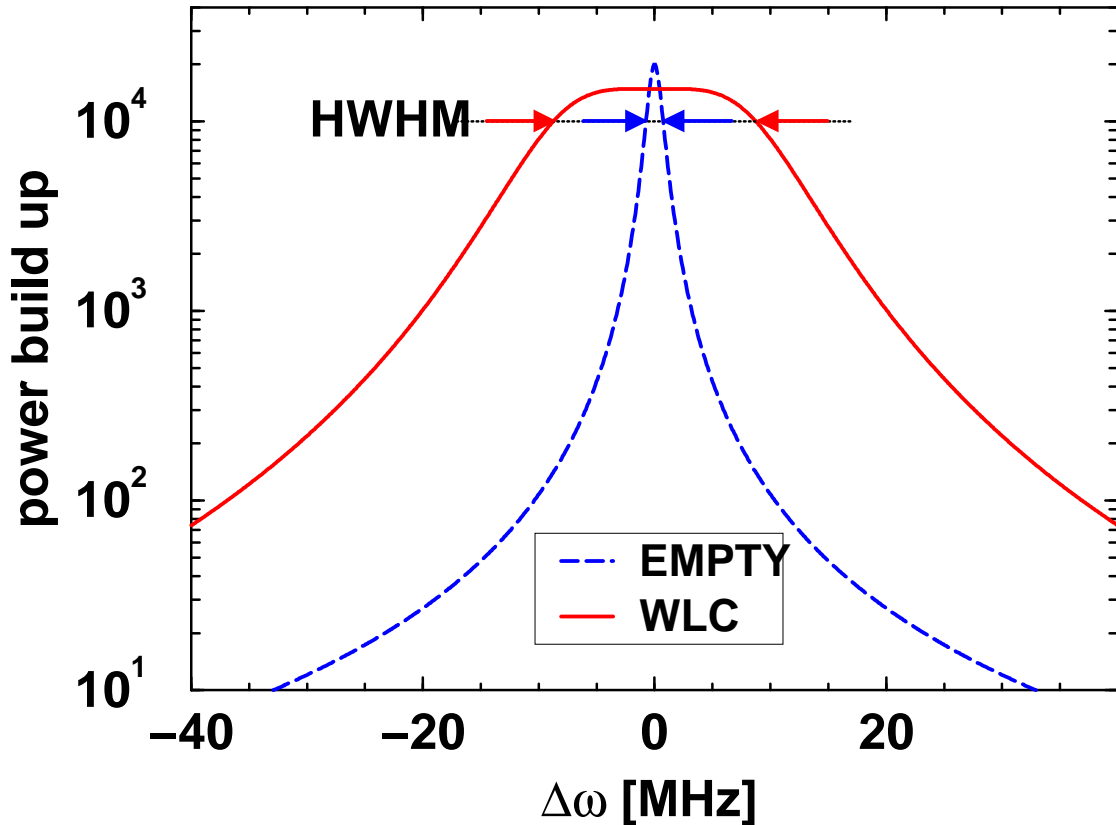
Figure 2.5: Power build up for empty and "white light" resonator: empty resonator, and resonator containing $N_{at} = 5 \times 10^{16} m^{-3}$ Ca atoms, strongly driven on the transition at $423nm$ with help of a perfectly resonant driving field with intensity $\Omega_D = 13.5 \times 2\pi 34 MHz$. The resonator is $1cm$ long, and the mirrors reflection coefficients are $R_1 = 0.99993$ and $R_2 = 0.99995$

the relations (2.23) and (2.22) which are also depicted in Fig 2.4. Once fixed the transition frequency and its line width γ, the dispersion and absorption are dependent on the strength of the driving field and the particle density involved.

Corresponding to a certain particle density, the strength of the driving field to obtain the value of the dispersion needed to fulfill the λ compensation is fixed.

But in this way also the residual absorption is defined.

As first example, we can observe that to obtain λ compensation with a particle density

of $N_{at} = 5 \times 10^{16} m^{-3}$ a driving field of $13.5 \times \gamma$ (with $\gamma = 2\pi 34 MHz$) would be needed. On the other hand (from 2.22) the corresponding residual absorption would be $\alpha_0 = 0.1\% m^{-1}$ and if we filled with such a medium a resonator of length $1cm$ and finesse 64×10^3 (empty), its finesse would become $\approx 33 \times 10^3$ decreasing of a factor ≈ 2. The bandwidth of the cavity would be increased by a factor ≈ 12 (see Fig2.5).

In the absence of driving field (i.e. $\Omega_D = 0$), to obtain λ compensation for Ca atoms, it would be needed a particle density of $N_{at} = \gamma \frac{4\pi}{3c_0\lambda_0^2} = 5 \times 10^{13} m^{-3}$. The residual absorption is in this case $\alpha_0 \approx 71\% m^{-1}$. This is about a factor 700 more than the one calculated in presence of the driving field and, recalling the expression (2.25), the finesse of the resonator would result dramatically decreased.

Figure of merit
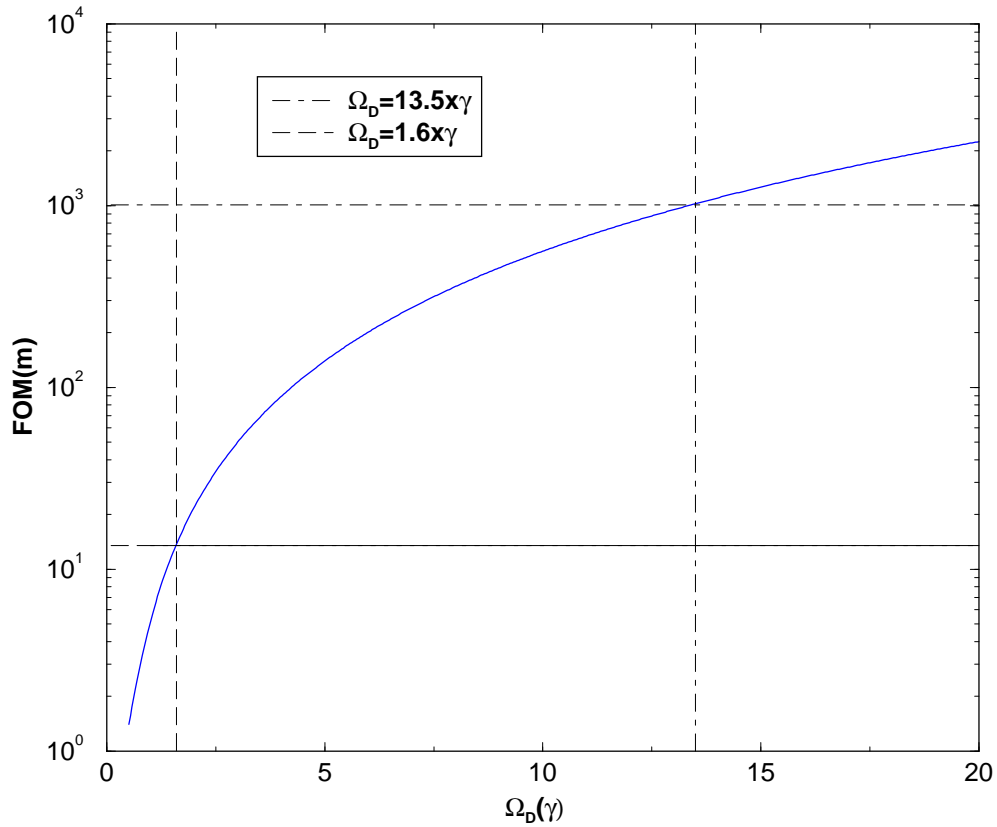
Figure 2.6: Figure of merit, ratio of dispersion to absorption, both calculated in at the transition function, normalized to $1/\omega_0$, as function of the driving field.

To take account of the modification of the characteristics of the resonator we need then to consider not only of the dispersion, but also the residual absorption. Furthermore we have to observe that, from relation (2.24), the presence of the medium decrease in any case the

power build up of the resonator.

To take account of both quantities it can be defined a further parameter, the figure of merit (Fig 2.6), as the ratio of dispersion on the resonance to residual absorption, normalized to the inverse of transition frequency.

$$FOM = \frac{\partial_\omega n_0}{-\frac{1}{\omega_0}\alpha(\omega_0)} = \frac{c_0}{\gamma}\frac{1 + 32[\Omega_D/\gamma]^4}{1 + 8[\Omega_D/\gamma]^2},$$

(2.33)

where the latter expression was calculated taking account of (2.23) and (2.22).

In absence of driving field the figure of merit results $\approx 1.4m$. For the strongly driven ($\Omega_D = 13.5\gamma$) λ compensated medium, the calculated factor of merit results $FOM \approx 1000m$.

Furthermore we can discuss the different power build ups of resonators represented in the Fig 2.5. The first curve represents the empty resonator, the second one a λ compensated medium obtained with a driving field of intensity $\approx 13.5 \times 2\pi 34MHz$. The height of the transmission peak is decreased of a factor ≈ 2 while the bandwidth is increased of a factor ≈ 12. The resonator parameter used for the calculations are: $l = 1cm$, $R_2 = 0.99995$. For the input mirror the impedance matching condition was used, then $\mathcal{T} = (1 - R_2)t_0$ and $\mathcal{R} = R_2 t_0^4$. The absorption experienced from the field passing through the medium is $t_m^2 = e^{-\alpha L_r}$.

3 Experimental setup

3.1   The experiment

Aim of this experiment was to measure phase shift and absorption profiles of a calcium atomic beam, when its optical properties are changed by applying a strong coherent light field [49]. A measuring method had been developed, utilizing a Mach Zehnder Interferometer with an electro-optical phase modulator within the reference arm [56]. It was used a combination of frequency modulation spectroscopy (FMS) [2], [53] and interferometry [56]. The first one provides the possibility to measure simultaneously phase shift and absorption. It allows furthermore to reach, at least theoretically and for the phase shift measurement (which is detected with FMS method) a shot noise limited sensitivity. Using high modulation frequencies, technical electronic and power noise could, in fact, be suppressed below the shot noise level of the optical field.

In the present configuration the absorption is not detected at modulation frequency and consequently the sensitivity is then limited by the power noise of the laser. As it will be shown later, the absorption could also be detected at twice the modulation frequency, which should improve the signal to noise ratio.

The interferometric method instead provides the possibility to avoid cross talking between the two signals (which would be a critical effect near the resonance, where absorption reaches the maximum while phase shift approaches zero).

In the configuration realized as input beam splitter was chosen a strongly unbalanced one. Consequently most of the probing laser power is injected in the reference arm. In this way the sample properties are not affected by the measurement.

Furthermore using the interferometer as a null instrument, renders its calibration, for the phase shift detection, a constant depending only on the half-wave voltage of the EOM and independent from the laser power. The calibration for the absorption was more complicated and will be explained in more details in the section describing how the signal is evaluated.

Figure 3.1: Measuring principle: laser systems (**probe** and **pump**) are represented. Both are in a **master-slave** configuration. Unwanted optical feedback are avoided with aid of optical diodes (**FI**). Both fields are frequency doubled, using a highly efficient ring resonator (**SHG**). Mode matching is optimized with a telescope **T**. The cavity is locked on the laser frequency using an (**HCD**) Haensch-Couillaud detector. Part of the blue radiation coming from the driving system is taken using a $\lambda/2$ plate and a polarizing beam splitter (**PBS**). A Frequency Modulation Spectroscopy (**FMS**) method is used to lock the laser frequency on the calcium transition. It consists of an electro-optical modulator (**EOM**) driven at (**LO**=$30MHz$), an **heat pipe** containing Ca vapors, a fast photodiode **PD**, an amplifier **G1**, a mixer and a further servo-loop (**G2**).

By means of a **PLL** (phase locked loop) the probing field is locked to the driving one with a variable offset provided by an **RF** generator. Driving field is $180MHz$ red shifted with an acousto-optical modulator (**AOM**): the beams are coupled in single mode optical fibers (**SMF**) and multi mode optical fiber (**MMF**). Laser frequencies are monitored with a **wave-meter** and the single mode operation is monitored with aid of a Fabry-Perot Interferometer (**FPI**). Both driving and probing fields enter the interferometer (**Mach Zehnder Interferometer**) via BS_{in} an input beam splitter. The interferometer, with a phase modulated reference arm (with an electro optical modulator **EOM** driven at $1.8MHz$) operates in a high vacuum environment and is seismic decoupled from the optical bench. Both lasers meet the atomic beam, produced with a calcium oven and mechanically chopped at $1.7kHz$, in the test arm. The arm length is changed using a piezoelectric **PZT** transducer acting on the mirror **M2**, and which is used to sweep the interferometer. It constitutes also the actuator which locks the interferometer for the low frequencies. The signal emerging from the interferometer is detected by two photodiodes (**PD1**, **PD2**) and subtracted. The DC component demodulated at $1.7kHz$ with aid of a dual lock in amplifier (**LI**) provides the absorption signal (α). The AC component demodulated at $1.8MHz$ and at $1.7kHz$ represent phase shift signal (φ).

In order to operate the interferometer, a light source had to be used: an ad hoc laser system had been also developed. Lasers, with their high spectral purity, are ideal sources for spectroscopic applications. In our case infrared laser diodes were chosen. It was then possible to obtain a compact and convenient light source. A Littrow setup with an optical grating was used [26] to reduce the line width of the lasers and to have the possibility to tune them [62], [58].

In this way it was possible to measure phase shift and absorption for the different laser frequencies [39], providing the complete profile of both optical properties.

Our aim was to study the $4s^2\,^1S_0 \rightarrow 4s4p\,^1P_1$ transition in Ca, which corresponds to a wavelength of $423nm$. In order for the laser to reach such a wavelength a frequency doubling ring resonator had to be implemented [5]. Two similar laser systems have been developed: the first (probing system) is used to scan the frequency on the resonance, while the second one, the driving system, was used to modify the sample properties. For the latter much more blue light power (at least $15mW$) was needed, while both lasers needed to be stabilized exactly on the resonance.

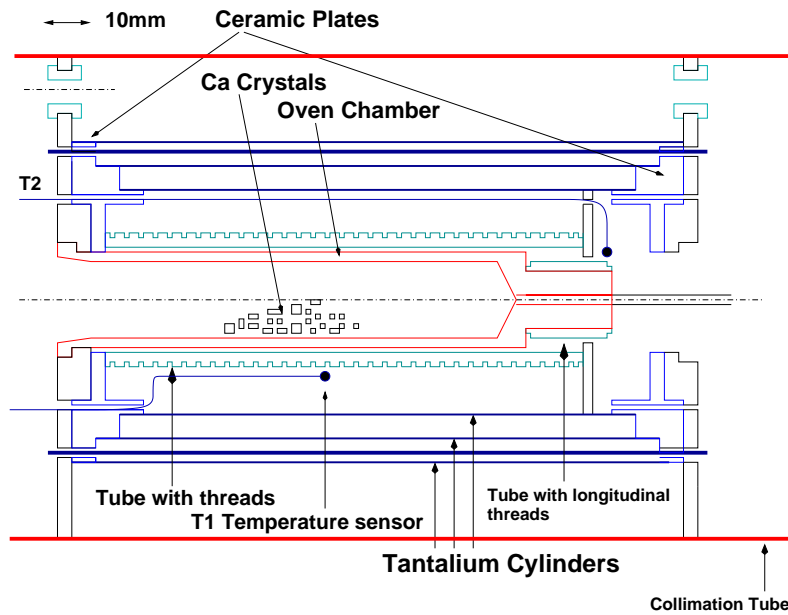A new Ca oven (depicted in Fig3.2) to produce the atomic beam, was designed and

Figure 3.2: Ca crystals are present in the oven chamber which is then warmed up using a ceramic tube with thread and tantalum coils. The oven is placed inside a collimation tube. Thermal dispersion is mostly avoided using ceramic connections. Tantalum cylinders are used to shield thermally the vacuum chamber from the oven. Two different and independent heating system are used for the whole chamber and the front part. Temperature is monitored with two different (**T1** and **T2**) sensors.

realised. It is positioned in an high vacuum ($p \approx 10^{-8}mbar$) chamber which is perpendicular to the chamber containing the interferometer (Fig.3.1). A collimator tube is used

to reduce the divergence angle of the atomic beam. The whole system has a cylindrical symmetry.

The distance between the oven and the interferometer can be changed ($\approx 30cm$) to obtain different collimation factor and particle densities. A typical value chosen for the collimation factor was $\approx 1 : 200$. It was possible to align the atomic beam with respect to the probing and pumping fields using vertical and horizontal micrometer screws. In this way the atoms meet the probing and pumping field under a right angle, avoiding in this way, shift of the transition frequency due to Doppler effect.

The oven (Fig 3.2) consists of a cylindrical metallic chamber surrounded by a ceramic tube with threads containing a tantalum wire ($\phi = 0.3mm$). The configuration used, does not avoid the creation of a magnetic field, but its intensity in the interaction zone, is less than the Earth's magnetic field one, which is anyway not shielded. The tube is enveloped with ceramic paper, to provide electrical insulation.

The temperature of the oven is monitored with a temperature sensor (thermocouple) fixed on the ceramic tube (actually outside the oven chamber). Temperatures of $\approx 1000°C$ were reached during the measurements. They corresponded to a particle densities of $\approx 6.7 \times 10^{15} m^{-3}$.

Thermal insulation between the oven and the vacuum chamber is obtained using a series of concentric tantalum cylinders, fixed to particularly shaped ceramic plates, which is itself fixed to the collimation tube.

The atomic beam is mechanically chopped at a frequency of $f_c = 1.7kHz$ (maximal chopping frequency of the motor is $4kHz$). This method avoids once more problems due to acoustic and seismic noise (since they have lower critical frequencies): f_c is inside a frequency interval where the noise spectrum of the interferometer is almost white.

3.2 The interferometer

3.2.1 Optical setup and theory of operation

Let us now consider the Mach Zehnder interferometer in Fig 3.3: an electromagnetic field entering it is given by the expression: $\vec{\mathcal{E}}_{in}(t) = \vec{\mathcal{E}}_0(t)exp(j\omega t)$ (where $j = \sqrt{-1}$).

We suppose that both the input and the output beam splitters are ideal; the equation $r_i^2 + t_i^2 = 1$, where r_i and t_i represent the reflectivity and transmission coefficient of the beam splitters, is then valid. It is also assumed that the mirrors M2 and M3 have reflectivity equal to one.

If we consider an empty Mach Zehnder interferometer, on the output photodiode 2 , the field when passing the test arm would be described by [55]:

$$\vec{\mathcal{E}}_{test} = \vec{\mathcal{E}}_0(t)r_1t_3e^{i(\varphi_1+\varphi_a+\psi_1)}, \qquad\qquad (3.1)$$
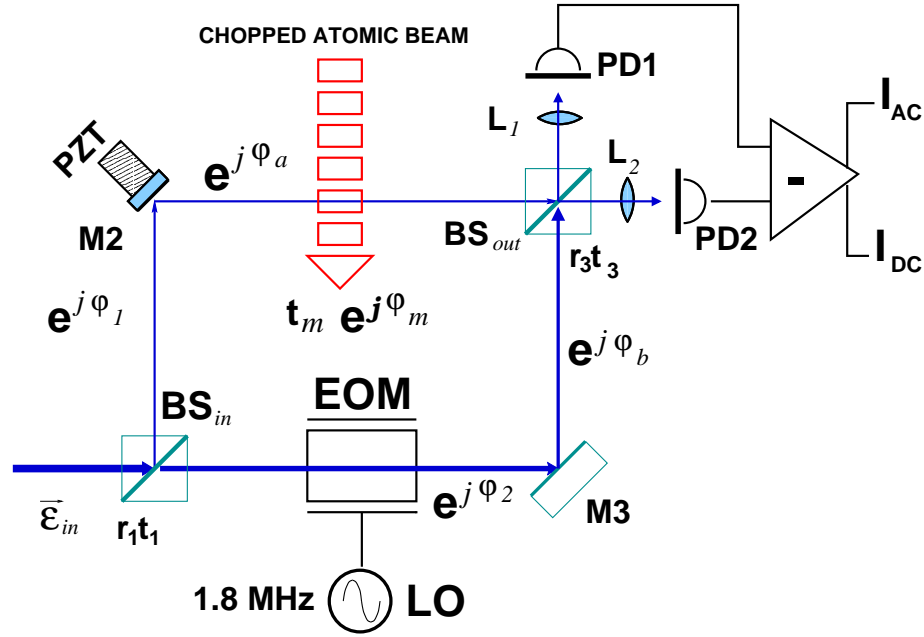
Figure 3.3: Optical setup of the interferometer. The input optical field $\vec{\mathcal{E}}_{in}$ enters the interferometer at the strongly unbalanced beam splitter (BS_{in}) (with reflecting and transmitting coefficients r_1 and t_1 respectively) and it is split between test arm and reference arm. The field passing the test arm experiences a total phase shift $e^{j(\varphi_1 + \varphi_a + \varphi_m)}$ due to the optical path and to the interaction with the atoms. The latter also causes an attenuation proportional to the transmission coefficient t_m. The field passing the reference arm is phase modulated by the **EOM** (electro optical modulator) driven by a **LO** (local oscillator) at **1.8MHz** . Both signals are then once more combined on the BS_{out}: output beam splitter (1:1) and sent to the **PD1** (photodiode 1) and **PD2** (photodiode 2). The difference of these two signals provides two outputs: the first one, the DC output, contains the absorption signal, while the high frequency output, once being demodulated, contains the phase shift signal

while the field passing the reference arm would be described by the relation:

$$\vec{\mathcal{E}}_{ref} = \vec{\mathcal{E}}_0(t) t_1 r_3 e^{i(\varphi_2 + \varphi_b + \psi_1)}, \tag{3.2}$$

we would obtain a signal, on the output photodiodes, which is proportional to $cos\Delta\varphi_L$. Here

$$\Delta\varphi_L = (\varphi_1 + \varphi_a) - (\varphi_2 + \varphi_b), \tag{3.3}$$

is the difference among the different phase shifts experienced from the field when it passes through the different arms.

Let us consider now our specific application: the test arm contains our sample, and within the reference arm an EOM is present. The field passing through the test arm, experiences a further phase shift φ_m and an absorption $(1 - t_m)$ due to the atomic beam. The expression for the field passing the test arm then becomes

$$t_m \vec{\mathcal{E}}_i e^{j\varphi_m}, \tag{3.4}$$

The field passing the reference arm experiences, on the other hand, a phase modulation due to the EOM. The expression of the input field becomes consequently

$$\vec{\mathcal{E}} \rightarrow \vec{\mathcal{E}} \times exp(jM_p \sin \Omega t) \tag{3.5}$$

where Ω and M represent the modulation frequency and the modulation index respectively. We can define furthermore:

- $\tilde{r} = r_1 r_3$: amplitude transmission coefficient for the transfer of the field from the input beam splitter to the photodiode 1 via the test arm

- $\tilde{t} = r_1 t_3$: amplitude transmission coefficient for the transfer of the field from the input beam splitter to the photodiode 2 via the test arm

- $\tilde{r}\kappa = t_1 t_3$: amplitude transmission coefficient for the transfer of the field from the input beam splitter to the photodiode 1 via the reference arm

- $\tilde{t}\tilde{\kappa} = t_1 r_3$: amplitude transmission coefficient for the transfer of the field from the input beam splitter to the photodiode 2 via the reference arm

If we then consider the difference between the intensity of the signals on both photodiodes, we have on the output $I^- = I_1 - gI_2$ where g is a gain factor which takes account of the difference in the sensitivity of the two detectors.

Expanding thereafter the expression for I^- using the Bessel functions of first kind ($J_m = J_m(M_P)$ represent the Bessel function of order m with the modulation index as argument) we obtain[56]:

$$\begin{aligned}
I^- =I_0 \Big[&t_m^2[\tilde{r}^2 - g\tilde{t}^2] + [(\tilde{r}\kappa)^2 - g(\tilde{t}\tilde{\kappa})^2] \\
&-2t_m \cos(\varphi_m + \Delta\varphi_L)\Big[\tilde{r}^2\kappa + g\tilde{t}^2\tilde{\kappa}J_0 \\
&-4t_m \cos(\varphi_m + \Delta\varphi_L) \\
&\times \sum J_{2n}\{\tilde{r}^2\kappa \cos(2n\Phi_1) + g\tilde{t}^2\tilde{\kappa} \cos(2n\Phi_2)\} \\
&-4t_m \sin(\varphi_m + \Delta\varphi_L) \\
&\times \sum J_{2n+1}\{\tilde{r}^2\kappa \sin[(2n+1)\Phi_1] + g\tilde{t}^2\tilde{\kappa} \sin[(2n+1)\Phi_2]\}\Big],
\end{aligned} \tag{3.6}$$

where $\Phi_i = \Omega t + (l_b + L_i) \times \Omega/c$ is the microwave phase (the phase shift experienced by the modulation field) and L_i represents the distances between the output beam splitter and both photodiodes.

We can then observe that the phase difference due to $(L_2 - L_1) \neq 0$ is very small, if we operate in the microwave frequencies. Variations of $L_2 - L_1$ due to mechanical (seismic and acoustic) noise does not significantly affect our measurement, and there is no need to

pay particular attention to these noise sources for the mechanical setup of the photodiodes (as it was considered for the interferometer).

The whole interferometer is instead operated in an high vacuum environment ($P \approx 5 \times 10^{-8} mbar$) to decouple it from acoustic noise. It is also seismic insulated from optical bench using a two stage mount consisting of three legs and an intermediate mass (of the same order of magnitude of the interferometer), decoupled from each other using a series of rubber cylinders. To reduce thermal drifts the optical components are connected via Zerodur rods.

If we demodulate the output signal at the modulation frequency or at its harmonic we can obtain a minimum signal for $\sin[\Delta\varphi_L + \varphi_m] = 0$ ("dark fringe") or $cos[\Delta\varphi_L + \varphi_m] = 0$ ("half fringe") which can be used to lock the interferometer.

It is important now to analyze the choice of the characteristics of our optical components [56]. We wanted to operate under conditions such that the optical properties of the sample are not affected by the probing field. For this reason a strongly unbalanced input beam splitter had to be chosen. The limit $I_{IZ} \ll I_0$ is then verified where I_0 is the probe field power and I_{IZ} is the laser power in the interaction zone with the sample. The fulfillment of this condition fixes consequently the reflectivity of the input beam splitter: $r_1^2 = I_{IZ}/I_0$. Let us now consider the expression (3.7) assuming that we have balanced photodiodes ($g = 1$). The maximal signal at modulation frequency and its harmonic is achieved when the expression $I_0 J_m(M_p)(\tilde{r}^2\kappa + g\tilde{t}^2\tilde{\kappa})$ becomes maximal.

But we have that:

$$I_0 J_m(M_p)(\tilde{r}^2\kappa + g\tilde{t}^2\tilde{\kappa}) = I_0 J_m(M_P) 2 r_1 r_3 \sqrt{1 - r_1^2}\sqrt{1 - r_3^2}, \tag{3.7}$$

and consequently the maximum corresponds to the choice of a balanced output beam splitter ($r_3^2 = 1/2$) and the expression (3.7) would become [56]

$$I_0 J_m(M_p)(\tilde{r}^2\kappa + g\tilde{t}^2\tilde{\kappa}) \approx \sqrt{I_{IZ}} \times \sqrt{J_m^2(M_P) I_0}. \tag{3.8}$$

It is then clear that the signal is produced by the beat of the optical field of the test arm with the sidebands (arising from phase modulation) of the reference arm.

Let us now assume that the loss induced in test arm is small. Consequently it is possible to substitute the coefficient t_m with the relative absorption of the test field power α_m considered that $t_m = exp(-\alpha_m/2) \approx 1 - \alpha_m/2$. If we now consider the expressions for the signal at DC, and at first harmonic, in the case of an interferometer locked on the "dark fringe" we have:

$$I_{DC}^- \approx I_0 \times \left[2J_0(M_P) r_1 t_1 \left(1 - \frac{\alpha}{2} + \frac{\delta g}{2}\right) + \frac{1}{2}\delta g - 4\left(r_1^2 - \frac{1}{2}\right)\delta R\right], \tag{3.9}$$

$$I_\Omega^- \approx -4 I_0 \times J_1(M_P) r_1 t_1 \varphi_m \times \sin\Omega t. \tag{3.10}$$

These expressions were derived expanding the signal respect to $\alpha_m, \varphi_m, \delta g$ and δR and neglecting second and higher order terms, after we suppose that g and r_3 differ from the ideal case for the quantities:

$g = 1 + \delta g$ and $\delta g \ll 1$

$r_3^2 = \frac{1}{2} + \delta R$ and $\delta R \ll 1$

Observing the expressions (3.9), (3.10) it is then evident that the DC signal contains the absorption term, while the demodulated signal contains the phase shift term.

If we considered the demodulation term at the second harmonic of the modulation frequency, we would have that:

$$I_{2\Omega}^- \approx -4I_0 \times J_2(M_P)r_1t_1 \left(1 - \frac{1}{2}\alpha + \frac{1}{2}\delta g\right) \times \cos 2\Omega t. \tag{3.11}$$

It can be observed, that information about absorption would also be contained in the second harmonic demodulated term, with a better signal to noise ratio (because of smaller contribution of unbalance and smaller electronic noise), but to use this signal further high frequency electronic would have been implemented.

We have furthermore to underline that with the use of this combination method, instead of a simple FMS, no cross talking effects are to be observed between the phase shift and absorption signal. Such effects would have been critical in the frequency interval (around transition) where we are interested to study the sample.

3.2.2 Operating the interferometer

In this section we are going to describe how the interferometer has been operated, how the signals have been detected and which feedback controls have been implemented. As already mentioned before, we use the differential output of both photodiodes. From the DC component of this signal, the absorption is obtained. From the demodulated signal at Ω (modulation frequency of EOM), the phase shift is obtained.

Let us now describe the way to operate the interferometer. The signals coming from the different output photodiodes are subtracted. The subtracter posses two different outputs: a DC output and an AC output (Fig 3.4).

The signal at the DC output is first amplified, then it passes through an 8th order filter (which is a a narrow band width filter with 8 zeros and 8 poles which consequently suppress the signal at all frequencies except the f_c we consider); using a dual-phase lock-in amplifier the signal is demodulated at the frequency of $f_c = 1.7kHz$, which is the frequency of the chopper motor (and the chopper itself is used as local oscillator for the lock-in amplifiers).

The signal obtained in this way is digitalized and sent to a computer which furthermore monitors the total status of the system (both SHG cavities, PLL, locking status of the interferometer).

The electronic scheme for the detection of the phase shift results more complex, because this signal is also used to lock the interferometer. The AC output of the difference signal of the photodiodes is first demodulated at $1.8MHz$ (EOM modulation frequency). The output of the mixer is amplified with a preamplifier which is a combination of a low-pass filter ($-20dB/dec$ for $f > 20kHz$) and three notch filters (for the harmonics of modulation frequencies). The signal goes then through two different paths (Fig3.4):

1. The first passes through an integrator ($-20dB/dec$ for $f < 1.1kHz$ and $-40dB/dec$ elsewhere) and an high voltage amplifier. it is used to drive the piezoelectric actuators which act on the mirror M2 of the interferometer (see Fig3.3), changing the length of one arm and providing the interferometer lock signal for the low frequencies ($f < 100Hz$):

2. In the second path the signal passes a bandpass filter whose transfer function shows a gain of $+40dB/dec$ for $f < 50mHz$, is proportional for $50mHz < f < 1kHz$, has a gain of $-40dB/dec$ for $1kHz < f < 20KHz$, and $-20dB/dec$ for $20kHz < f < 32kHz$ and proportional for $f > 43kHz$. The DC gain of the filter can be changed, depending on the signal in the interferometer and its alignment.

The output of the bandpass filter is also split in two parts: one part of it passes a 8th order filter, and is then demodulated to $1.7kHz$ (chopper motor frequency) using a second lock-in amplifier: it goes then to the computer, which records it.
The other part of the signal is also used to lock the interferometer for the higher frequency interval ($f > 100Hz$)(where the piezo would become unstable because of its own mechanical resonances): the signal is high voltage amplified and then goes to the EOM. The EOM, which can be represented as a capacitor, is driven in a resonant way, to reach a voltage of $250V_{pp}@1.8MHz$ with aid of a variable inductance.
With this configuration the calibration of the signal is defined and not depending on the laser power, and it is the reason why we can affirm that the interferometer is used as an active null instrument. The half voltage of the EOM ($U_\lambda = 380V$) defines the correspondence between the signal and the phase shift experienced by the laser beam. The lock of the interferometer is then obtained using both the EOM and the piezoelectric actuators which move the mirror M2.
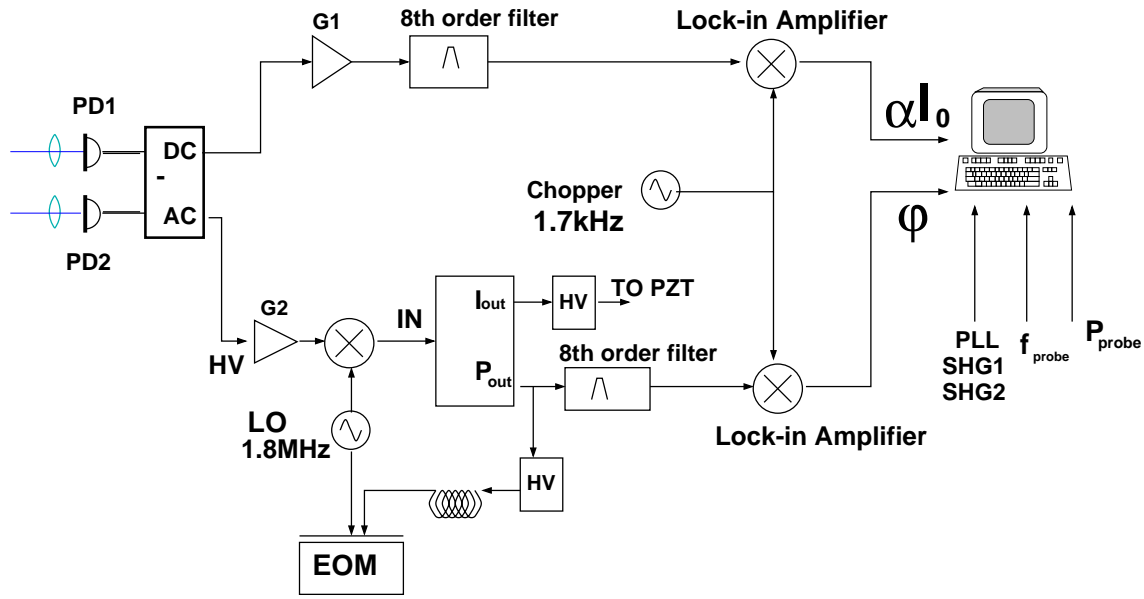
Figure 3.4: Schematic for the operation of the interferometer. **DC** signal of the differential output is first amplified (**G1**), then passed through an 8th order filter, and is then demodulated at $1.7kHz$ using a dual phase **lock-in amplifier**: absorption signal is obtained. **AC** signal from the differential output is used to obtain the phase shift and to lock the interferometer. It is amplified (**G2**) and demodulated at $1.8MHz$ (EOM modulation frequency). The emerging signal goes to a servo loop which provides two outputs: I_{out} (integrator) and P_{out} (proportional). The first one (I_{out}) is once more filtered, then high voltage amplified (**HV**) and used to drive the (**PZT**) piezoelectric actuator to lock the interferometer in the low frequencies interval ($f < 100Hz$). The proportional output (P_{out}) is furthermore split: it passes an 8th order filter, used to suppress the higher harmonics, subsequently demodulated at $1.7kHz$ (using a second lock-in amplifier) and provides in this way the phase shift signal. The same output (P_{out}) is also used, with aid of an high voltage amplifier (**HV**) and an inductance (to resonant drive the EOM) to lock the interferometer on the dark fringe in the higher frequencies interval. Both phase and absorption signals go to a computer which also monitors the status of: the **PLL** (phase locked loop), the **SHG1** and **SHG2** (second harmonic generators of both systems), the P_{probe} (power of the probing laser) and its frequency (f_{probe})

A detailed noise analysis [56] showed that the optimal choice of the modulation index depended on the relative power noise of the laser. It was chosen to operate the interferometer on the "dark fringe". This choice allowed us to detect the absorption from the DC differential signal, as equation (3.9) clearly shows. Consequently the optimal modulation index corresponding to the minima of detectable absorption and phase shift resulted $M_P \approx 1.5$ [56].

3.3   The laser system

For our spectroscopic intents we needed a compact and easy to handle, stabile, laser source. Our aim was to simultaneously change the optical properties of the sample and measure them. Two similar laser systems had been developed: one of them had to remain locked on the transition (driving system) and to provide enough power to change significantly the properties of the sample (at least 15mW blue power had to be reached). The probing system had to be continuously swept around the resonance to provide the profiles measurement.

The system developed consists of two IR diode lasers, used in a master-slave configuration, and a ring resonator containing a $KNb0_3$ crystal is used as second harmonic generator (**SHG**), which provides the desired wavelength.

3.3.1   The infrared (IR) laser system

Master Laser

Master Lasers are infrared laser diodes of the series $SDL5410$. These $GaAlAs$ laser diodes are available for the wavelength $852 \pm 10nm$, and operate in a single longitudinal mode, with a maximal output power of $100mW$ at $120mA$ of driving current.

To reach a good tunability and a stabile single mode operation, the output facet was anti reflex coated (suppressing the reflectivity to about 10^{-5}). Implementing the AR coating modifies slightly the characteristics of the laser diode. The threshold current becomes higher ($\approx 35mA$), which represents also the operating current. In this way was reachable a power of about 20mW, in a single mode operation. A special mounting unit for the laser diode was developed to ensure maximal stability and a good thermal contact with the laser diode case. The mounting unit, and consequently the laser case, had to be temperature stabilized using an active Peltier element. To this aim it was used a particular alloy $CuSn8$: it consists of 80% copper and 8% tin, has thermal capacity of $75W/(m \times K)$ and an expansion coefficient of $18 \times 10^{-6}K^{-1}$ [26].

An external optical feedback was implemented using a grating ($1400Lines \ mm^{-1}$ and $\approx 20\%$ efficiency for first order) in a Littrow configuration [58]. The grating is fixed on the mounting. Its position (i.e. the angle between the emerging laser and the grating itself) is adjustable using a micrometer screw and a piezoelectric element. The latter provides then the possibility to tune the laser: a slope of $\approx 0.5GHz/V$ was reachable. A detuning of the laser frequency was also obtainable by changing the temperature of the mounting, and consequently the length of the resonator constituted by the diode with the grating: a variation of $\approx 10GHzK^{-1}$ was possible, provided that to change the frequency continuously (preventing the so-called "mode- hopping") steps of $\approx 0.1K$ had to be used.

The total tunability of the diode was of about $20nm$, but the continuous tunability (between

two different modes) was of some GHz, which is also suited for our application: it is in fact possible to observe both the transition frequency and the Rabi side band structure.

The strongly divergent light emitted from the laser diode had to be collimated, and a
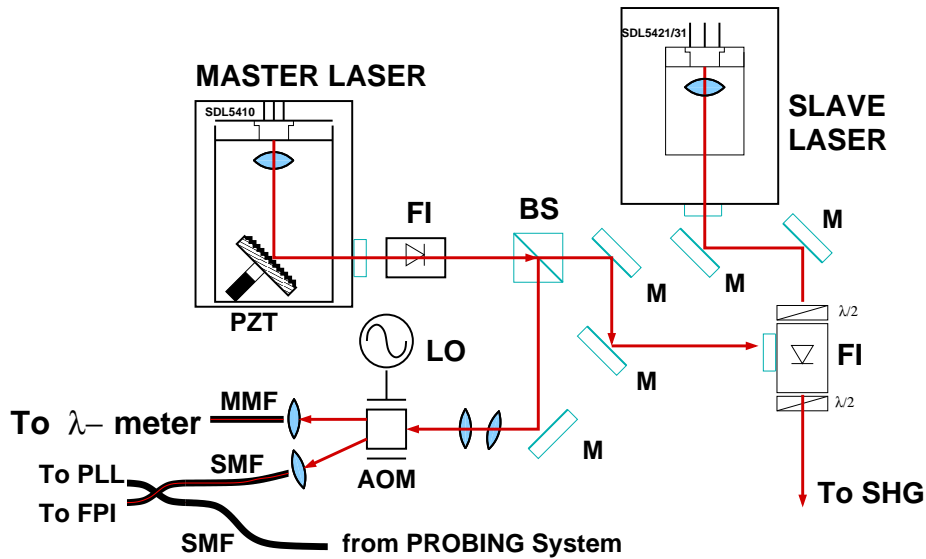

Figure 3.5: Scheme of injection lock: the master laser in the Littrow setup is represented with the (**PZT**) piezo electric transducer acting on the grating. Light from the SDL5410 is collimated using a collimator lens. It passes a Faraday isolator (**FI**) and a beam splitter (**BS**) . Part of the radiation is injected in the slave laser, using two mirrors (**M**) and a further Faraday Isolator. In the driving system the second output of the BS, after passing a telescope constituted by two lenses L_1 and L_2, is coupled in an acousto-optical modulator (**AOM**) driven at $180MHz$. The red shifted output radiation, injected in a single mode fiber (**SMF**), is coupled with the field coming from the probing system and the beat signal obtained is sent to the phase locked loop (**PLL** to lock the probing on the driving field). The unperturbed output of the AOM is sent, through a multi mode fiber (**MMF**) to a wave-meter to monitor the radiation frequency. For the probing system a slightly different configuration is chosen: the second output of the beam splitter is directly injected to a SMF. With the use of two couplers, three outputs are provided: the first one goes to wave-meter, the second to a Fabry Perot interferometer (**FPI**) the third is coupled to the driving field.

lens (Thorlabs5230TM-B, $f = 4.5mm$) had to be used (Fig 3.5). After passing Faraday Isolator (optical diode, Gasaenger, DLI-1, $60dB$ isolation), to avoid optical feedback from the subsequent part of the experiment [61] the output beam is split into two parts (beam splitter 1:1). The first one is used to:

- Monitor the longitudinal single mode operation (using a scanning Fabry Perot inter-
  ferometer)

- Monitor the wavelength of the laser with aid of a super stabile reference laser (λ

meter)

- Lock the pump and probe system optical frequencies (digital phase locked loop)

The other part is then injected into the slave laser, using a second Faraday Isolator. The light of master laser enters through a side window, and, because of its direction of polarization, the beam is "forced" to go into the direction of the slave laser. Master and slave lasers have then exactly the same optical path, and slave laser can be injection locked on the master laser [26], [30], [16].

Slave Laser

For the slave laser a similar laser diode is used, with higher emitting power. This configuration does not use a grating, in this way the laser diodes (SDL5420, SDL5430) can be driven with a higher current without problems due to optical feedback. SDL5420 and SDL5430 provide a maximum IR power of 150 and $200mW$ when operated at max 200 or $250mA$ respectively.
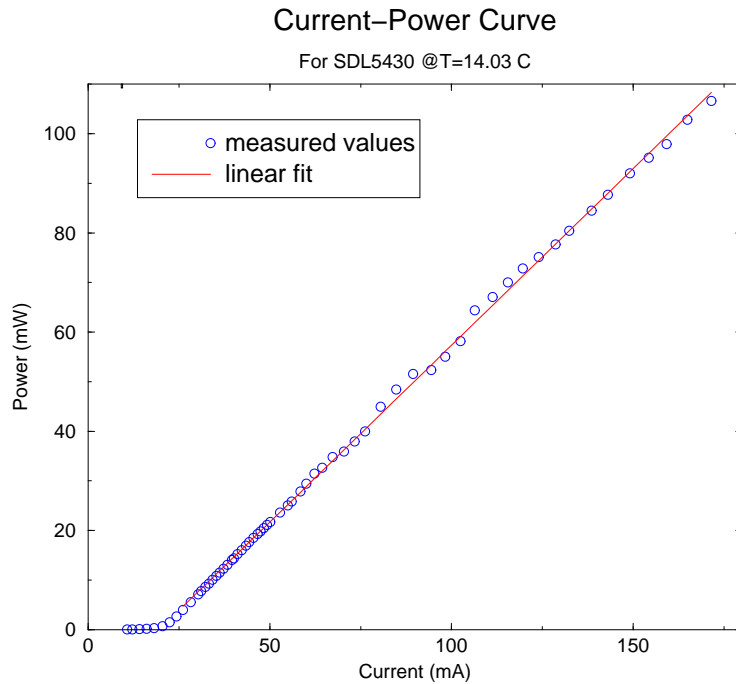

Figure 3.6: Characteristic curve for the laser diode SDL5430. Emitted power as function of the driving current is represented. With a linear fit it was obtained: $dP/dI = 0.7127(28)W/A$ and $I_{thr} = 19mA$

The direction of the field polarization is fixed. Using an optical diode, optical feedback of the slave laser to the master laser direction is prevented and, simultaneously, optical feedback from the SHG cavity to the slave laser is avoided. In this way the slave laser is forced

to work in the same way the master laser does. Using this master-slave configuration we are the able to obtain a laser source which has, at least in some driving current interval, the same single mode operation, the tunability, the same frequency stability like the master laser, and higher emitting power.

Both master and slave lasers are seismic and acoustic decoupled from the optical bench and the environment using metallic boxes (which can be closed) positioned on heavy metal plates, placed between two rubber sheets. The boxes are also filled with silicon gel, to avoid problems due to air humidity condense on the laser diodes.

Observing in fact the power vs. temperature curve (Fig 3.7) to obtain the maximal power, the temperature of the laser diode has to be stabilized to temperature ($T = 8.5°C$) which is below the room temperature.

Because of the necessity to obtain as much infrared power available, the laser diode SDL5420 has been substituted with an SDL5430, which has a bigger maximal output power. The measured characteristics of this different laser diode are depicted in Fig3.7, Fig3.6, and Fig3.9 .
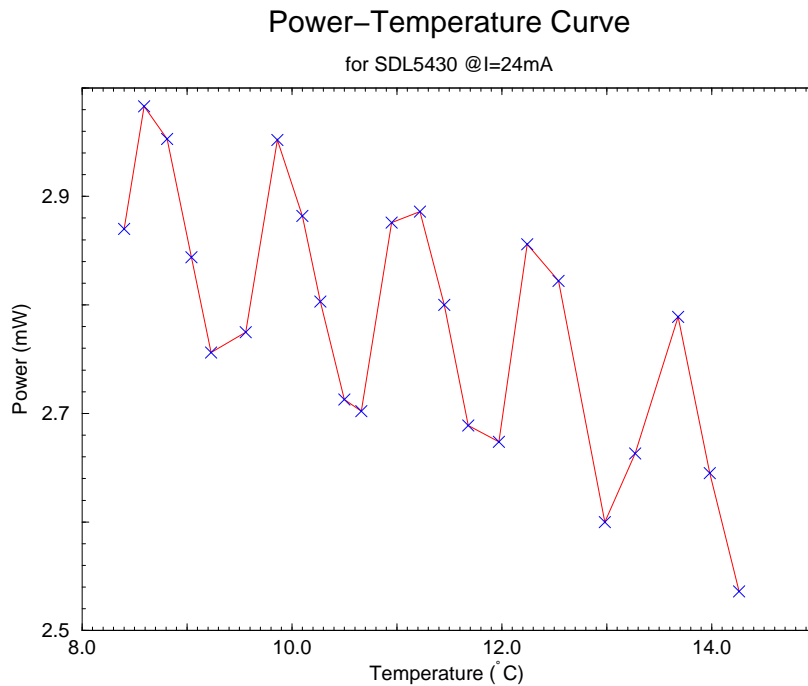

Figure 3.7: Characteristic curve for the laser diode SDL5430. Emitted power as temperature function. Driving current is 24mA

3.3.2   Second Harmonic Generation (SHG)

An important part in the optical setup is the second harmonic generation (**SHG**) cavity. In order to obtain a strongly driven two level system, with properties suited for applications inside a "white light cavity", "high" blue power radiation at $423nm$ was needed. The requirements, as for example illustrated in the [49], are, for a particle density of $N_{at} = 5 \times 10^{-10} cm^{-3}$, a driving field of Rabi frequency $\Omega_d = 13.5 \times 2\pi 34 MHz$, corresponding to an intensity of $\approx 870mW/mm^2$.

To this purpose a ring resonator had been developed as second harmonic generator.

Second harmonic generation is a nonlinear effect obtained by the polarization of an anisotropic medium (as crystals are), and is caused by frequency mixing phenomena of the fundamental wave with itself. In our case the anisotropic medium is constituted by two a-cut $KNbO_3$ crystals ($9mm$ and $15mm$ long for probing and pumping system respectively).

To obtain a second harmonic generating process the **phase matching condition** has to be fulfilled. This results in the necessity for the refraction indices for the fundamental field (n_1) and for the second harmonic (n_2) to be the same:

$$n_1 = n_2 \tag{3.12}$$

To fulfill this condition it can be applied an electric field, it can be adjusted the direction of the beam axis relative to the crystal one, or it can be varied the crystal temperature [4]. The last method was used in our experimental setup. As expressed both in [65], [5] the temperature for the phase matching was, in our case $\approx -13°C$. The crystal, surrounded by an indium film to optimize its thermal conductivity, was fixed in a special mounting unit, which was cooled with a Peltier active element. The mounting and the crystal were protected from unwanted condense with a Plexiglas case, where Natrium flowed continuously.

The relation between the fundamental (P_1) and second harmonic power (P_2) is quadratic, i.e.:

$$P_2 = \alpha P_1^2, \tag{3.13}$$

where the proportionality constant α is dependent from the crystal properties, and the geometrical properties of the Gaussian fundamental field.

The optimizing of second harmonic generation has been theoretically analyzed by Boyd and Kleinmann [4]. Following their analysis, the second harmonic generated beam possess the same focus and the same confocal parameter like the fundamental field.

Furthermore to obtain the maximal conversion efficiency two conditions have to be fulfilled [4]:

- The focus of the fundamental field has to lay in the middle of the crystal

- Between the crystal length L_k, and the confocal parameter of the fundamental wave (b_1) the following relation has to be valid:

$$\xi_{bk} = L_k/b_1 = 2.84, \tag{3.14}$$

where the confocal parameter is expressed by the relation [27]:

$$b_1 = 2\pi \frac{w_1^2}{\lambda_1} n_1, \tag{3.15}$$

where λ_1 represents the wavelength, w_1 is the focus radius of the fundamental wave, and n_1 is the refraction index of the crystal.

Fixed consequently the length of the crystal, the geometrical properties of the beam in the crystal are fixed.

The ring cavity, in the bow-tie configuration (depicted in Fig (3.8)), was used to increase the IR power, and, consequently, the achievable blue power.

The cavity consists of four mirrors: M1 and M2 are plane mirrors, the latter is glued on a tiny and fast piezo element which allows to scan the cavity or to lock it to the laser frequency. The PZT is itself glued on a compact and adjustable mount.

M3 and M4 are two curved mirrors, with the same radius of curvature R. M4 has an high transmissivity for $427nm$ and is also used to focus the emerging from the resonator one. The mirror axes are tilted of an angle $\theta = 6°$ with respect to the radiation propagation direction. The characteristics of the mirrors, their curvature radii, the angle θ, define the cavity geometry.

Let us consider a laser beam with a transversal intensity distribution that can be described by a Gaussian. Then, at point z of its propagation direction, it is given by its complex parameters:

$$\frac{1}{q(z)} = \frac{1}{R(z)} - i\frac{\lambda}{\pi w(z)^2}, \tag{3.16}$$

where $R(z)$ is the wavefront local radius of curvature, $w(z)$ is the local radius (radius of the beam, corresponding to a decrease of $1/e^2$ of the intensity with respect to the maximum), and λ is the wavelength of the field.

The relations between $R(z)$, $w(z)$, $z = 0$ (position of the focus) and w_0 (radius in the focus) are expressed by:

$$R(z) = z \left[1 + \left(\frac{\pi w_0^2}{\lambda z}\right)^2\right] \qquad w^2(z) = w_0^2 \left[1 + \left(\frac{\lambda z}{\pi w_0^2}\right)^2\right] \qquad . \tag{3.17}$$

Depending on the characteristics of the resonator we can then describe our Gaussian beam in every point of the propagation direction.
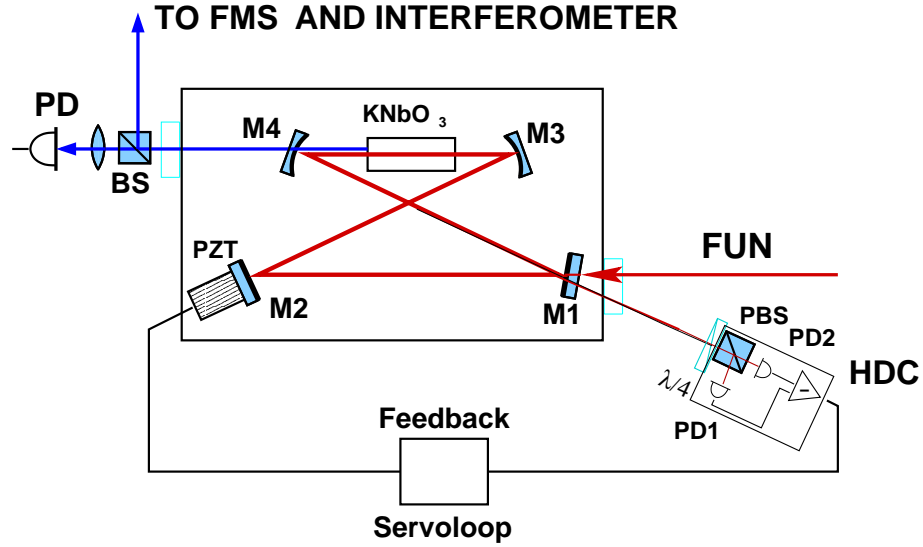
Figure 3.8: Schematic of the Second Harmonic Generator setup. **FUN** (fundamental field) from the slave laser enters the cavity through the mirror **M1**. The **PZT** piezoelectric transducer glued to mirror **M2** allows to scan the cavity and is the actuator to lock it on the laser frequency. The reflected beam goes to **HCD** Haensch- Couillaud Detector: it passes the $\lambda/4$ plate, becoming circular polarized. When the cavity is in the resonance condition the output of the **PBS** (polarizing beam splitter) are two, perpendicular to each other, linearly polarized fields, with equal amplitude. The signals on both photodiodes **PD1** and**PD2** are equal. Their difference is equal to zero.

The $KNbO_3$ crystal is cooled to $-13°C$ to obtain the phase matching condition. The output mirror M4 posses an high transmissivity for the blue wavelength ($427nm$) and, simultaneously, focus it. The second harmonic is transmitted. The emerging beam is divided into two parts using a beam splitter **BS** . The output to **PD** photodiode is used to monitor the output power. The second output goes to the interferometer.

 If we place the crystal, which has fixed dimensions and characteristics, centered between the curved mirrors M3 and M4, the condition for the confocal parameter (see equation 3.14), defines the focus radius we want to obtain in this point. The dimensions of the second focus of the cavity, which is centered between the plane mirrors M1 and M2, are then dependent on the total length of the cavity and the focal length of the curved mirrors. It is then possible to study different configurations which fulfill the given conditions. In our case, the desire to obtain the most compact configuration led to a choice of $f = 25mm$, $L \approx 0.60m$ (length of the path in the cavity) and an angle of $\theta = 6°$.

It has to be observed that our SHG cavity has an intrinsic ellipticity due to the use of tilted mirrors. A slightly tilted lens, in fact, has a different focal length in the different directions (vertical and horizontal). If we suppose it is α the tilting angle about a vertical, then the focal length of the lens is transformed following the relation:

$$f_{hor} = f_0\xi \qquad\qquad\qquad f_{ver} = f_0/\xi, \qquad\qquad (3.18)$$
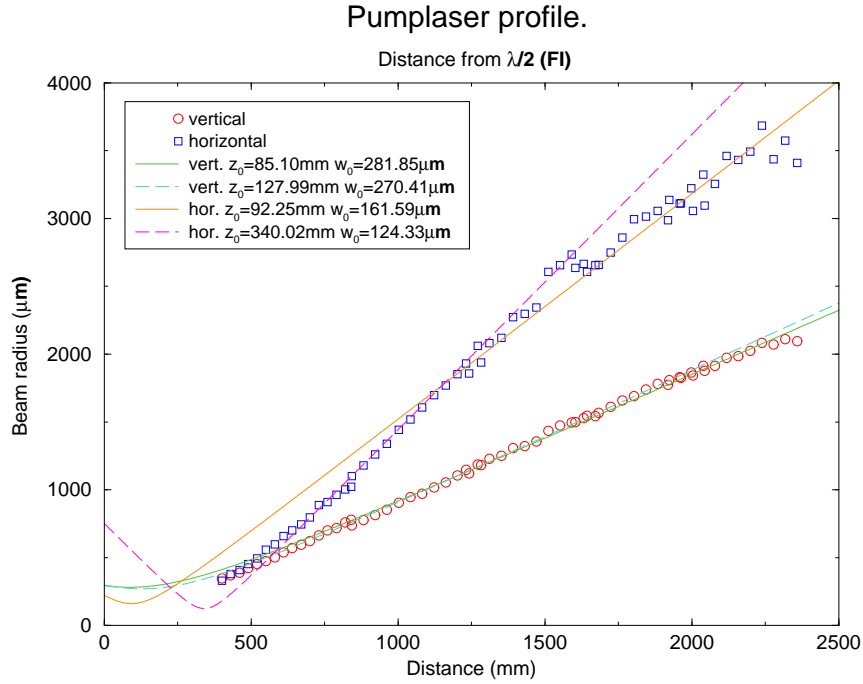
Figure 3.9: Beam radius for the horizontal and vertical direction as function of the distance in the propagation direction. The points represent the experimental values. Continue lines are the profiles fitted to the experimental values. Solid and long dashed lines correspond to different weights attributed to the points. Great divergence in the beam was in fact observed. The focus positions and focus radii are calculated from the fitted curves

where $\xi = cos\alpha$ when the tilting direction is horizontal and $\xi = 1/\cos\alpha$ when the tilting direction is vertical and f_0 represents the focal length of the lens. Subsequently for our case:

$$f_{hor} = \frac{R}{2}\cos\alpha \qquad\qquad f_{ver} = \frac{R}{2}/\cos\alpha. \qquad (3.19)$$

The required focus radii are different for the horizontal and the vertical directions. In our case, for the driving system (crystal length $15mm$) the conditions were:

$$w_{0\,hor} = 288.8\mu m, \qquad\qquad w_{0\,vert} = 255.8\mu m. \qquad (3.20)$$

The transmissivity of the input mirror (M1) determines impedance matching condition of the fundamental wave in the resonator. 100% impedance matching corresponds to a complete coupling of the fundamental wave in the resonator.

In this case, the transmission coefficient of the input mirror t_1 is equal to the losses of the field in one round trip through the resonator.

If only the linear losses of the fundamental wave in the resonator were considered, the fulfillment of the impedance matching would correspond to an optimal value on the coupling

mirror transmission equal to [24]:

$$T_1 = \frac{\mathcal{L}}{2} + \sqrt{\frac{\mathcal{L}^2}{4} + \eta P_1},$$ (3.21)

where $\eta = P_2/(P_1)^2$ is the nonlinear conversion loss due to second harmonic generation and $\mathcal{L}$ represent the linear losses in the cavity.

The expression is valid only in absence of any other linear losses. For the crystal used, a BLIRA (BLue enhanced Infra-Red Absorption) effect was observed [23]. These losses are proportional to the blue power and consequently to the square of the infrared internal power (see 3.13). An imperfect impedance matching was then observed: the latter resulted in fact $\approx 70\%$ when using the $150mW$ laser diode and was decreased to less than 60% after the implementation of the $200mW$ laser diode.

We are now ready to discuss the coupling of a 'real' laser beam to the cavity, and the experimental results we achieved. First we have to fulfill a mode matching condition, between the laser and the resonator. A laser beam coming from a laser diode has in fact have a strong ellipticity and an astigmatism. Furthermore, in one of the direction (the vertical or the horizontal, depending how the polarization direction of the diode was chosen) strong interference effects, due to the big divergence of the laser output, and a finiteness of the output surface, causes the appearance of higher transversal laser modes, which can not be described by a TEM_{00}. These higher modes however represent losses in the frequency doubling process, because they are not coupled in the resonator. For what concern the beam produced by the laser, our aim was:

- To correct the astigmatism and the ellipticity of the laser beam

- To mode match our laser to the SHG cavity

To obtain these conditions a combination of two different lenses is used. The first lens, is placed in one of the two position in which, according to eq.(3.16) the beam is circular. This lens is used to correct the ellipticity and the astigmatism of the beam.

For a Gaussian beam passing through a lens, the local radius of curvature of the wavefront is in fact changed. Tilting the lens of a specific angle θ in the horizontal or in the vertical direction (depending on the characteristics of the beam), it is possible to obtain a circular beam after the lens.

A second lens can then be used to obtain the mode matching in the SHG cavity: we want the focus of the beam and its dimensions to be exactly the ones required by the cavity.

 In particular we can report the measured properties of a laser diode of the series SDL5430. As first step the perpendicular intensity distribution, as function of the distance along the propagation direction, for both the horizontal and the vertical planes, was measured, using a Super Beam Analyzer. The results achieved are depicted in Fig 3.9. With help of a
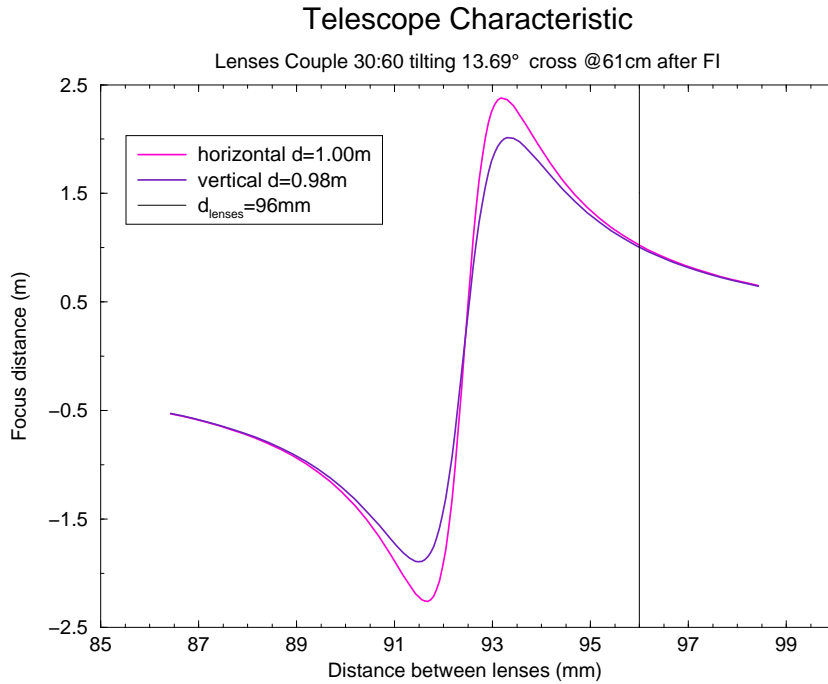
Telescope Characteristic

Figure 3.10: Focus distance as function of distance between lenses, for a telescope constituted of a 30mm focal length and a 60mm focal length lenses. The first lens is tilted in the vertical direction of an angle of 13.64°

fitting method to a Gaussian profile, the foci positions and the dimensions of vertical and horizontal beam could be determined.

It was then possible to calculate the position in which the first lens had to be placed i.e. where the beam results circular.

For any kind of focal length, a tilting angle was then defined, following the condition that the radii of curvature have to be the same after the lens in both the horizontal and the vertical plane.

The focal length of the second lens and its distance from the first one, is then defined if we impose that the focus of the beam is in the middle of the $KNbO_3$ crystal in the cavity (which position with respect to the laser is then fixed), and the desired dimensions of the beam focus (3.20).

In order to strongly drive the Ca atoms we needed to obtain as much blue power as possible.

The series SDL5420 laser diode has maximal infrared power of $150mW$ corresponding to $200mA$ of driving current. The maximal blue power experimentally obtained was of $\approx 17mW$ (when injecting $\approx 70mW$ IR in the SHG), and it had been used for a series of measurements. It was then substituted with one of the series SDL5430 which can provide up to $200mW$ IR power at $250mA$ of driving current.
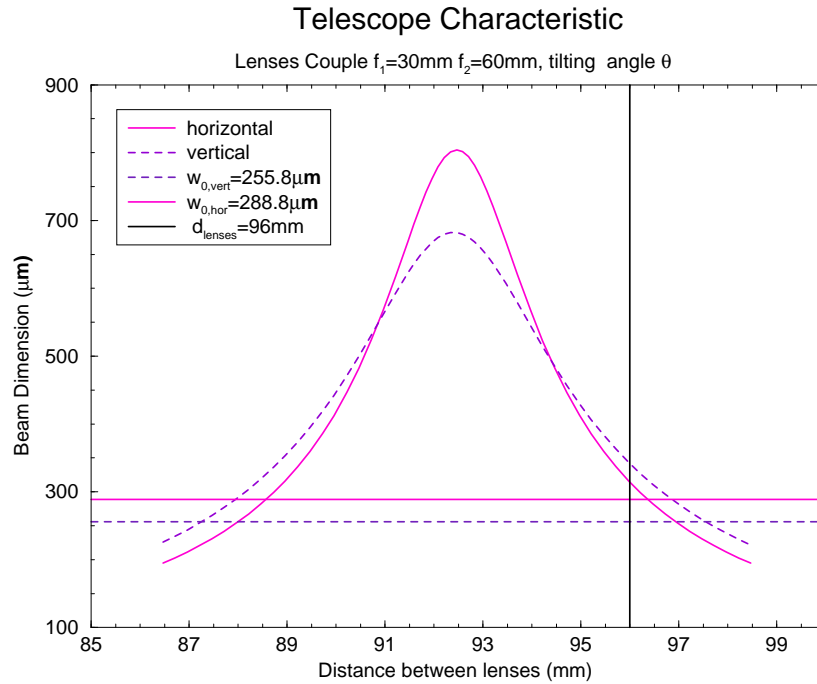
Figure 3.11: Beam radius in the focus after the telescope. It consists of two lenses of focal length 30mm and 60mm respectively, the first tilted by $\theta = 13.6°$ and placed at $61cm$ after Faraday isolator. Function of distance between the lenses.

The obtained beam was then characterized as showed in Fig 3.9.

Any significant improvement of the produced blue power was unfortunately observed.

The lack of improvement was due to several reasons.

First, one of the requirements of our laser diode was to have an AR coating in the output facet, to yield a more stabile and easier to obtain injection lock. The only available AR coated SDL-5430 had a so-called G1 case, instead the C one which had been previously used. The main characteristic of this case is that it is round. This causes a loss of definition in the polarization direction, and consequently an increasing in the losses when passing the Faraday isolator. Furthermore, although the collimator lens was used and its position optimized, a very poor quality in the transversal beam was observed in the horizontal direction, together with a big divergence of the beam (an observable radius of $\approx 2cm$ at a distance of 2m). This naturally caused a great indetermination in the measurement of the transversal beam (see Fig 3.9), which rendered more difficult the choice of an optimal telescope configuration and consequently a poor coupling of the IR beam in the second harmonic generator.

An increase of the BLIRA effect with the increasing IR injected power was furthermore observed.

The SHG cavity was then characterized at different IR injected powers (changing the driv-

P_{in}	$58mW$	$80mW$	$101mW$	$126mW$	$134mW$	$149mW$
Int. loss (%)	5.64	5.73	6.73	6.85	7.30	7.15
Mode matching (%)	56.8	54.5	56.0	55.7	56.6	58.3
Int. Power (mW)	550	710	769	930	930	1100
Conv. efficiency (%)	2.5	2.6	2.8	2.3	2.7	2.0
Conv. loss (%)	1.6	2.2	2.6	2.6	3.1	2.7
Linear loss (%)	2.5	2.6	2.8	2.3	2.7	2.0

Table 3.1: Second Harmonic Generator parameters. In correspondence of different values of input infrared powers (P_{in}), obtained changing the diode driving current, the transmitted infrared and blue power, and the IR reflected power, were measured. Consequently the mode matching in the resonator, the internal loss, internal power, conversion loss and linear loss could be calculated

ing current of the laser diode).

The different cavity characteristics, calculated using a model for a ideal cavity, are reported in the table (3.1): corresponding to different driving currents of the diode SDL5431, and consequently of the IR power injected in the SHG, the IR and blue transmitted power, as well as the IR reflected power were measured.
A further experimental difficulty was then observed. The phase match condition (3.12) requires that the refraction index for the fundamental and second harmonic to be the same. This condition is obtained by cooling the crystal. Practically the resonator is scanned using the piezo and the signal on the photodiode is observed (see Fig 3.8). The crystal is then cooled down to $-13°C$. The temperature is then optimized observing the blue signal on the photodiode, and the cavity is locked using the Haensch- Couillaud detector. A difference between the optimal temperature in the scanned and the locked condition was then observed (some 1/10 of $°C$) . The difference resulted to be bigger as the input infrared power (and consequently the internal infrared power) was increased. In this way the SHG could not work under optimal conditions.
The increasing of the infrared power available did not result then, in the expected increase of blue power.
To change then significantly our experimental condition, a completely different kind of laser should instead be used. A solution could be represented by blue laser diode which are recently experiencing a great development and which characteristics are being continuously improved: at present, for example, 5mW blue cw laser diodes are available, and since very recently pulsed 30mW blue are also available.

3.4   The feedbacks

3.4.1   Locking the SHG on the laser frequency: Haensch - Couillaud Detector

The first of the feedback systems we had to use, comprehends the stabilizing of the cavity on the laser frequency. To this aim an Haensch- Couillaud method [17] was used.

The presence in the cavity of an element (the crystal) which is sensitive to the polarization direction, causes a dependence of the reflected light from the polarization direction.

The Haensch-Cuillaud method is based on the presence of a polarizer in the cavity. The scheme we used is represented in Fig 3.8. Let θ be the direction of the polarizer. The incoming field can be decomposed into two components, one perpendicular and the other parallel to θ. The first component is completely reflected from the cavity, and in the plane wave approximation

$$E_\perp^r = E_\perp^i \sqrt{R_1}, \tag{3.22}$$

where R_1 represents the reflectivity of the entrance mirror M1. On the other hand the component parallel to the polarizer is transmitted in the cavity and experiences, in a round trip a determined phase shift [17]. The resonance condition is reached when this phase shift becomes zero. In this case the reflected field results still linearly polarized. When the resonance condition is not fulfilled the field have instead an elliptical polarization.

The reflected beam passes through a $\lambda/4$ plate and then a polarizing beam splitter. At its outputs two photodiodes are present.

In case of resonance, the linearly polarized field [1] is transformed in two linear polarized fields with the same amplitude: the photodiodes then detect two equal signals (supposing that their electronic amplification is exactly the same). The resonance condition corresponds to a zero signal.

Out of resonance the elliptical polarized beam is a combination of left and right circular polarized fields with different amplitudes. Consequently the two linear polarized beams have different amplitudes and the difference signal of the two photodiodes differs from zero.

The difference signal is expressed with the relation [17]:

$$I_a - I_b = I_i 2 cos\theta \sin\theta \frac{T_1 R \sin\delta}{(1-R)^2 4R \sin^2 \delta/2R}, \tag{3.23}$$

---

[1]which can be represented as a combination of a right and left circular polarized field of the same amplitude

where δ is the phase shift difference and R is the amplitude ratio between two successive round trips, the latter determining the cavity finesse. In this way this scheme provides an error signal which can be used for servo locking the cavity length on the laser frequency.

3.4.2 Locking the laser on the transition: FMS

Fundamental to our application is that both lasers are locked on the transition which had to be studied.

To lock the driving system on transition, a frequency modulation spectroscopy (FMS) method had been used [3] [53]. This method, developed by Bjorklund at the end of the seventies, provides the possibility to measure the dispersion and absorption profiles of a specific sample.

The beam, which frequency is ω_c passes through a phase modulator driven sinusoidally at a radio frequency [2]. A modulation index $M_{FMS} \approx 0.13$ was chosen. In this way it is possible to produce a strong carrier of frequency ω_c and two sidebands which frequencies are, respectively $\omega_c \pm \omega_m$. The obtained beam passes the sample (an heat pipe containing Ca vapors). Assuming that the sample has an absorption coefficient $\alpha(\omega)$ and refraction
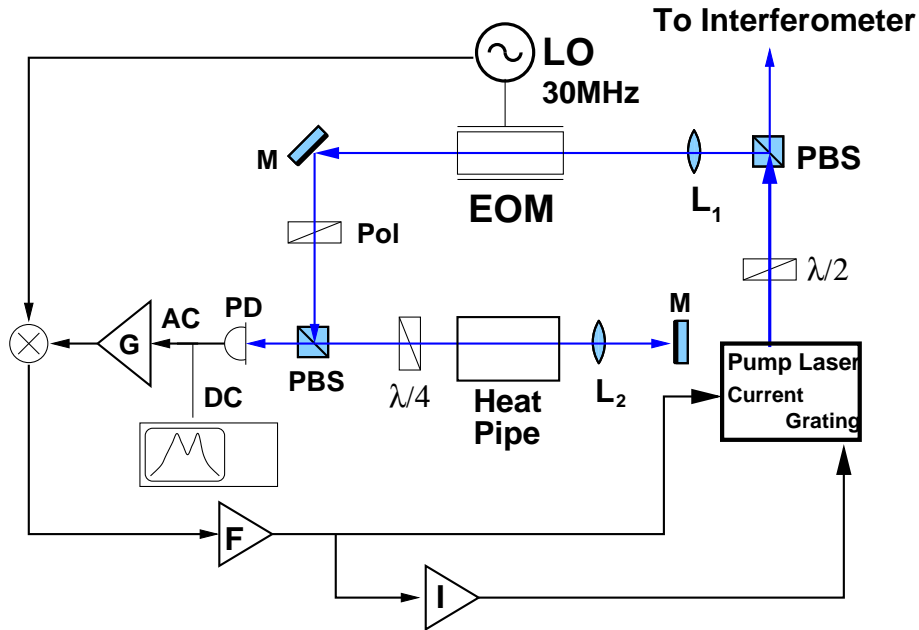
Figure 3.12: Frequency Modulation Spectroscopy: **PBS**: polarizing beam splitter, L_1, L_2: lenses to optimize the geometry of the beam, **EOM**: Electro optical phase modulator, **Pol**: polarizer, **M**: plane mirror, **PD**: fast photodiode, **G**: amplifier, **LO**: local oscillator (30MHz), **F**: filter, **I**: integrator

---

[2] in our configuration $\omega_m = 30MHz$ which is of the same order of magnitude of the spectral width of the medium ($34MHz$)

index $n(\omega)$, each component of the electrical field experiences an amplitude transmission and a phase shift. The signal is then detected with a fast photo detector, it is expressed by the relation [2]:

$$I(t) = \frac{cE_0^2}{8\pi}e^{-2\delta_0}[1 + (\delta_{-1} - \delta_1)M\cos\omega_m t + (\phi_1 + \phi_{-1} - 2\phi_0)M\sin\omega_m t], \quad (3.24)$$

where $\delta_i = \alpha_i L/2$ represents the absorption and $\phi_i = n_i L(\omega_c + i\omega_m)/c$ the phase shift experienced by the lower sideband, the carrier, the higher sideband corresponding to $i = -1, 0, 1$ respectively.

In our case the modulation frequency is great enough that the sample is probed by a single isolated sideband, and the losses and phase shift experienced by both the carrier and the other sideband are constant. Then the expression for the signal becomes:

$$I(t) = \frac{cE_0^2}{8\pi}e^{-2\delta_0}[1 - \Delta\delta M\cos\omega_m t + \Delta\phi M\sin\omega_m t]. \quad (3.25)$$

The demodulated signal provides subsequently a dispersive signal which can be used as an error signal for servo locking the laser frequency on the transition.

Let us now describe how the method was implemented. The setup is depicted in Fig 3.12. Part of the output of the blue power, coming from the SHG cavity of the driving system is taken using a combination of an half wave plate and a polarizing beam splitter. In this way it is possible to fix the power coupled the FMS. The beam passes first a lens L_1 which is used to focus the beam in the interaction zone. A good signal-to-noise analysis requires a power density which is ≈ 3 times the saturation intensity of the transition ($I_{Sat} \approx 1.2mW/mm^2$ [59]). This condition fixes the wanted dimensions in the interaction zone, provided that the power taken from the principal beam (which goes further to the interferometer) is of $\approx 2mW$; consequently $w_{hor} \approx 260\mu m$ and $w_{vert} \approx 360\mu m$. The characteristics of the beam are such that the confocal parameter results, in both direction, bigger then the length of the interaction zone, assuring a good collimation.

The laser beam goes then through the electro optical modulator, which provides the sidebands at $30MHz$. A second lens L_2 is dimensioned to reconstruct exactly the geometry of the beam (its radius and position of the focus) after the first passage of the heat pipe. Using of a polarizer the polarization direction of the beam is fixed, and unwanted components are suppressed. Using a combination of a polarizing beam splitter and a $\lambda/4$ plate it is possible to pass twice the heat pipe, containing Calcium vapors, obtaining an higher absorption signal. The emerging from heat pipe beam results in fact linear polarized in a direction orthogonal to the input one. Passing the polarizing beam splitter it is completely transmitted in the direction of the detecting photodiode (fast photodiode with a $30MHz$ bandwidth). The photodiode has two outputs: the DC output provides a signal which is used to monitor the absorbed signal. The AC output is used as an error signal to lock the laser on resonance. The signal is in fact first amplified using two low noise, high frequency

amplifiers (Minicircuits ZFL500LN and ZFL1000LN) which provide $42dB$ gain. Then it is demodulated, and passes a 1st order low pass filter to suppress the modulation frequency and its harmonics ($-3dB$ at $640Hz$).

The error signal obtained in this way is used to lock the laser frequency on the transition frequency. We have to observe that the frequency noise is due to noise in the driving current of the laser diode and in the tension applied to the grating which fixes the frequency of the master laser. The error signal enters a servo loop which transfer function is constant up to $100Hz$, decreases with $40dB/dec$ up to $1kHz$ and decreases with $20dB/dec$ at higher frequencies. The emerging signal is then be split into two parts and it is used as feed back for both phenomena. The first one is used for the feed back signal of the laser driving current, while the second output passes a further integrator (which transfer function decreases with $20dB/dec$ from DC to $200Hz$ and then decreases with $40dB/dec$ for $f > 200Hz$). The low frequency (DC) servo loop signal is used (after passing an high voltage amplifier) with the piezo acting on the grating which posses own mechanical resonance frequencies at $\approx 2kHz$. The cross over frequency of both servo loops is lower then $200Hz$.

In this way it was possible to lock the laser frequency on the transition.

3.4.3 Locking the probe on pump laser: digital phase lock

A further step in the development of the required setup comprehends a mechanism which provides the possibility to lock the frequency of the probing system on the transition frequency and simultaneously scan it around the resonance. The second requirement is provided giving the possibility to fix a variable offset between the probing laser frequency and the transition and to change it continuously. The scanning interval should theoretically run from 0Hz (to measure absorption and phase shift on the resonance) and some 100MHz which is required to characterize the optical properties in correspondence of the so-called Rabi side bands frequencies (see 2.6), which are proportional to the amplitude of the applied driving field.

Our aim was fulfilled developing a method to lock the probing field to the driving field which is itself locked to the transition by means of the already described frequency modulation spectroscopy: master laser of the probing field is then coupled to the master laser of the driving field with a variable offset frequency.

Let us consider two electromagnetic fields described by the expressions: $\mathcal{E}_{\mathcal{A}}e^{i\varphi_A(t)}$ and $\mathcal{E}_{\mathcal{B}}e^{i\varphi_B(t)}$, where φ_A and φ_B describe the phases of both fields which are dependent from time.

We can then consider the expression of the difference of the two phases as [55]:

$$\Delta\varphi(t) = \varphi_A(t) - \varphi_B(t) = \phi_{LO}(t) + \delta\varphi(t), \qquad (3.26)$$

with $\delta\varphi \ll 1$ and ϕ_{LO} is the frequency of the local oscillator provided by a strong stabile HF generator.

The beat signal of the two fields is then limited by the phase noise of the local oscillator.
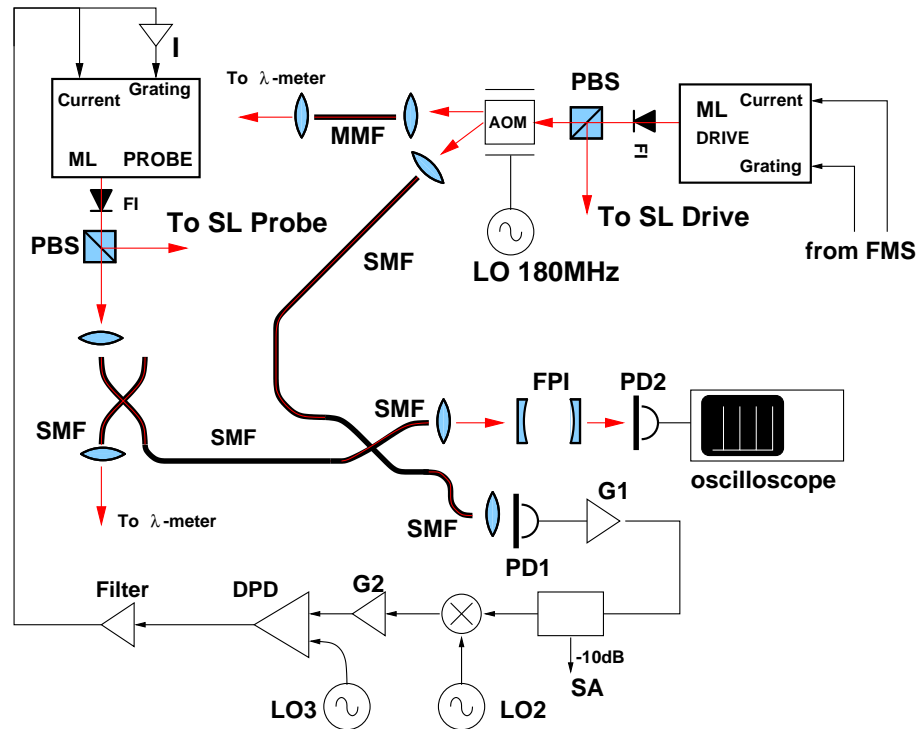

Figure 3.13: Phase Locked Loop: Part of the beam from master laser (**ML**) is taken with help of a polarizing beam splitter (**PBS**): for the driving system it is red shifted of $180MHz$ using an **AOM**. The beam is then coupled in a (**SMF**) single-mode fiber. The second output of the AOM (not shifted) is coupled in a (**MMF**) multi-mode fiber and sent to the wave-meter, which monitors its frequency, with a $100MHz$ precision. The same happens to the probing field which is not, on the other hand, red shifted. The two signals are mixed with aid of a coupler and the beat signal emerging, is detected with a fast ($2GHz$) photodiode (**PD1**) .

It is then amplified with two **HF** amplifiers (**G1**), which provide a total gain of $40dB$. Part of the signal is monitored using the spectrum analyzer (**SA**). The rest of it is then demodulated with a signal coming from the high frequency generator **LO2** ($1kHz...3GHZ$). The output is furthermore amplified (**G2**) and demodulated with the signal coming from the local oscillator (**LO3**=$20MHz$). It goes then to the servo loop used to lock probing on pumping laser. The servo loop acts, as it happened in the **FMS** on both the grating piezo (for the lower frequencies) after passing a further integrator, and the driving current.

Considering in fact that the frequency of the driving system is stabilized, a change in the local oscillator frequency corresponds to a scan of the second laser frequency. The reachable frequency is then in principle limited only by the electronic used, and it does not depend on physical variable.

To develop a phase locked loop it is then necessary to implement a phase detector. For this purpose a digital phase/frequency detector was developed, following the model proposed by Prevedelli et al. [37]. The laser beams coming from masters of both driving and probing

systems are injected into two single mode optical fibers, which are subsequently coupled to each other. It is important to underline that the frequency of the driving laser is shifted of $180MHz$ with respect to red with aid of an acoustic optical modulator. In this way the transition frequency corresponds to a frequency of $180MHz$ instead of $0MHz$, giving the possibility to scan the interval both left and right with respect to the transition (Fig 3.13).

The field emerging from the fiber is the beat frequency of the two incoming fields. It is detected using a fast photodiode ($2GHz$, DC-power $\approx 0.5mW$). The signal is then amplified using two high frequency amplifiers (Minicircuits ZFL-2500VH, $0.01...2.5GHz$, $20dB$) with a total gain of $40dB$. $10dB$ of it are then decoupled using an HF decoupler and sent to the spectrum analyzer used to monitor the beat signal. The rest of the signal is sent to an analogical mixer and is then demodulated with the signal coming from the high frequency generator (Rodhe and Schwarz, SMT3 which frequency can vary between $1kHz$ and $3GHz$). In this way it is possible to vary continuously the frequency of the probing field with respect to the transition frequency.

We have though to underline the presence of two phenomena which limit the possible interval of scanning the laser frequency. First we have to take account of the interval in which the injection lock condition is verified. Normally this interval is of some GHz but an aging process of the laser diode was observed, and its reduction. Furthermore it is unlikely that the transition frequency corresponds exactly to the center of this interval. It was then impossible to carry out a perfectly symmetrical scan around this frequency.

Furthermore the signal coming from the HF generator can not vary continuously in the whole working interval. It was observed that, for certain frequencies, an internal switch happened and the laser had problems in remaining locked when passing them.

These phenomena naturally limited the possibility to scan the laser over a bigger frequency interval.

The demodulated signal was furthermore amplified (using Minicircuits $ZFL1000VH$, $0.01 - 1GHz$, $28dB$), sent to a fast TTL converter and then to the phase lock detector.

The latter has two symmetrical inputs: to the first one goes the beat and demixed signal, to the second one goes the output of a TTL local oscillator (whose frequency is $20MHz$).

In the detector two registers are present : the first one increases by one for every period of the first input, while the second one decreases by one for every period of the second input. The stand of both registers is then added and the result, converted once more to an analogical signal and passing a 2nd order low pass filter (with a cutting frequency of $4MHz$), provides then the phase error signal for the servo loop.

To have a stabile servo loop, the transfer function has to decrease as $-20dB/dec$ $(1/f)$ in correspondence of the unity gain frequency. As this is the intrinsic characteristic of the phase detector (which transform a phase error in a frequency error), then the servo loop which has to be implemented, has to be proportional in correspondence of the unity gain frequency.

A servo loop had been implemented to the probing system, as was done for the pump laser. It acts on the laser diode driving current (for the higher frequencies interval) and on the piezo acting on the grating of the master laser.

The servo loop transfer function possess then a proportional characteristic for frequencies lower than $f_1 = 20Hz$ and higher than $f_2 = 20kHz$ while decreases with $20dB/dec$ in the interval between f_1 and f_2. The servo signal goes to the current driver and to the piezo after passing an integrator and an high voltage amplifier.

The result was the reaching of a line width for the laser of less than $100kHz$, which is enough for our spectroscopic aims. It was than possible to implement a frequency sweep with steps of $10kHz$ and a width of $\approx 300MHz$.

4 Experimental results

4.1 Introduction

In the preceding chapter it was described the experimental setup, and how it was used. We are now able to show the results achieved during different measurement sessions.

A comparison is also made with the theoretical prediction we obtained which were derived from the model of the strongly driven Two Level Atom (TLA). A discussion is also presented about the performances offered by the medium created if put inside an optical cavity, together with the perspective for future developments.
The discussions were in fact multiple, following the evaluation of the results obtained .

- We first performed a series of test measurements in the absence of the driving field. In this way it was possible to evaluate the validity of the method, and to ensure that no cross talking between the absorption and dispersion signals was observed. The correspondence between the expected two-level atom spectrum and the measured spectrum was verified.

- We then started increasing the power of the driving field with the help of a combination of neutral density filters with different transmission coefficients (which can vary between 1% and 91%). It was then possible to evaluate the behavior of both phase shift and absorption as a function of the driving field.

- A fitting method had been developed: it provided the coefficients for the theoretical curve describing the profiles for different driving fields. It was then evaluated the values of both phase shift (or, better, the value of the derivative of the index of refraction with respect to frequency) and absorption at the transition frequency.

- A comparison between the achieved characteristics and the desired ones is performed. Is the medium, prepared in this way, suitable for application inside a resonator? Do the performances of the optical resonator change significantly under the present conditions?

Regarding these last questions, an extra discussion follows. In general we have that the phase shift and absorption profiles correspond to the predicted ones. Furthermore a decreasing of both dispersion and absorption on the resonance is observed. In the profiles it is possible to recognize both the so called Rabi side bands while the structure of the profile around the transition (which possesses a smaller signal to noise ratio) is still well resolved. It was also possible to observe that the decrease in the absorption with increasing pump laser power was stronger than the decrease in dispersion. For both of them a good agreement with the predicted theoretical curves was observed.

4.2   The profiles

4.2.1   Absorption and dispersion profiles

First both absorption and dispersion profiles were measured in absence of the driving field. The different measurements performed are depicted in Fig4.1.

The probing laser system provides $\approx 5.7mW$ of blue power at the output of the **SHG** (Second Harmonic Generator). This is much more than the power necessary to probe the atoms without saturating them. The beam is consequently attenuated using the neutral density filter combination OD 0.04 + OD 0.5 + NG 4 (corresponding to transmissions of 91%, 32% and 26% respectively) until we obtained at the output photodiodes of the interferometer $PD1 = 120\mu W$, $PD2 = 125\mu W$, which correspond to $\approx 40\mu W$ power in the interaction zone. The beam is slightly elliptical and astigmatic, even if corrected with help of two lenses one of them tilted. The dimensions of the beam waists in the horizontal and vertical planes are $w_{hor} = 135\mu m$ and $w_{vert} = 133\mu m$ respectively, and the distance of the foci in the interaction zone are $\Delta z_{hor} = 1.08 \times 10^{-4}m$ and $\Delta z_{vert} = 2.35 \times 10^{-2}m$ respectively. This corresponds to a probing field intensity of $\approx 730\mu W/mm^2$, while the saturation intensity is $I_{sat} = 1.2mW/mm^2$ [59]. Hence, saturation effects due to the test field are not to be expected.

The represented phase shift and absorption, expressed in $mrad$ and $1 - exp(-\alpha l_{int}) \approx \alpha \times l_{int}$ respectively, (where l_{int} represents the length of the interaction zone with the atoms which is $\approx 1mm$) are function of the probing field frequency.

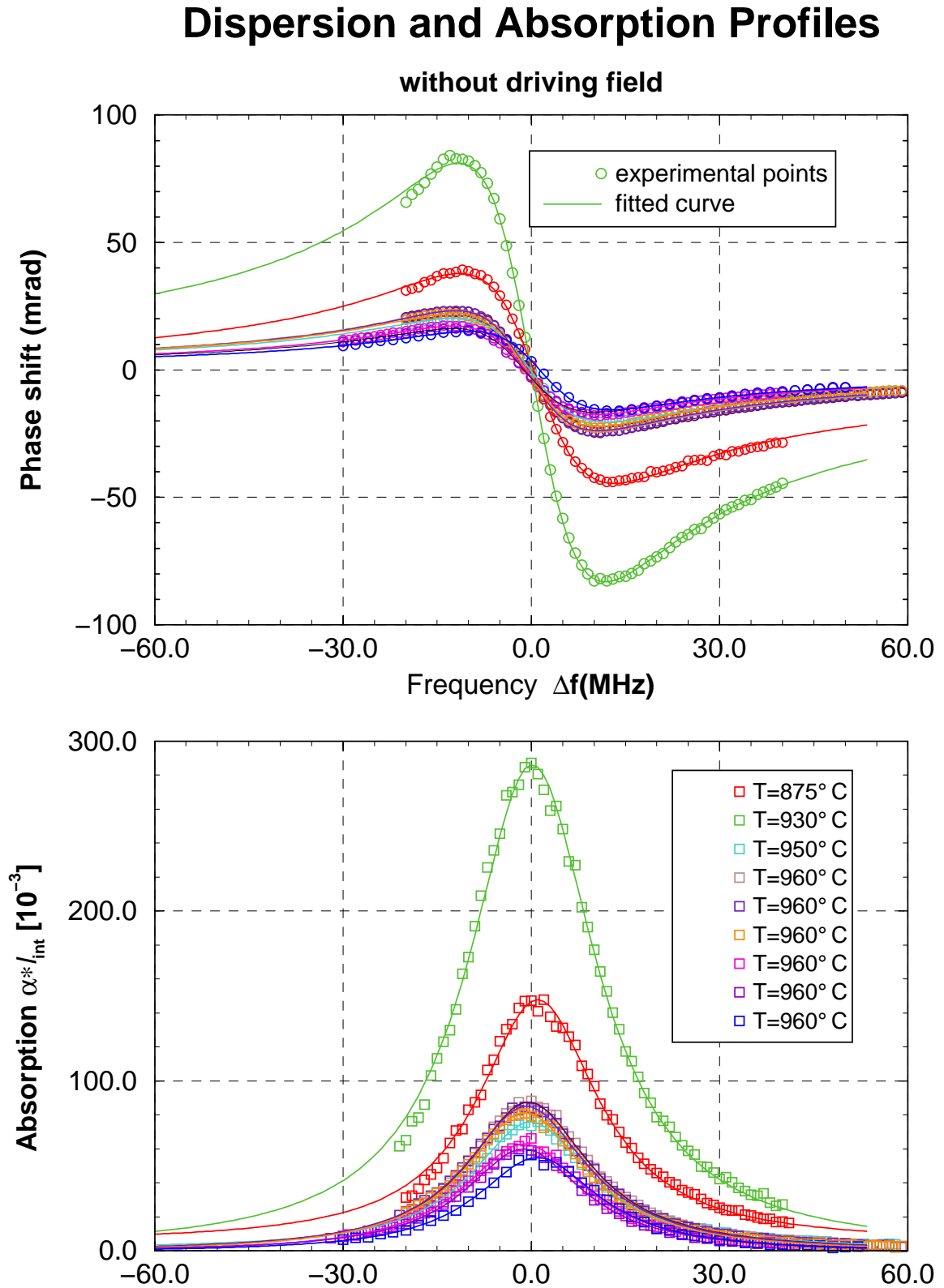# Dispersion and Absorption Profiles

without driving field

Figure 4.1: Profiles of dispersion and absorption in the absence of the driving field for different oven temperature. The values of the fitted parameters are reported in tables 4.1 and 4.2. The different corresponding temperatures are also reported.

The frequency scan varied between $\approx -20MHz$ and $\approx 60MHz$, where the transition frequency corresponds to $0MHz$.

The results represented are obtained using a calibration procedure to calculate phase shift and absorption from voltage signals. It is described in the following section.

4.2.2   Calibration of the signals

Let us first consider the laser and fix its optical frequency. Passing the atoms the beam experiences a certain phase shift φ and an absorption α.

The atomic beam is chopped and consequently the resulting phase shift signal has the form of a square wave, centered around u_0^P, with a height equal to $\hat{u}_P$.

Such a signal goes to the lock-in dual amplifier (Fig 4.2). Its output signal provides the rms value $(u_0^P/\sqrt{2})$ of the Fourier component at 1.7kHz (chopping frequency) of the input signal $(\hat{u}_P 2/\pi)$, multiplied by a factor G_B corresponding to the gain of the bandpass filter (8 zeros and 8 poles filter) used to suppress the higher harmonics of the signal.
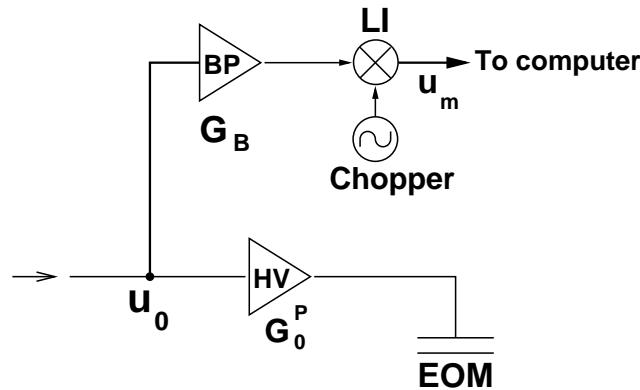

Figure 4.2: Schematic for the calibration of the phase shift signal: the signal u_0 passes a bandpass filter (**BP**), with gain G_B and then enters the lock-in dual amplifier (**LI**). The output signal u_m goes to the computer. u_0 is also used to lock the interferometer through the electro optical modulator (**EOM**), after passing an high voltage (**HV**) amplifier with gain G_0^P

The measured signal at the output of the lock-in amplifier takes consequently the form:

$$u_m = \frac{2}{\sqrt{2}\pi}G_B u_0 = \frac{\sqrt{2}}{\pi}G_B u_0. \tag{4.1}$$

The phase shift corresponding to a particular voltage on the EOM can be derived by considering the G_0^P gain of the high voltage amplifier for the EOM, and its half wave voltage

u_λ. The relation between the phase shift experienced and the voltage measured then results:

$$\varphi = \frac{2\sqrt{2}}{u_\lambda} \frac{G_0^P}{G_B} u_m. \tag{4.2}$$

The latter represents a constant calibration factor, depending on the gain of some of the electronic components and from the half wave voltage on the EOM, u_λ.

For the absorption signal the procedure is similar, but the fact that the calibration factor is dependent on the power of the probing laser has to be considered. Furthermore it should be noted that the absorption signal, is contained in the DC component of the interferometer output, and consequently it is dependent on the modulation index of the EOM[1] as it is not demodulated at $1.8MHz$, as it is done for the phase shift.

Let us now describe the procedure to calculate the calibration factor for the absorption signal. In expression (3.9) we have the difference of the DC component of the photodiodes, under the hypothesis that their gain is the same, not considering higher order terms. It can be written in the form:

$$I_0 2 J_0(M_P) r_1 t_1 [1 - \alpha/2] \cos \varphi = \hat{u}(M_P)[1 - \alpha/2] \cos \varphi, \tag{4.3}$$

where the term J_0 is dependent on the modulation index and I_0 represents the laser field intensity injected in the interferometer. To determine the latter the u_A^0 is measured: it is the peak to peak value on the photodiodes, when the interferometer is swept, the EOM is off (and consequently $M_P = 0$) and no atoms are present in the interaction zone (i.e. $\alpha = 0$). Under the hypothesis that the interferometer is locked on the "dark fringe" (and consequently $\cos \varphi = 1$) we have that $u_A^0 = 2\hat{u}(M_P = 0)$. In general:

$$\frac{\hat{u}(M_P)}{\hat{u}(0)} = J_0(M_P), \tag{4.4}$$

and consequently

$$\hat{u}(M_P) = J_0(M_P) \frac{u_A^0}{2}. \tag{4.5}$$

It is now necessary to apply exactly the same procedure used for the calibration of the phase shift signal, and to consider that the lock-in dual amplifier provides the rms value of the Fourier component at $1.7kHz$ of the signal i.e. $u_F^A = \hat{u}(M_P)\alpha/\sqrt{2}\pi$. Once more it is necessary to consider both the gains of the preamplifier G_{PR} and of the bandpass filter G_B^A (4.3). Consequently the signal at the output of the lock-in amplifier is expressed by:

$$u_{LI}^A = \frac{1}{\sqrt{2}} G_{PR} G_B^A \hat{u}(M_P) \frac{\alpha}{\pi} = \frac{1}{\sqrt{2}} G_{PR} G_B^A \frac{J_0(M_P) u_0^A}{2} \frac{\alpha}{\pi}. \tag{4.6}$$

---

[1]It was also observed that this modulation index was not constant, causing an uncertainty in the calibration factor; it was then monitored during the laser scan

Consequently the relation between the absorption coefficient α and the tension measured at the output of the lock-in amplifier is:

$$\frac{\alpha}{2} = \frac{\sqrt{2}\pi}{G_{PR}G_B^A J_0(M_P)u_A^0} u_{LI}^A. \tag{4.7}$$

We have observed that the calibration factor does not remain constant, depending on the modulation index M_P. To take account of possible variation in the laser power, consequently the term u_A^0 has be written in the form:

$$u_A^0 \rightarrow u_A^0 \frac{u_{PR}}{u_{PR}^0}, \tag{4.8}$$

where:

- u_{PR}^0 represents the voltage on the photodiode which measures the laser power at the output of the **SHG** at the analog to digital converter used to monitor the laser power signal, in absence of the atoms and with the interferometer aligned.

- u_{PR} is the same signal monitored during the measurement, in the presence of the atoms.

The schematic for the measurement is represented in Fig4.3.
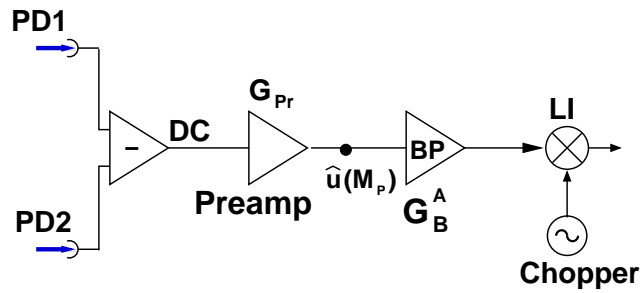
Figure 4.3: Schematic for the calibration of the absorption signal

4.2.3 The profiles in absence of the driving field

The measured profiles were fitted using the theoretical expression for the absorption and dispersion derived from the density matrix of a two level atom which experiences the presence of two different (classical) electromagnetic fields. For the evaluation of the density matrix the approximation of a very weak probing and a variable driving field was used.

N_{at}	$x_0 \times 10^{-2}$	g	$a \times 10^{-2}$	$\partial_\omega n(\omega_0)$
0.3917(15)	1.12(15)	0.6908(63)	-3.35(15)	-715.98
0.7714(22)	0.24(10)	0.6955(44)	-0.92(21)	-1493.02
0.1924(35)	-0.46(70)	0.6999(28)	-0.094(35)	-370.12
0.2222(41)	-1.92(68)	0.6997(28)	-0.377(38)	-427.46
0.2212(41)	-2.27(67)	0.6802(27)	-0.293(38)	-437.82
0.2074(50)	-2.52(89)	0.6756(26)	0.057(32)	-413.27
0.1623(34)	-2.83(28)	0.6759(36)	-0.127(28)	-323.16
0.1539(53)	-3.31(12)	0.6740(28)	-0.183(40)	-307.35
0.1446(53)	3.97(13)	0.6687(44)	-0.257(39)	-291.14

Table 4.1: Fitted values in the absence of driving field: N_{at} is particle density (in units of 10^{16} particles per m^3), x_0 detuning of the resonance frequency, g line width of the transition (both in natural line width units literature value $\gamma_1 = 2\pi \times 34MHz$), a offset, $\partial_\omega n(\omega_0)$ is the value of the index of refraction derivative calculated on the transition frequency (multiplied for a factor 10^{-10} and in units of MHz^{-1}). Values calculated from the phase shift curves

The mathematical expression of the function [55] is reported in (2.18) and has already been discussed.

The parameters fitted are:

- The particle density N_{at}, which can vary due to variation of the oven temperature.

- The detuning of the probing laser to transition frequency x_0: it can deviate slightly from zero because of the transition frequency detuning due to the imperfect orthogonality between the atomic beam and the probing laser beam.

- The natural line width g, expressed in units of $\gamma_1 = 2\pi \times 34MHz$

- The "Rabi-Frequency" dp also expressed in units of γ_1, which is proportional to the amplitude of the driving field through the relation (2.6).

- A variable offset a.

- The detuning of the driving laser frequency ω_d, when the atoms are driven, due to the imperfect orthogonality between the **driving** field, and the atomic beam (Doppler effect).

N_{at}	$x_0 \times 10^{-2}$	$g \times \gamma$	$a \times 10^{-2}$	$\alpha(\omega_0)$
0.3348(33)	3.03(32)	0.6878(14)	4.79(1.26)	147.82
0.6708(54)	0.41(22)	0.7322(12)	-0.32(2.17)	286.24
0.1755(73)	-0.34(13)	0.6758(55)	0.93(20)	75.90
0.2068(69)	-1.28(11)	0.6875(45)	-0.63(18)	87.71
0.2014(59)	-2.35(95)	0.6979(40)	-0.86(16)	85.18
0.1924(79)	-2.94(13)	0.6957(56)	-1.04(21)	81.13
0.1501(91)	-3.35(17)	0.7075(91)	-1.25(34)	62.87
0.1418(97)	-3.55(21)	0.6784(96)	-0.56(29)	75.48
0.1310(12)	2.87(28)	0.6987(13)	-1.04(37)	54.92

Table 4.2: Parameters fitted values: N_{at} particle density (in unities of 10^{16} particles for m^3), x_0 detuning of the resonance frequency, in bandwidth unity (literature value $2\pi \times 34MHz$), g line width of the transition in bandwidth unity, a offset. $\alpha(\omega_0)$ is the absorption at the transition frequency in m^{-1}. Values calculated from the absorption curves

With respect to the latter question it has to be underlined that this effect could not be completely avoided because of difficulties inherent to the actual setup of the experiment. It is in fact of first importance to achieve the maximum orthogonality possible between the probing field and the atomic beam. They can be considered to be laying in the horizontal plane, orthogonal to each other.

Let us now consider the driving field: it **cannot** lay exactly on the probing field, otherwise it would cause the presence of an additional signal (or actually, noise) at the output of the interferometer: so it cannot lay in the same horizontal plane containing the probe and atomic beam. But it should also be orthogonal to the latter, to avoid problems in the shifting of the transition frequency due to the Doppler effect. The probing and pumping field then lay in the vertical plane perpendicular to the atomic beam, with an angle θ between them.

On the other hand the driving field is coupled into the interaction zone with help of the second input of the input beam splitter of the interferometer (see Fig3.1). Consequently the angle θ results small (less than $3°$). In the actual configuration it is otherwise quite hard to align the driving field exactly in the vertical plane. The consequence is then the presence of a slightly horizontal angle which corresponded in the measurement to a detuning of the transition frequency, proportional to the strength of the driving field.

The first set of measurements realized, in absence of driving field, was used to observe the evolution of the particle densities with time and oven temperature.

In this way, the evolution of the particle densities was monitored over several hours. The current in the heating of the oven was constant. As expected, the density showed a strong fluctuation during the first hour (before an equilibrium was reached in the oven chamber), afterwards it remained almost constant for ≈ 3 hours, and then it started to decrease. Because the signal to noise ratio is strongly dependent on the number of particles present in the atomic beam, it was decided that the measurement should be interrupted and the oven chamber filled with Calcium once more.

4.2.4 The fitting method

Let us now observe the functions to which we want to fit the measured profiles. For the phase shift as a function of the detuning x from the transition frequency (x_0) the following relations are in fact valid:

$$f(x) = a + 10^3 l_{eff} \frac{\omega_0}{c_0} \times \frac{1}{2} \Re(\chi(x)), \tag{4.9}$$

where

$$\chi(x) = N_{at} \times 3\pi \frac{c_0^3}{\omega_0^3} \times g \frac{1}{2E_p} \times \rho(x), \tag{4.10}$$

and

$$\rho(x) = E_p \times \frac{(1 + dp^2 \times Q_1^\star(x)/P_1^\star(x))}{(x - x_0 - ig_2)} \frac{ig}{P_0(x)}. \tag{4.11}$$

Part of the parameters are described in the preceding section. Furthermore, we have that c_0 represents the velocity of light in a vacuum, ω_0 is the transition frequency. E_p is the Rabi side band corresponding to the probe field; it is set to 10^{-6} in the fit procedure, because we are assuming the presence of a very weak probing field. l_{int} is the interaction length (set to $1mm$ in the fitting procedure). The terms $P_1^\star$, $P_0(x)$, and $Q_1^\star$ are the ones reported and discussed in (2.21).

It is possible to observe that part of the parameters are strongly connected to each other and have a correlation which is, at least for some of them (i.e., N_{at} and g or dp and x_0), almost equal to one.

Consequently the fitting procedure presented some difficulties.

Its aim is in fact to minimize the function $\chi^2 = \frac{\sum_i [y_i - f(x)]^2}{n - m - 1}$ (reduced χ^2) where y_i are the experimental points and $f(x_i)$ is the function to be fitted, which depends on various parameters. When the parameters are connected and correlated to each other, there is the risk of getting stuck in a local minimum of the function χ^2 instead of a global one: the result is then strongly dependent on the initial values chosen for the parameters.

Our aim is then to find a global minimum of this function with respect to the parameters

described in the preceding section.

A method has been used which should bypass the difficulties of finding local minima. This method, developed by W.L. Price, has been analyzed relating to the detection of gravitational waves [32] where quite precise methods are useful in the analysis of the signals.

Let us suppose we want to find the global minimum of a function f of m parameters, each of which can vary between a maximum and a minimum. In our case this interval is defined considering the physics of the variables considered.

Let us then choose N different combinations of these parameters, each of them chosen randomly in its variation intervals. Each combination of the m (6 in our case) parameters represent a trial point for the function χ^2.

In this way we are able to build a grid, of dimensions $N \times (m+1)$. Each column of the array corresponds to one of the $m = 6$ parameters, and to each row of this array corresponds the trial point and the function χ^2 which has to be minimized, calculated for the particular combination.

We can then obtain the structure:

$$\begin{pmatrix} x_{11} & x_{12} & x_{13} & x_{14} & x_{15} & x_{16} & f_1 \\ x_{21} & x_{22} & x_{23} & x_{24} & x_{25} & x_{26} & f_2 \\ x_{31} & x_{32} & x_{33} & x_{34} & x_{35} & x_{36} & f_3 \\ ... & ... & ... & ... & ... & ... & ... \\ x_{N1} & x_{N2} & x_{N3} & x_{N4} & x_{N5} & x_{N6} & f_N \end{pmatrix}$$

It is then possible to identify the row corresponding to the maximum value of $f = \chi^2_{max}$. Then the process of minimizing the function can begin.

The first trial point is chosen in the following way: seven (corresponding to $m+1$) points in the array are randomly chosen and the centroid ($G = \frac{\sum_i x_{i1}}{6}$) of the first six is calculated. Then it has to be considered:

$$P = 2 \times G - R_{m+1}. \tag{4.12}$$

The function χ^2 is then evaluated at the point P and its value is compared with χ^2_{max} of the grid. If $\chi^2(P) < \chi^2_{max}$ then the point P is substituted for the point corresponding to the χ^2_{max}, and the procedure is repeated. In all other cases the latter happens without making the substitution.

The process is stopped when the maximum number of iterations has been reached (a typical value was 50000 iterations), or when the χ^2 function reaches a limit, which could also be fixed (typically a value of 1 was chosen).

The fitted function is then calculated for the parameters value which minimize the χ^2 function.

Using this procedure the set of N points tend to cluster to the minima because of the random process of choosing the points which constitute the grid. Some trial points, on the

other hand, can also be far away from the local minima, so it is possible to get out of them. It can be demonstrated [32] that with increasing number of iterations the distribution of the grid points will tend to a Gaussian distribution. If the dimension of the grid is large enough, the mean value of this distribution will be coincident with the global minimum. Using this method it was possible to fit our different curves and to determine the values of the parameters. A good correspondence between the curves and the measured values could then be observed (see Fig 4.1). Furthermore the fitting method was tested increasing the total number of the trial points and of the maximum iterations, without significant changes in the results. Once the fitted curves had been calculated, it was also possible to evaluate the values of both absorption and dispersion at the transition frequency.

4.2.5   Fitted curves

As can be observed in the representation of the absorption and dispersion profile measurement of Fig4.1, the agreement between the experimental curves and the fitted ones is very good.

In tables (4.2) and (4.1) the calculated values of the fitted parameters from the absorption and dispersion curves are represented.

It can be underlined that the already illustrated evolution in the particle densities was observed, while, as to be expected, the line width of the transition remains almost constant.

The experimental value of the natural line width of the transition is $\approx 22MHz$ which can be compared to the expected result of $34MHz$ [59] which was found in the literature. On the other hand the value we calculated corresponds to the one given by Hiller [22], derived from life time measurements as function of Ca atomic density.

The difference between the values is to be attributed to radiation trapping effects which play a role under conditions of atomic densities, velocities and spatial dimensions similar to ours [22], [23].

The observed detuning of the transition frequency from the zero value corresponds to a residual transversal Doppler shift well below the natural line width.

The corresponding values calculated from the absorption curves are approximately the same. The slight difference in the particle density can be attributed to the major role played by the offset when fitting an even instead of an odd function.

Furthermore if we observe the value of the derivative of phase shift and the absorption on the transition frequency, both of them, as expected, are dependent on the particle densities. The errors given to the fitted values are purely statistical ones deriving from our fitting process.

N_{at}	x_0	g	a	dp	ω_D
0.05359(17)	0.0902(82)	0.6401(33)	-0.1099(84)	0.0737(11)	-0.0975(84)
0.04414(13)	0.1086(90)	0.7267(39)	-0.1397(73)	0.0743(79)	0.0423(11)
0.05149(22)	0.1069(92)	0.6757(46)	-0.0557(59)	0.1031(50)	0.0391(49)
0.058166(17)	0.0687(77)	0.6375(29)	-0.0626(19)	0.1180(01)	-0.2204(52)
0.047197(55)	0.1237(24)	0.5632(11)	-0.0376(19)	0.13748(39)	0.9292(11)
0.068831(10)	0.1386(33)	0.6220(13)	-0.0920(11)	0.2208(44)	0.0826(25)
0.039934(19)	0.0693(11)	0.7608(19)	0.1222(29)	0.3209(68)	0.0742(34)
0.063921(11)	0.0138(67)	0.7531(16)	0.0319(70)	0.4100(63)	0.0359(55)
0.034986(12)	0.1176(31)	0.9000(18)	0.0269(69)	0.4154(68)	0.0657(31)
0.034606(21)	-0.0056(24)	0.7314(23)	0.0271(73)	0.6478(13)	-0.0445(12)

Table 4.3: Fitted parameters values: N_{at} particle density (in units of 10^{16} particles for m^3), a offset, x_0 detuning of the resonance frequency, g line width of the transition, dp Rabi frequency, ω_d detuning due to driving field. All the latter parameters are expressed in $\gamma_1 = 2\pi 34 MHz$ units. Values calculated through the fitting of the dispersion curves

4.2.6   Increasing the driving field

The next step in the realization of our negative dispersive transparent medium was to drive the atoms with the help of the pumping field and observe the evolution of the phase shift and absorption profiles.

The different measurements of the profiles corresponding to increasing driving powers are presented.

The maximum achieved power was $\approx 14.7mW$ at the output of the SHG frequency doubling cavity. It corresponded to $\approx 12.4mW$ at the input of the interferometer. The use of the concept of a strong unbalanced interferometer, and the use of the same input beam splitters for the probing and pumping field (through the two different inputs) allows the pump beam to be almost completely coupled into the test arm.

Even in this case a telescope with the first lens tilted is used to optimize the beam geometry of the driving field at the interaction zone: it is in fact necessary for the power distribution of the driving field to be almost constant, and for its radius to be much bigger then the probing one, so that the atoms which are probed experience a constant driving power.
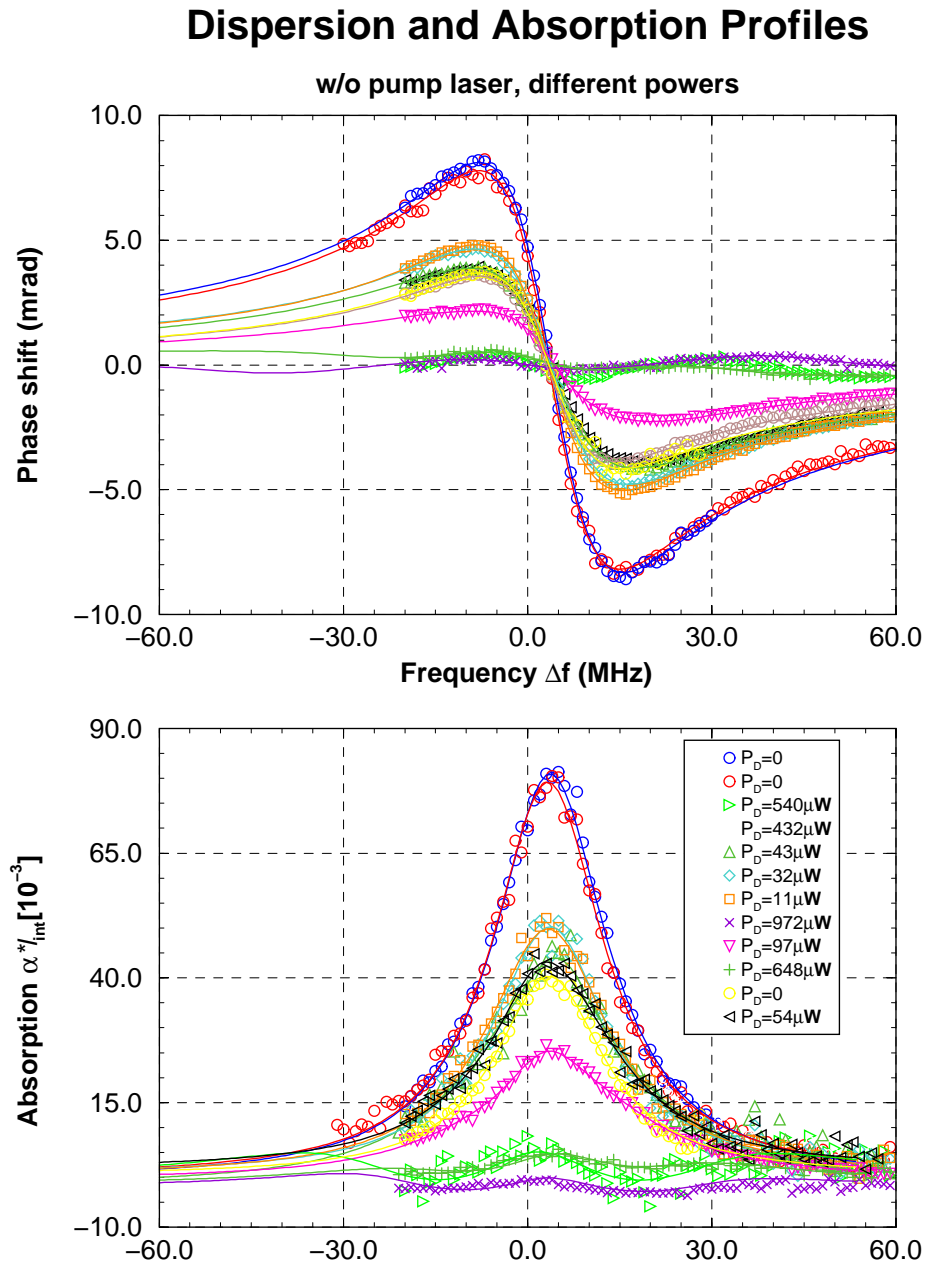
Dispersion and Absorption Profiles

Figure 4.4: Absorption and dispersion profiles corresponding to different driving field powers. The driving field varies between $0 mW$ (no driving field) and $\approx 1.2 mW$ (9% of transmission). The decrease in both dispersion and absorption, compared to the curve without the driving field, has to be observed. For the stronger driving fields it is also possible to observe the structure of the Rabi side band. The asymmetry of the the frequency scan with respect to the transition frequency, due to problems of the laser system, allow to observe only the right side band.

4 Experimental results

The values for the beam geometry obtained are then:

- $w_{hor} = 308\mu m$ in the horizontal and $w_{vert} = 366\mu m$ in the vertical direction for the beam waist.

- $b_{hor} = 1.25m$ in the horizontal and $b_{vert} = 1.99m$ in the vertical direction for the confocal parameters.

- $\Delta z_{hor}/b_{hor} = 0.18$ in the horizontal and $\Delta z_{vert}/b_{vert} = -0.015$ in the vertical direction for the foci distance from the interaction zone.

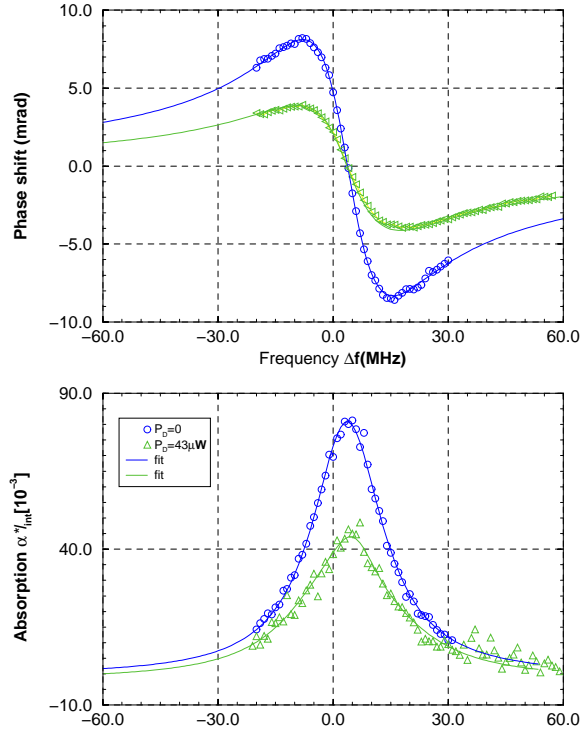Consequently the maximal intensity of the driving field in the interaction zone is $\approx 3.30 mW/mm^2$.

Figure 4.5: Absorption and dispersion profiles for no driving and weak driving field ($\approx 43\mu W$). It is possible to observe only the decreasing of the dispersion and of the maximum value of the absorption curve. No Rabi sideband structure is observable. The fitted values of the parameters are reported in Tables (4.3, 4.4)

In this case the fitting method developed was particularly useful, because of the increasing in the number of parameters to be fitted.

N_{at}	$x_0 \times \gamma_1$	g	a	dp	ω_D
0.20749(17)	0.0500(83)	0.7000(33)	-0.8442(76)	0.4182(55)	0.0523(27)
0.09731(26)	0.0500(90)	0.5671(46)	-2.1377(98)	0.3772(63)	0.0913(33)
0.19460(43)	0.0500(77)	0.5670(37)	-2.1375(87)	0.3772(27)	0.0913(39)
0.14744(27)	0.6108(58)	0.6540(65)	-0.6483(53)	0.1427(46)	0.0828(45)
0.21538(38)	0.1394(63)	0.8981(53)	-2.8308(69)	0.3862(35)	0.0877(68)
0.21259(18)	0.0768(44)	0.6028(62)	0.2400(45)	0.0880(62)	-0.3103(89)

Table 4.4: Fitted values for the variables: N_{at} particle density (in units of 10^{16} particles per m^3), x_0 detuning of the resonance frequency, dp Rabi Frequency, ω_d detuning due to driving field, g line width of the transition in bandwidth units (literature value $2\pi 34 MHz$), a offset. Values calculated from the absorption curves

The particular case where the driving field is still quite weak (Fig 4.5), had to be treated with particular attention. In this case in fact, the Rabi side bands, whose distance to the transition is proportional to the amplitude of the field, are not clearly resolved and their structure is superimposed onto the transition structure. The measured profiles are represented in Fig 4.4.

Firstly it can be observed that a decrease in both the absorption and the dispersion profile occurs. The profiles near the transition frequency are still well resolved.

Two different curves corresponding to a driving field of $0mW$, and $0.041mW$ (0% and 0.4% of the pumping field respectively) are depicted in Fig4.5. In the driven curve ($P_D \approx 50\mu W$) it is possible to observe the decrease in both the profiles. In Fig 4.6 two curves are instead compared, one measured in the absence of the driving field ($\Omega_D = 0MHz$) and the second one for a strong driving field ($\Omega_D = (2\pi)22MHz$). In this case it is possible to observe both (left and right) Rabi side band structures. The atoms also exhibit gain without inversion near the bare atomic resonance ($\alpha \cdot l_{int} < 0$)[20]. For no driving, the fitted parameters are: $N_{at} = 7.513(17) \times 10^{14}m^{-3}$, $\Delta f_0 = 32(26)kHz$, $g = 23.701(78)MHz$ from the dispersion and $N_{at} = 6.12(11) \times 10^{14}m^{-3}$, $x_0 = -2.27(20)MHz$, $g = 22.10(65)MHz$ from the absorption. For the driven atoms the fitted parameters are: $N_{at} = 6.76(18) \times 10^{14}m^{-3}$, $x_0 = -2.58(54)MHz$, $g = 20.84(75)MHz$, $\Omega_D = (2\pi)21.85(15)$, and $\Delta f_{drive} = 1.60(37)MHz$ for the dispersion and $N_{at} = 6.91(28) \times 10^{14}m^{-3}$, $x_0 = -1.19(71)MHz$, $g = 21.6(14)MHz$, $\Omega_D = (2\pi)22.62(20)$, and $\Delta f_{drive} = 1.50(51)MHz$ for the absorption.

The fitted values of our physical variables corresponding to different driving fields are represented in tables (4.3) and (4.4).
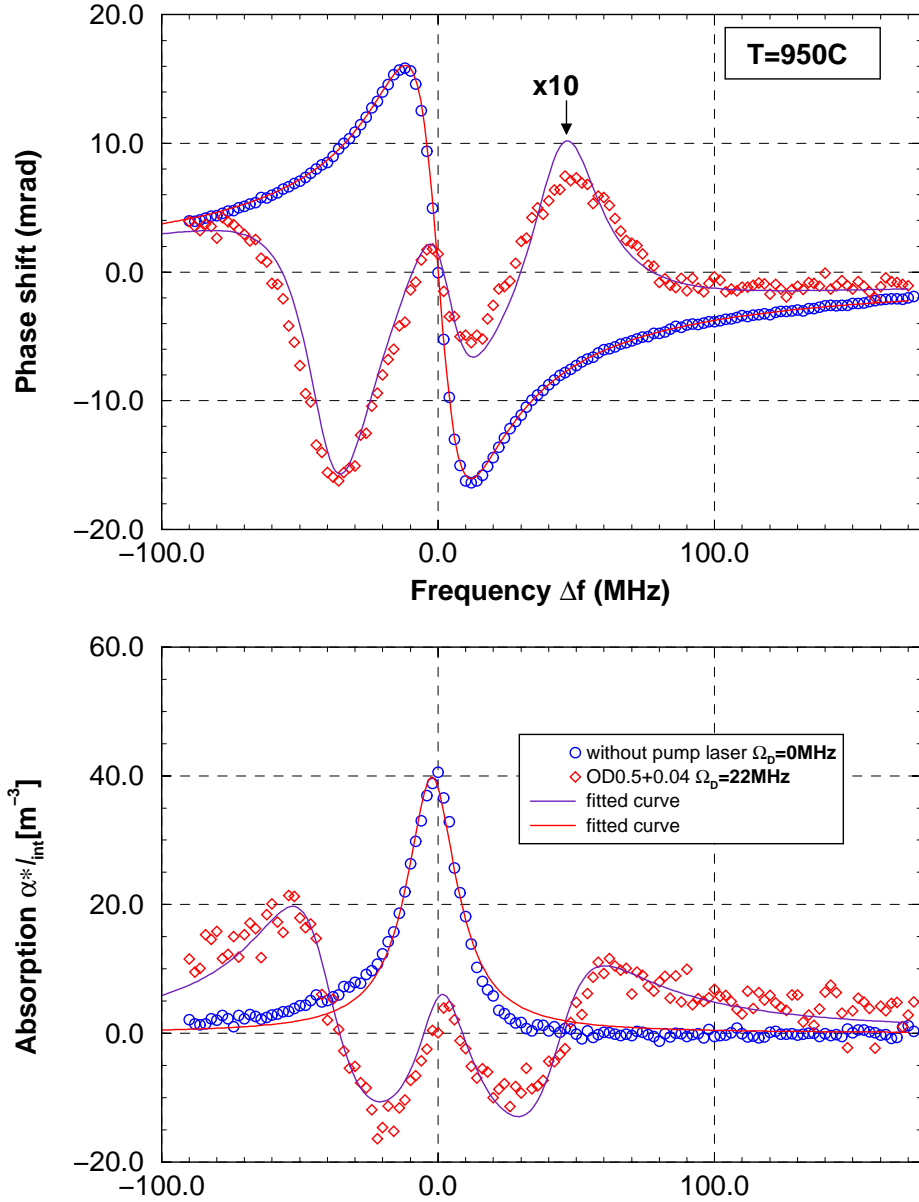
Figure 4.6: Absorption and dispersion profiles for no driving ($\Omega_D = 0 MHz$) and strong driving ($\Omega_D \approx 22 MHz$). The Rabi side band structure is clearly resolved. For the driven atoms both the fitted curve and the experimental points are multiplied by a factor 10 to render the comparison easier . For no driving, the fitted parameters are: $N_{at} = 7.513(17) \times 10^{14} m^{-3}$, $x_0 = 32(26) kHz$, $g = 23.701(78) MHz$, from the dispersion and $N_{at} = 6.12(11) \times 10^{14} m^{-3}$, $x_0 = -2.27(20) MHz$, $g = 22.10(65) MHz$ for the absorption. For the driven atoms the fitted parameters are: $N_{at} = 6.76(18) \times 10^{14} m^{-3}$, $x_0 = -2.58(54) MHz$, $g = 20.84(75) MHz$, $\Omega = (2\pi)21.85(15)$, and $\Delta f_{drive} = 1.60(37) MHz$ for the dispersion and $N_{at} = 6.91(28) \times 10^{14} m^{-3}$, $x_0 = -1.19(71) MHz$, $g = 21.6(14) MHz$, $\Omega = (2\pi)22.62(20)$, and $\Delta f_{drive} = 1.50(51) MHz$ for the absorption.

If we then analyze the results obtained, it is important to underline that, as expected, the line width of the transition remains a constant and its value is comparable with the one calculated in the absence of a driving field.

With respect to the strongest driving field ($\approx 600 \mu W$) the signal to noise ratio is strongly reduced, but the Rabi side band located at $\approx 12 MHz$ and the profile structure around the transition frequency are still quite well resolved.

4.3   Dispersion and absorption on the transition

Once it was possible to fit the measured experimental values, to the curves which represent phase shift and absorption for a two level atom in the presence of an electromagnetic field (or, to be more precise, two electromagnetic fields one of them very weak), it was possible, with aid of the fitted curve to calculate both absorption and phase shift at the transition frequency. These results could then be compared with the curves which are derived from the theory.

In fact we have the expressions for absorption and the derivative of the index of refraction, calculated at the transition as a function of the driving field (Rabi-sideband frequency):

$$\alpha_{P,0} = 2\frac{\omega_0}{c_0} N_{at} \frac{3\pi c_0^3}{2\omega_0^3} \frac{1}{[1 + 8(\Omega_D/\gamma_1)^2]^2} \tag{4.13}$$

$$n'_{P,0} = \frac{2}{\gamma_1} N_{at} \frac{3\pi c_0^3}{2\omega_0^3} \frac{1 + 32(\Omega_D/\gamma_1)^4}{[1 + 8(\Omega_D/\gamma_1)^2]^3} \tag{4.14}$$

which asserts that the absorption decreases more strongly than dispersion.

In the expression above, ω_0 represents the transition frequency, c_0 is velocity of light in a vacuum, N_{at} is the particle density, Ω_D is the Rabi sideband frequency and γ_1 is the natural line width of the transition.

We then had the possibility to make a comparison of the values obtained using the fitting method, and the corresponding theoretical curves.

It must be underlined that both the theoretical curves have a multiplication factor dependent on the particle densities and, in the case of the dispersion, the natural line width of the transition which has to be considered. Therefore to render possible the comparison between the results obtained during different measurement sessions, where at least the particle density had to be different, a sort of normalization had to be done. In fact n'_0 and α_0 were first calculated and then these values were normalized to a particle density $N_{at} = 1 \times 10^{16} m^{-3}$, which is of an order of magnitude comparable with the one achieved during the experiment.

In this way it is possible to analyze the different results achieved. In the log-log representation of Fig4.8 the experimental points for the weakest values of the driving field are
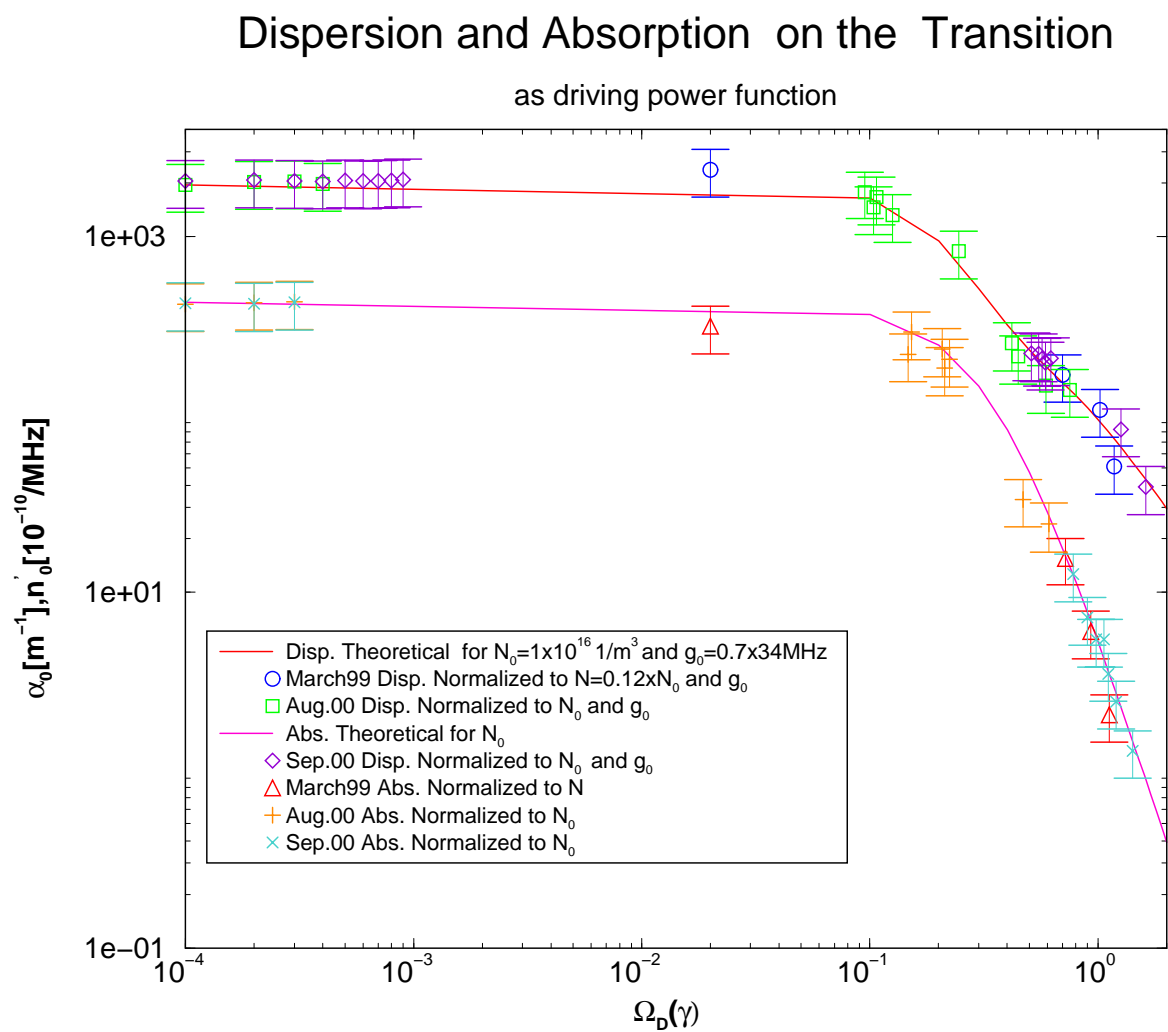
Figure 4.7: Absorption and dispersion at the transition frequency as a function of the driving field. Values normalized to $N_{at} = 1 \times 10^{16} m^{-3}$
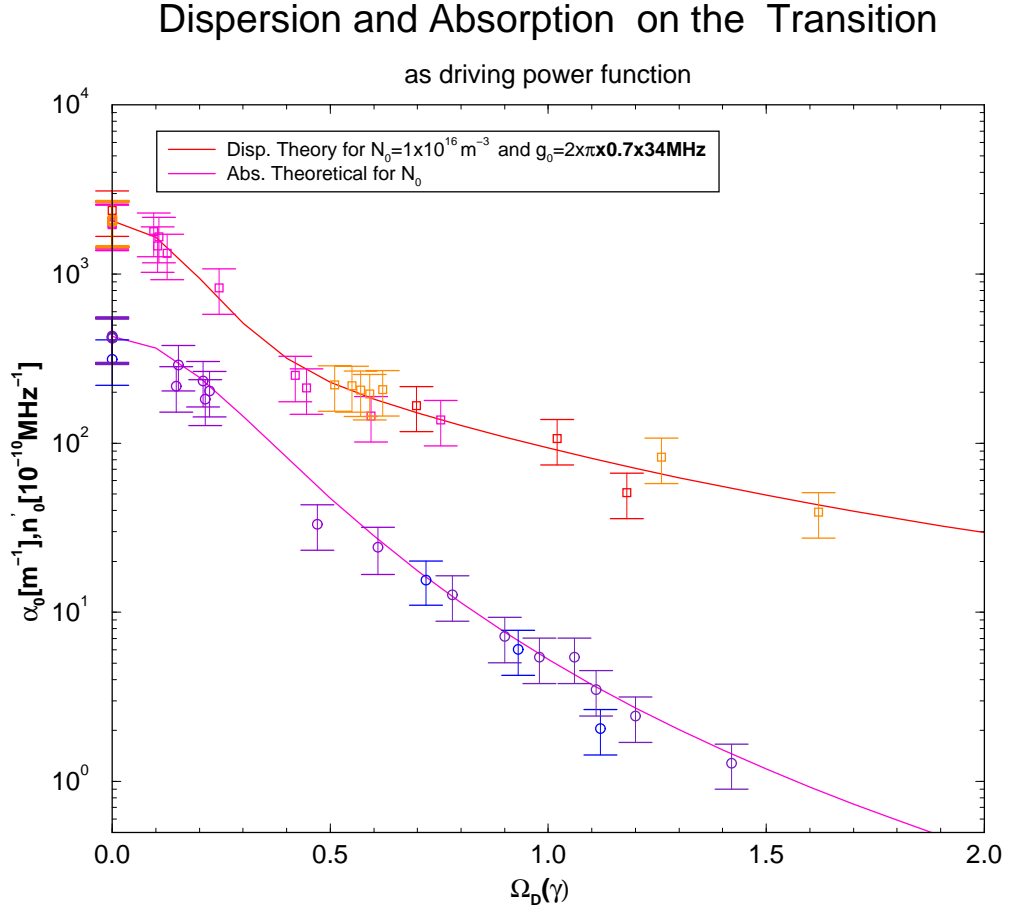
Figure 4.8: Absorption and dispersion at the transition frequency as a function of the driving field. Values normalized to $N_{at} = 1 \times 10^{16} m^{-3}$. Linear representation

actually the ones calculated in the absence of the driving field ($\Omega_D = 0$). It can also be noticed that the regime where the decreasing of the absorption is stronger than that of the dispersion was reached.

With respect to the maximal driving field available, which corresponds to a power in the interaction zone of $\approx 12mW$, and consequently to a saturation parameter of $S = (2\Omega/\gamma)^2 = 6.8$ the values of $d_\omega n_0 = -(4.8 \pm 1.0) \times 10^{-10} MHz^{-1}$ for dispersion, corresponding to $\alpha_0 = (0.18 \pm 0.04)\% cm^{-1}$ for the residual absorption are achieved.

4.4 The medium in a cavity

Let us consider now, what would happen if we filled an optical resonator with a medium under the conditions we were able to achieve. We have in fact already observed that the presence of a medium in an optical resonator changes its properties.

4 Experimental results

First we need to recall the equation defining the transfer function of the resonator, as the ratio of the transmitted to injected intensity. We then have:

$$\frac{I^t}{I^{in}} = \frac{\mathcal{T}^2}{(1-\mathcal{R})^2} \frac{1}{1 + 4\frac{\mathcal{R}}{(1-\mathcal{R})^2}\sin^2\frac{\Delta}{2}},$$ (4.15)

where $\mathcal{R}^2 = R_1 R_2(t_m^2)$, $\mathcal{T}^2 = T_1 T_2 t_m^2$ and R_1, R_2, T_1, T_2 represent the reflection and transmission coefficient of the input 1 and output 2 mirrors, t_m is the amplitude transmission coefficient and $\frac{\Delta}{2} = \Phi_m = \frac{\omega}{c_0} n(\omega) L_r$ is the phase shift experienced by the field in a round trip due to the presence of the medium in the cavity under the hypothesis that the mirrors do not cause a further phase shift. If the condition (2.30) is verified then the wavelength of the field in the medium becomes independent from its frequency: we can talk of λ compensation: the dispersion of the medium compensates the frequency dependence of the vacuum wavelength.

We have to recall that to obtain a λ compensated medium for Ca at the transition at $423nm$, the dispersion should consequently reach the value $n_0' = -2.2 \times 10^{-10} MHz^{-1}$. In this case the band width of the resonator would increase with respect to an empty one.

We have still to underline that the enlarging of the resonator bandwidth is limited by the frequency interval where in the development of $n(\omega)$ around ω_0 (transition frequency) higher order terms can be neglected.

We want to practically analyze the conditions which were achieved experimentally, and if it would be meaningful to insert such a medium inside a resonator: we have in particular to take account of the modification in the bandwidth of the resonator and of its finesse considering that they are not any more inverse proportional. From the relations 4.14 and 4.13 we observe that once the transition frequency and its line width γ are fixed, the dispersion and absorption are dependent on the strength of the driving field and the particle density involved.

As a first example, we can observe that to obtain λ compensation at a particle density of $N_{at} = 5 \times 10^{16} m^{-3}$ a driving field of $13.5 \times \gamma$ (with $\gamma = 2\pi 34 MHz$) would be needed. On the other hand (from 4.13) the corresponding residual absorption would be $\alpha_0 = 0.1\% m^{-1}$ and if we filled a resonator of length $1cm$ and finesse 64×10^3 (empty) with such a medium, its finesse would become 33×10^3 decreasing of a factor ≈ 2. The bandwidth of the cavity, as derived from Fig 2.5, on the other hand would be increased by a factor ≈ 12.

Let us consider now the not driven TLA: to obtain λ compensation for Ca atoms which not strongly driven, (i.e. $\Omega = 0$), we would need a particle density of $N_{at} = \gamma \frac{4\pi}{3c_0\lambda_0^2} = 5 \times 10^{13} m^{-3}$. On the transition a not driven atom is strongly absorptive and the corresponding residual absorption is $\alpha_0 \approx 71\% m^{-1}$, which is about a factor of 700 more than the one obtained in presence of the driving field: considering that the height of the transmitted power is dependent on the absorption coefficient, it is easy to realize that it would

not have much sense to insert a strong absorptive medium inside a resonator. To calculate the modification of the characteristics of a resonator we need then to take account not only of the dispersion, but also of the residual absorption.

In order to take account of both quantities it is possible to consider the figure of merit, as the ratio of dispersion on the resonance to residual absorption, normalized to the inverse of the transition frequency.

$$FOM = \frac{\partial_\omega n_0}{-\frac{1}{\omega_0}\alpha(\omega_0)} = \frac{c_0}{\gamma}\frac{1 + 32(\Omega/\gamma)^4}{1 + 8(\Omega/\gamma)^2} \tag{4.16}$$

In the absence of a driving field the resulting figure of merit is $FOM \approx 1.4m$. For the strongly driven ($\Omega = 13.5\gamma$) λ compensated medium, the calculated figure of merit is on the other hand $FOM \approx 1000$.

Considering the relations (4.14), and (4.13), we can see that the most interesting result is the one corresponding to the maximum driving power we could achieve. Let us then analyze this case.

For a driving power of $\approx 12mW$ we fitted a Rabi side band value of $\Omega/\gamma = 1.6$, corresponding to a saturation parameter $S = (2\Omega/\gamma)^2 \approx 10.2$. The dispersion is $n_0' = (-39 \pm 12) \times 10^{-10}MHz^{-1}$ and the residual absorption $\alpha_0 = (1.28 \pm 0.38)\%m^{-1}$. These values were calculated for a particle density of $N_{at} = 1 \times 10^{16}m^{-3}$. The corresponding figure of merit is consequently $FOM \approx 13.6m$. It is approximatively a factor ten bigger than the not driven case and a factor approximatively 74 less than the strongly driven case.

In the absence of a driving field the measured values of dispersion on the resonance and residual absorption were $n_0' = -2060 \pm 620 \times 10^{-10}MHz^{-1}$ and $\alpha_0 = 422 \pm 127m^{-1}$ respectively with a calculated factor of merit of $\approx 2.18m$. Consequently the dispersion was decreased by a factor ≈ 53 and the absorption by a factor ≈ 330. Once more we can observe that the regime where absorption decreases more strongly than dispersion was achieved. We consequently increased the figure of merit by a factor ≈ 6. On the other hand, comparing the results achieved with the ones theoretically calculated, we can observe that the conditions achieved were far away from the ones desired in order to obtain an enlargement of the resonator bandwidth without losing in the transmitted intensity.

Furthermore we observe that for the particle density created and the driving field utilized, no λ compensation condition was achieved. Supposing the driving field had been fixed to the maximum achievable, i.e. $P \approx 12mW$, $\Omega/\gamma = 1.6$, then the particle density needed to achieve λ compensation would have been $N_{at} = 0.02 \times 10^{16}m^{-3}$, but the corresponding residual absorption would have been $\alpha_0 = 7.25\%m^{-1}$. Under these conditions the finesse of the cavity would be $\mathcal{F} \approx 1065$: it would have resulted dramatical decrease. Furthermore we observe that in the present experimental condition, using such a low particle density would have drastically decreased the signal to noise ratio, and it would have

become extremely complicated to distinguish the profiles.

Finally we can conclude that:

- the theoretical stronger decrease in the absorption with respect to dispersion was demonstrated, illustrating that in principle it is possible to realize a "white light resonator".

- to reach a more useful regime the absorption should be furthermore suppressed, i.e. a stronger driving field should be used. To this aim a completely different laser system should be developed.

4.5   Realizing a "White light resonator"

As described in the preceding section with our experimental setup we were able to realize a negative dispersive with decreased absorption medium. We also were able to demonstrate the correspondence between the obtained values of dispersion and absorption at the transition frequency for different values of the driving power, and the curves calculated for a strongly driven two level atom.

The next logical step would have been to insert such a medium inside an optical resonator in order to realize a "white light cavity".

The latter step was on the other hand avoided because of multiple reasons.

First it is necessary to underline that the stronger decrease of absorption with respect to dispersion for increasing driving field was experimentally demonstrated, but the $\lambda -compensation$ condition necessary to increase the resonator bandwidth had not been achieved. Furthermore the value of the residual absorption, which is fundamental in the finesse of the cavity (see 2.25) and in the transmitted power 2.24, had not been sufficiently suppressed.

The two quantities which play an important role in the evolution of the dispersion and absorption on the transition frequency, once the frequency and its line width have been fixed, are the particle density and the strength of the driving filed.

Let us discuss the first quantity.

The maximal particle density achieved with the experimental setup realized (heating a fresh filled oven up to temperature of $\approx 1000°C$) was of $\approx 0.67 \times 10^{16} m^{-3}$, while the stabile value was of $\approx 0.2 \times 10^{16} m^{-3}$. The latter is a factor ≈ 25 less than the needed one to obtain an increasing of a factor 10 of the bandwidth of the cavity, obtained strongly pumping the atom with a driving field of Rabi frequency $\Omega_D = 13.5\gamma_1$. Such substantial increasing was not easy to obtain using an heated chamber (oven) to obtain an atomic beam.

A possible solution could be obtained using the medium inside a magneto-optical- trap (MOT): for such system a combination of laser and magnetic field are used to to confine

and cool atomic samples. Such a scheme was for example realized by Zinner et al. [64] using a magneto-optical trap operating on the $^1S_0 \rightarrow^1 P_1$ transition at $422.79nm$, and using a re-pump technique to the $5s5p$ $^1P_1$ state. With such configuration the trap lifetime reached $50msec$, limited by the residual gas in the vacuum chamber. They were able to achieve an atomic density of $2.0 \times 10^{16}m^{-3}$ within a radius of $r = 0.5mm$ for the trapped ensembles at a temperature of $3mK$. This density is "only" a factor ≈ 10 bigger than the one we achieved with the atomic beam.

It is also necessary to consider that they used, to slow down the atoms, exactly the same transition we wanted to strongly drive, i.e. the driving field frequency and the MOT laser frequency result to be the same. If inserting the driving field the atoms were any more confined. Using such system would result then not convenient for our purposes.

On the other hand, even if we overwhelmed the problem of the particle density, the difficulties from the not strong enough driving field should still be present.

We have already mentioned that laser diodes are particularly suited, considering their compactness, their easy tunability, the convenience, the narrow emission line width, for spectroscopic intents. Furthermore, the experimental setup would have resulted more compact and easier to operate, if a blue laser diode had been used. $5mW$, cw, single mode blue laser diodes are available but their power, if perfectly suited for the probing system, would not be enough for the driving one. Since recently, around $420nm$ pulsed laser diodes are available with a maximal emitting power of $30mW$. It corresponds to a saturation parameter $S = (I/I_{sat}) \approx 71$ while the condition needed to obtain a "white light resonator" requested a saturation parameter of $S \approx 730$ [56]. Such laser diode would then still not be suited to obtain the desired conditions.

A further possible solution would have been to substitute the diode lasers with a completely different laser system. An eligible candidate would have been a Ti:Sa laser pumped by an argon ion laser which typical output can vary between 150 to $1000mW$ at $800nm$, but the implementation of such a system had to be excluded for financial reasons.

The problems arising from the necessity of the frequency doubling would have not been in any case overwhelmed.

Until now it seems that the implementation of a "WLC" using strongly driven alcium atoms can not be performed due to technical problems.

A possible solution could be represented by a different atomic system, which could show anomalous dispersion at a point of vanishing absorption. The Λ system (3- Niveau system), constituted by Cs atoms was analyzed by M. Mueller [35].

The two hyperfine levels of the ground state $6s_{1/2}$ (corresponding to quantum number $F = 3, 4$) can be coupled to hyperfine level ($F' = 4$) of the excited state $6p_{3/2}$, by means of a coupling field Ω_{ac} and a probing field Ω_{ab}. From the expression of the derivative of the density matrix calculated for such a system [35], it was possible to simulate the behavior of both the absorption, the dispersion and furthermore their ratio, as function of the

probing field intensity, and for different values of the coupling field and the coherent time of the two lower levels (or better its inverse γ_0). A typical result obtained is depicted in Fig 4.9, where all the quantities reported are expressed in function of the natural linewidth of the transition γ. In the Fig 4.9 are depicted both the derivative of index of refraction and the ratio between the latter and the residual absorption.
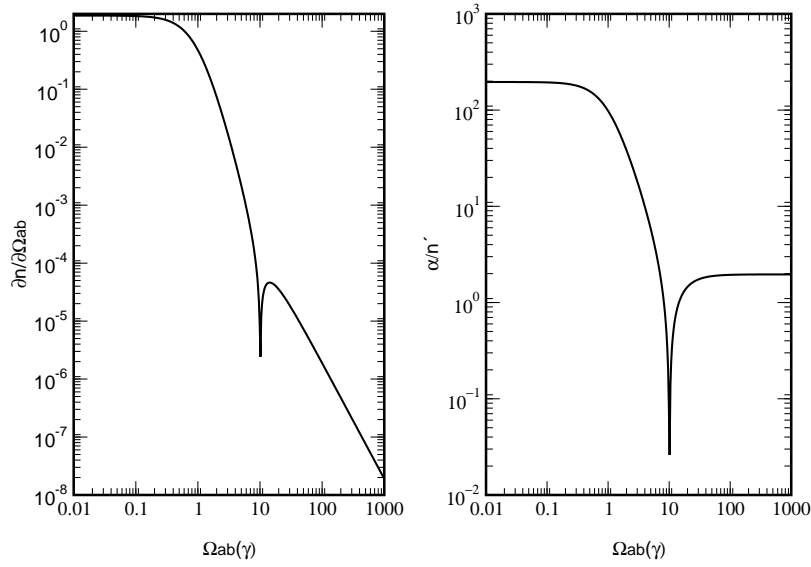

Figure 4.9: Dispersion and residual absorption to dispersion ratio as probing field function. Quantities expressed in natural linewidth units. Calculated values for $\gamma_0 = 0.1$ and $\Omega_{ac} = 3$.

The parameters Ω_{ac} and γ_0, the first representing the intensity of the driving field (expressed by its Rabi frequency) were optimized to the values respectively 3 and 0.1.

The minimum in the figure depicting the dispersion represents a point where the sign changes : for stronger values of the probing field the dispersion becomes anomalous.This is the interval interesting for our application. On the other hand, looking at the curve which represents the ratio of residual absorption to dispersion it has to be observed, that in the interesting interval the ratio tends, with increasing probing field intensity, to a constant value. It is subsequently not possible, to decrease the residual absorption as much as desired, as it were in principle possible with the strongly driven two level system, where, for increasing driving field, the dispersion decreases less than the absorption. We have to

conclude that also a Λ system as not suited for our application.

An atomic system involving a double-Λ scheme was analyzed by Wicht et al. [57], and it consists of a four level system, with two lower and two upper levels. The two lower levels $|b\rangle$ and $|b'\rangle$ are coupled through the first upper level $|c\rangle$ with a strong coupling field of Rabi frequency Ω_k and "zero detuning" $\omega_k = \frac{1}{2}(\omega_{cb} + \omega_{cb'})$. The second upper probing level $|a\rangle$ decays radiatively to the lower levels with damping constants $\gamma = \gamma'$. The radiatively decay relaxation constants of $|c\rangle$ to $|b\rangle$ and $|b'\rangle$ are $\gamma_c = \gamma_{c'} = \gamma$. Indirect pumping rates $\tilde{r}$ and $\tilde{r'}$ are applied between $|a\rangle$ and $|b\rangle$ or $|b'\rangle$ without establishing an additional coherence. The small longitudinal relaxation constants between $|b\rangle$ and $|b'\rangle$ is $\gamma_b = \gamma_{b'} = 10^{-3}\gamma$. The values calculated in the simulation, for the particle density and the field strength are $N = 2 \times 10^{16} m^{-3}$ and $\Omega_k = 2.22\gamma$ respectively, and result to be very promising.

Such a system could be furthermore studied in order to analyze the possibility of its experimental realization.

4.6   Superluminal group velocity

Over the last few months a new kind of application suited for negative dispersive media was developed [10], [52].

An experiment was in fact performed by Wang and coworkers [52] using a negative dispersive medium in order to observe faster than c propagation of light pulses without experiencing large absorption or reshaping, which resulted in controversial interpretation in experiments of such kind performed in the past [7].

It is possible to describe the principle underlying such experiment and to make a comparison between the characteristics of the medium used by Wang and coworkers and our strongly driven calcium atoms. The question will follow, if the medium we realized would be suited to observe a faster than c light pulse propagation velocity.

First it is important to remind the sense of the faster than c light pulse propagation. It has to be considered a light pulse of frequency ν and bandwidth $\Delta\nu$ entering a medium with refraction index $n(\nu)$. The group velocity of the pulse propagation would consequently be $v_g = \frac{c}{n_g}$ where n_g represents the group velocity index $n_g = n(\nu) + \nu\frac{dn(\nu)}{d\nu}$. To avoid a reshaping of the signal the group velocity index has to remain constant over the pulse bandwidth $\Delta\nu$. Recently the modification of the optical properties of a medium using coherent light sources has been used, considering a normal dispersion region, to decrease the group velocity up to $8msec^{-1}$ ([21], [25]).

On the other hand using an **anomalous** dispersive medium, considering once more the expression for the group velocity index, it is possible to obtain a region of large negative

values of $\nu \frac{dn}{d\nu}$. Conversely the group velocity can exceed c (and even become negative). The latter, even if quite counterintuitive does not violate causality. As affirmed by Wang et al.: "The observed superluminal light pulse propagation is not at odds with causality, being a direct consequence of classical interference between its different frequency components in an anomalous dispersion region"[52]. They also affirm: "As remarked by Lord Rayleigh, the group velocity of a light pulse is the result of interference between its various frequency components. Here we note that the measured negative and superluminal group velocity of a light pulse propagating through a transparent anomalous dispersive medium is due to the physical effect of "rephasing". Specifically, inside an anomalous dispersion medium, a longer wavelength (redder) component of a light pulse has a slower phase velocity, contrary to the case of normal dispersion medium. Conversely , a shorter wavelength component (bluer) has a faster phase velocity. Inside a medium of refractive index n, the effective wavelength of a light ray is modified: $\lambda' = \lambda/n$, where λ is the vacuum wavelength. Therefore, in a sufficiently strong anomalous dispersion medium, the redder incident ray will have a shorter wavelength and hence become a bluer ray, while an incident bluer ray will have a longer wavelength to become a redder ray. This results in an unusual situation where the phases of the different frequency components of a pulse become aligned at the exit surface of the medium earlier than even in the case of the same pulse propagating through the same distance in a vacuum."

In the last years Chiao and coworkers showed the theoretical possibility to obtain anomalous dispersion in a transparent medium and that a region of anomalous dispersion can be created in order to reach a faster than c group velocity with almost no pulse distortion using a gain doublet ([47]). In their experiment, Dogariu and coworkers, using two closely spaced Raman peaks observed an anomalous essentially lossless region, measuring a negative group velocity index of $n_g = -315(\pm 5)$ [11]. The propagation time of $\frac{L}{v_g} = n_g \frac{L}{c}$ is needed for a light pulse to transverse a medium of length L. The time difference for the same pulse to transverse the medium or vacuum is subsequently given by the expression $\Delta T = \frac{L}{v_g} - \frac{L}{c} = (n_g - 1)\frac{L}{c}$ and when $n_g < 1$ this delay time results negative.

Consequently the pulse propagation through a vapor cell, which was measured, resulted to be 315 times of the vacuum light propagation time (which is $\frac{L}{c} = 0.2 nsec$).

It results consequently interesting to calculate which would be the time propagation for a pulse passing our anomalous dispersive medium. Once more the conditions to be analyzed correspond to the strongest driving field. This corresponds in fact to the a region where the absorption could be considered suppressed enough in order to let us observe a pulse passing a cell of length $1cm$. In order to calculate the group velocity index the have to consider the derivative of refractive index with respect to frequency.

Dogariu and coworkers measured a derivative of refraction index which was $\approx -9474 \times 10^{-10} MHz^{-1}$ (corresponding to a variation of the refraction index of -1.8×10^{-6} over a frequency interval of $1.9 MHz$). Our calcium atoms on the other hand presented a deriva-

tive which was of $\approx -2067 \times 10^{-10} MHz^{-1}$ (i.e. a factor ≈ 4.5 smaller) for a not driven system, which was furthermore decreased up to $\approx -39.13 \times 10^{-10} MHz^{-1}$ for the strongly driven case.

If we then calculated the group velocity index, we would obtain ≈ -16 which is a factor ≈ 20 less than the Dogariu's one. Our light pulse velocity would then be ≈ 16 times faster than c. On the other hand, in our case the absorption resulted much more suppressed: we in fact obtained a value of $\alpha_0 = (0.18 \pm 0.04)\% cm^{-1}$, while Dogariu reported a value of 40% in the transmitted intensity.

Finally, we can conclude that our medium was designed considering its use inside an optical resonator: it was then designed to obtain λ compensation at a point of vanishing absorption; particular attention was in fact paid to the suppression of the residual absorption which plays a fundamental role in the magnitude of the transmitted peaks. That is why, even if following the same principle (observing anomalous dispersion at a point of zero absorption) our medium would be not perfectly suited to observe faster than c light pulse propagation.

5 Conclusion

Aim of this experiment was to demonstrate the possibility of realizing an anomalous dispersive transparent medium using a strongly driven two level system. Such medium could be in fact result interesting to realize both a broad band high finesse optical cavity or to obtain faster than c propagation pulses.

With help of a strong coherent field, stabilized on the $4s\,^1S_0 \rightarrow 4s4p\,^1P_1$ Ca transition by means of an Fm-spectroscopy, the optical properties of the medium were modified, and were measured using a much weaker laser field .

In the first chapter of this work it is presented a brief description of the theory of the strongly driven two level system, and the characteristics necessary to realize a transparent λ- compensated medium are discussed. It is also illustrated which would be the performances of such a medium when inserted inside an optical resonator.

In the second chapter the experimental setup which had been implemented to realize the anomalous dispersive medium and to measure its absorption and phase shift spectra is presented. The laser systems are illustrated, together with the performances of the frequency doubling cavity, used to obtain the desired wavelength, when an higher power infrared laser diode had been implemented. Furthermore the optical setup used is presented: to obtain an high sensitive and simultaneous measurement of both phase shift and absorption, it was used a Mach Zehnder interferometer with a phase modulated reference arm. To enhance the particle density in the interaction zone, a new configuration for the atomic oven was projected and realized. The performances of the measuring system together with the operating method are described.

In the third chapter are presented the measurements which were realized. Both phase shift and absorption spectra were for the first time systematic investigated in absence of the driving field and for different driving field intensities. The correspondence with the theoretical model of the strongly driven two-level system, which has been discussed in first chapter, could be verified.

5 Conclusion

Furthermore it is observed, as predicted, the stronger decreasing of the absorption with respect to the dispersion with increasing pumping power. For the strongest available driving field, corresponding to a Rabi frequency of $\Omega_D = 2\pi 54.4 MHz$, a measured value for the dispersion of $-39 \pm 12 \times 10^{-10} MHz^{-1}$ was obtained, decreased of a factor ≈ 50 with respect to the not driven atoms. Meanwhile the residual absorption was of $1.28 \pm 0.38\% m^{-1}$, decreased of a factor ≈ 330 with respect to the not driven atoms. Consequently the figure of merit (2.33) takes the value $\approx 13m$, increased of a factor ≈ 6 with respect to the not pumped case. On the other hand a value of $\approx 1000m$ is needed in order to obtain a "white light cavity".

In the reached conditions, even if the λ compensation had been reached, the suppression of absorption could not be considered sufficient in order to realize a White Light Cavity, but it is possible to affirm that, at least theoretically, it is realizable, by mean of an anomalous dispersive transparent medium obtained strongly driving a two level system.

In order to further increase the absorption suppression, a stronger driving field should be used. An analysis of the available possibilities to overwhelm this technical difficulty was also performed.

Furthermore a brief analysis of different atomic systems which could be eligible to realize such kind of application was also performed. The Λ term scheme, which is realizable with Cs by means of the hyperfine splitting of the fundamental state, and which at first sight resulted promising, had to be excluded after a more detailed analysis, which is also reported. Still available would be a double-Λ-system, and a more detailed analysis of such system, and the possibility of its experimental realization could be performed in the future.

76

Bibliography

[1] Biaggio, I., Kerkoc, P., Wu, L.S., Guenter, P., Zysset, B., *Refractive indices of ortho-hombic $KNbO_3$ II. Phase matching configurations for non linear optical interactions*, J. Opt. Soc. Am. B **9**, 507 (1992)

[2] Bjorklund, G. C. and Levenson, M. D., *Frequency Modulation (FM) Spectroscopy, Theory of Lineshapes and Signal-to-Noise Analysis*, Appl. Phys. B **32**, 145-152 (1983)

[3] Bjorklund, G.C., *Frequency- modulation spectroscopy: a new method for measuring weak absoprtion and dispersions*, Opt. Lett. **5**, 15 (1980)

[4] Boyd, G.D., Kleinmann, D.A., *Parametric interaction of focused Gaussian light beams*, J. Appl. Phys., **39**, 3597 (1968)

[5] Brozek, S., *Effiziente Frequenzverdopplung mit Diodenlasern*, Diploma Thesis, Hannover, Germany, 1995

[6] Brozek, O.S., Quetschke, V., Wicht, A., Danzmann, K., *Highly efficient cw frequency doubling of $854nm$ GaAlAs diode lasers in an external cavity*, Opt. Commun., **146**, 141 (1998)

[7] Chiao, R.Y., *Superluminal (but causal) propagation of wave packets in transparent media with inverted atomic population*, Phys. Rev. A, **48**, R34 (1993)

[8] Cohen-Tanoudji, C., *Frontiers in laser spectroscopy*, Les Houches Summer School 1975, Session 27, edited by R. Balian

[9] Demtroeder, W., *Laserspektroskopie*, 3. Edition, Springer Verlag Berlin, 1993

[10] Dogariu, A., Kuzmich, A., Wang, L.J., *Pulse propagation at negative group velocity in a transparent medium*, in OSA Trends in optics and Photonics **57**, Electronic and laser science conference, Thechnical Digest (OSA Washington D.C.), (2001)

[11] Dogariu, A., Kuzmich, A., Wang, L.J., *Transparent anomalous dispersion and superluminal light pulse propagation at a negative group velocity*, Phys. Rev. A **63**, 053806 (2001)

[12] Fleischhauer, M.,Keitel, C.H., Scully, M.O., Su, C., Ulrich, B.T., Zhu, S.Y., *Resonantly enhanced index of refraction without absorption via atomic coherence*, Phys. Rev. A **46**, 1468 (1992)

[13] Fleischhauer, M., Scully, M.O., *Magnetometer based on atomic coherence and possible application to the search for P and T violating permanent electric dipole moments of atoms*, Quantum Semiclass. Opt. **7**, 297 (1995)

[14] Fleischhauer, M., Scully, M.O., *Quantum sensitivity limits of an optical magnetometer based on atomic phase coherence*, Phys. Rev. A **49**, 1973 (1994)

[15] Grynberg, G., Cohen-Tanoudji, C., *Central resonance of the Mollow absorption spectrum: physical origin of gain without population inversion*, Opt. Commun. **96**, 150 (1993)

[16] Hadley, R., *Injection locking of diode lasers*, IEEE J.Quantum Electron. QE-**22**, 419 (1986)

[17] Haensch, T.W., Couillaud, B., *Laser frequency stabilization by polarization spectroscopy of a reflecting reference cavity* Opt. Commun., **35**, 441 (1980)

[18] Haroche, S., *Dressed atoms: a theoretical and experimental study of the physical properties of atoms interacting with radiofrequency photons*, Annls. Phys. (Paris), **6**, 189, 327 (1971)

[19] Harris, S.E., *Lasers without inversion: Interference of lifetime-broadened resonances*, Phys. Rev. Lett. **62** 1033 (1989)

[20] Hartig, W., Walther, H., *High-resolution spectroscopywith and frequency stabilization of a cw dye laser*, Appl. Phys. **1**, 171 (1973)

[21] Hau, L.V., Harris, S.E., Dutton, Z., Behroozi, C.H., *Light speed reduction to 17 metres per second in an ultracold atomic gas*, Nature **397**, 594 (1999)

[22] Hiller, W., *Lebensdauermessungen in Singulett-System des Ca I-Spektrum*, Diploma Thesis, Hannover, Germany, 1980

[23] Kibble, B.P. Copley, G., Krause, L., *Effect of imprisonment of radiation in sodium vapour on the measured lifetime of th* $3\,^3P$ *states*, Phys. Rev. 1539 (1967)

[24] Polzik, E.S., Kimble, H.J., *Frequency doubling with* $KnbO_3$ *in an external cavity*, Opt. Lett. **16**, 1400 (1991)

[25] Budker, D., Kimball, D.F., Rochester, S.M., and Yashchuk, V.V., *Non linear magneto-optics and reduced group velocity of light in atomic vapor with slow ground state relaxation*, Phys. Rev. Lett., **83**, 1767 (1999)

[26] Klausing, H., *All solid state Lasersystem bei* $\lambda = 423nm$, Diploma Thesis, Hannover, Germany, 1996

[27] Kogelnik, H., and Li, T., *Laser beams and resonators*, Appl. Optics **5**, 1550 (1966)

[28] Kuzmich, A., Dogariu, A., Wang, L.J., *Signal velocity, causality, and quantum noise in superluminal light pulse propagation*, in OSA Trends in optics and Photonics **57**, Electronic and laser science conference, Thechnical Digest (OSA Washington D.C.), (2001)

[29] Liang, J.Q., Katsuragawa, M., Fam Le Kien, Hakuta, K., *Slow light produced by stimulated Raman scattering in solid hydrogen*, in OSA Trends in optics and Photonics **57**, Electronic and laser science conference, Thechnical Digest (OSA Washington D.C.), (2001)

[30] Lang, R., *Injection locking properties of semiconductor lasers*, IEEE J.Quantum Electron. QE-**18**, 259 (1982)

[31] Lohdahl, P., Soerensen, J.L., and Polzik, E.S., *High efficiency second harmonic generation with a low power diode laser*, Appl. Phys. B **64**, 383 (1997)

[32] Milano, L., Barone, F., and Milano, M., *Time domain amplitude and frequency detection of gravitational waves from coalescing binaries*, Phys. Rev. D **55**, 4537 (1997)

[33] Mollow, B. R., Phys. Rev. **188**, 1969 (1969)

[34] Mueller, G., Mueller, M., Wicht, A., Rinkleff, R.-H., and Danzmann, K., *Optical resonator with steep internal dispersion*, Phys. Rev. A **56**, 2385, (1997)

[35] Mueller, M., *Zerstoerungsfreie Quantenmessungen*, Ph.D. Thesis, Hannover, (2000)

[36] Padmabandu, G.G., Welch, G.R., Nikonov, D.E., Lukin, M.D., Scully, M.O., *Laser oscillation without population inversion is a sodium atomic beam* , Phys. Rev. Lett. **76**, 2053 (1996)

[37] Prevedelli, M., Freegarde, T., Haensch, T.W., *Phase locking of grating tuned diode lasers*, Appl. Phys. B, **60**, 241, (1995)

[38] Quang, T., Freedhoff, H., *Index of refraction of a system of strongly driven two level atoms*, Phys. Rev. A **48**, 3216 (1993)

[39] Quetschke, V., *Heterodynes Laserinterferometer zur simultanen Absorptions- und Dispersionsmessung*, Diploma Thesis, Hannover, Germany, 1996

[40] Rautian, S.G., Sobel'man, I.I., *Line shape and dispersion in the vicinity of an absorption band, as affected by induced transitions*, Soviet Phys. JETP **14**, 328 (1962)

[41] Scully, M.O., Zhu, S.Y., Gavrielides, *Degenerate quantum-beat laser: Lasing without inversion and inversion without lasing*, Phys. Rev. Lett. **62**, 2813 (1989)

[42] Scully, M.O., *Enhancement of index of refraction via quantum coherence*, Phys. Rev. Lett. **67**, 1885 (1991)

[43] Scully, M.O., Zhu, S.Y., Fearns, H., *Lasing without inversion*, Z. Phys. D **22**, 471 (1992)

[44] Zhu, S.Y., Scully, M.O., Fearns, H., Narducci, L.M., *Lasing without inversion*, Z. Phys. D **22**, 483 (1992)

[45] Sobel'man, I.I., *Introduction to the theory of atomic spectra*, Pergamon press, Oxford, 1972

[46] Spano, P., Piazzolla, S., Tamburrini, M., *Frequency and intensity noise in injection locked semiconductor lasers: theory and experiment*, IEEE J.Quantum Electron. QE-**22**, 427 (1986)

[47] Steinberg, A.M., Chiao, R.Y., *Dispersionless, highly superluminal propagation in a medium with a gain doublet*, Phys. Rev. A **49**, 2071 (1994)

[48] Stenner, M.D., Gauthier, D.J., *Quantum limits to superluminal pulse advancement*, in OSA Trends in optics and Photonics **57**, Electronic and laser science conference, Thechnical Digest (OSA Washington D.C.), (2001)

[49] Szymanowski, C., Wicht, A. Danzmann, K., *On negative dispersion without absorption in bichromatically driven two-level systems* J.of Mod. Optics **44**, 1373-1392 (1997)

[50] Szymanowski, C., Keitel, C.H., Dalton, B.J., Knight, P.L., *Switching between Rayleight-like and Lorentzian lineshapes of the dispersion in driven two-level atoms*, J.of Mod. Optics **42**, 985 (1995)

[51] Szymanowski, C., Keitel, C.H., *Enhancing the index of refraction under convenient conditions*, J. Phys. B **27**, 5795 (1994)

[52] Wang, L.J., Kuzmich, A., Dogariu, A., *Gain assisted superluminal light propagation*, Letters to nature **406**, 277 (2000)

[53] Whittaker, E.A., Gehrtz, M., Bjorklund, G.C., *Residual Amplitude modulation in laser electro-optic phase modulation*, J. Opt. Soc. Am. B **2**, 1320 (1985)

[54] Wicht, A., Mueller, M., Rinkleff, R.-H., Rocco, A., and Danzmann, K., *Experimental demonstration of negative dispersion without absorption*, Opt. Commun **179**, 107 (1999)

[55] Wicht, A., *Anomale Dispersion, kohaerente Medien und Weisslichtresonatoren*, Ph.D. Thesis, Hannover, 1998

[56] Wicht, A., Mueller, M., Rinkleff, R.-H., Rocco, A., and Danzmann, K., *A phase-modulated interferometer for high-precision spectroscopy*, Appl. Phys. B **70**, 821 (2000)

[57] Wicht, A., Danzmann, K., Fleischauer, M., Scully, M.O., Mueller, G., and Rinkleff, R.-H. *White light cavities, atomic phase coherence and gravitational wave detectors*, Optics Commun. **134**, 431 (1997)

[58] Wieman, C.E., Hollberg, L., *Using diode lasers for atomic physics*, Rev. Sci. Instrum. **62**, 1 (1991)

[59] Witte, A., Kisters, Th., Riehle, F., Helmke, J., *Laser cooling and deflection of a calcium atomic beam*, J. Opt. Soc. Am. B **9**, 1030 (1992)

[60] Wynands, R., Nagel, A., *Precision Spectroscopy with coherent dark states*, Appl. Phys. B, **68** (1999)

[61] Wynads, R., Diedrich, F., Meschede, D. Telle, H.R., *A compact tunable* $60dB$ *Faraday optical isolator for the near infrared*, Rev. Sci. Instrum. **63**, 5586 (1992)

[62] Tartwjik, G.H.M., Lenstra, D., *Semiconductor lasers with optical injection and feedback*, Quantum seimiclass. Opt **7**, 87 (1995)

[63] Yariv, A., *Quantum Electronics*, John Wiley & Sons, 1989, New York

[64] Zinner, G., Biennewies, T., Riehle, F., *Photoassociation of cold Ca atoms*, Phys. Rev. Lett. **85**, 2292 (2000)

[65] Zysset, B., Biaggio, I., Guenter, P., *Refractive indices of orthorhombic* $KNbO_3$ *I. Dispersion and temperature dependance*, J. Opt. Soc. Am. B **9**, 380 (1992)

Acknowledgments

I first would like to thank Prof. Danzmann for giving me the possibility to to work within his group and providing the best working conditions. He was also always very supportive. Even though the natural difficulties this experience resulted of great importance for both my scientific and personal development.

My deep thanks to Dr. Rolf-Hermann Rinkleff: he followed the different phases of the work and was always available for discussions, share his experience, and giving support and motivation in the hardest part of the experiment. He also never regret to spend many hours in the laboratory to help me overwhelm my "physical" limits. Also in the final part, the writing of this thesis, his advice and support was always precious.

I wish also to thank Dr. Andreas Wicht who guided me in my first steps in experimental atomic physics and into German lab language. He also was always ready to answer and discuss my questions, even when they came in form of e-mail to U.S.A.

I also wish to thank the whole technical staff. Herr Heiko zur Muehlen with his precious knowledge of electronics and who was always available for a last minute repairing. Herr Jochen Klaus and Herr Lehmann from the mechanical workshop, who were able to decipher my "Picasso" technical drawings and developed from them working mechanical components. All the people in the mechanical workshop were very kind and helpful, even when my German explanations and requests were not very clear. In particular I would like to thank Herr Philip Shauzu for modifying many times a collimator lens holder without (apparently) complaining.

I wish also to thank Prof. Milano for helpful discussion about fit methods.
I would also like to thank all my colleagues for the different and helpful discussions occasions. In particular I would like to mention: Andreas Freise who provided infinite support in trying to match my brain waves to the computer ones (without much success), Dr. Geppo Cagnoli, who spent one of his free week-end working with me, Valerie Nadeau who helped to correct some weird English expressions, Dr. Benno Wilke for starting and hosting the International Evening, Dr. Patrick Kloevekorn for being a friend and for providing a software resurrection of my dead screen-saver fish, all the many people who supported me in such unpleasant occasions as bike accident, and the people who are my friends now.

I also would like to thank Frau Kirsten Naceur, who welcomed me in Germany and helped to smooth the cultural shock.

Last but not least I want to thank Fabiomassimo, who still wants to share his life with me. It would be long to list the occasions when his help or support were necessary to hold on, but without them this work would not be here.